SUSTAINED MICROGLIAL IMMUNE RESPONSES

IN AN SIV/MACAQUE MODEL OF HIV CNS DISEASE

by

Audrey Claire Knight

A dissertation submitted to Johns Hopkins University in conformity with the requirements

for

the degree of Doctor of Philosophy

Baltimore, Maryland

March 2020

**ABSTRACT**

Human Immunodeficiency Virus (HIV) central nervous system (CNS) disease
remains a significant clinical issue in the post-antiretroviral therapy (ART) era. Although the
severity of HIV CNS disease has decreased with ART, the prevalence has not changed. It is
hypothesized that chronic inflammation in the CNS despite effective viral suppression is
critical to the pathogenesis of HIV CNS disease. As one of the immune cells in the brain that
is also chronically infected with HIV, microglia are of particular interest.

In this dissertation, we characterized chronic microglial immune activation in an
SIV/pigtailed macaque model of HIV CNS disease. We characterized in this model the
expression colony stimulating factor 1 receptor (CSF1R), a classic tyrosine kinase receptor
that is constitutively expressed on cells of the myeloid lineage that is essential for the
survival of microglia. Additionally, overexpression of CSF1R has been associated with
several neurodegenerative diseases, including Alzheimer's disease (AD) and amyotrophic
lateral sclerosis (ALS). In animals with SIV encephalitis, we found that CSF1R was
significantly elevated in brain compared to uninfected animals. Interestingly, CSF1R protein
levels remained elevated in the brains of ART-suppressed SIV-infected animals, suggesting
that CSF1R plays a role in the persistence of HIV CNS disease in the post-ART era.

We also characterized a similar receptor, triggering receptor expressed on myeloid
cells 2 (TREM2). TREM2 is similarly associated with AD and ALS, and there is significant
crosstalk between TREM2 and CSF1R via DNAX adaptor protein 12 (DAP12).
Consequently, TREM2 and CSF1R have many of the same downstream signaling effects in
microglia. While TREM2 and CSF1R both significantly increase in SIV encephalitis,
TREM2 returns to baseline levels with suppressive ART. This shows that while similar,

TREM2 and CSF1R have unique roles in neuroinflammation, particularly in the context of chronic, suppressed SIV infection.

Finally, we performed a pilot pre-clinical drug trial in suppressed, SIV-infected pigtailed macaques with PLX3397, a small-molecule CSF1R inhibitor. PLX3397 was kept onboard after animals were released from ART. PLX3397 treatment reduced the number of microglia both *in vitro* and *in vivo*. While PLX3397 had no effect on plasma viral rebound, treatment prevented viral rebound in the cerebrospinal fluid of one animal. Additionally, PLX3397 treatment changed the morphology of the remaining microglia from an ameboid, activated state to a resting/surveilling state. The work presented in this dissertation provides a unique insight into the mechanisms of chronic inflammation in the CNS of SIV-infected pigtailed macaques lays the groundwork for future preclinical drug trials to treat HIV CNS disease.

**ACKNOWLEDGEMENTS**

IHC and ISH up and running. I would not have been able to start those projects without your hard work and assistance. And thank you to the rest of the Mankowski group members, Dr. Lisa Mangus, Dr. Marcelo Bustamante, Dr. Katie Mulka, Megan McCarron, and Clarisse Solis. You all have created an incredible environment for me to complete my PhD.

I also want to thank the Pathobiology program director, Dr. Lee Martin. You have always been an incredible advocate for me and the rest of the Pathobiology students. Thank you for continuing to support all of us and for providing an incredible environment for us students. Also, thank you to Stacey Morgan, the Pathobiology program administrator. I absolutely would not have been able to graduate without all of her help filling out forms, getting me signed up for classes on time, and keeping our program running. I also want to thank all of the students of the Pathobiology program. You have been incredible peers to learn from and work with over the last five years.

I want to thank the members of the incoming class of 2015, Lionel, Nivi, Swathi, Yea Ji, and Janelle. I would not have made it through my first two years of coursework and lab work without your help and support. I want to especially thank Janelle. You were my first friend in Baltimore and have been such an incredible source of love and support throughout my time at Hopkins. I am so grateful for your friendship. I also want to thank my two closest friends, April and Elizabeth. You have been my most constant and most enthusiastic sources of support and love since we were 13. Thank you for always being there for me. You both mean the world to me.

Thank you to my fiancé, Mark. You came into my life halfway through this process, which is never easy. Thank you so much for always keeping me grounded, for reminding me

of the good things and helping me move past the negative. Thank you for always giving me a reason to smile and to laugh, even when I felt like the world was falling apart.

Finally, thank you to my family: my brothers Adam and Evan, and my parents. Whenever I doubted my abilities, you were always there to remind me of how proud you were of my accomplishments and reassured me. When I was growing up, I never wanted to go into science, because both my parents were scientists. I wanted to be my own person and make my own way. Now as I am an adult and a professional scientist, I realize how lucky and blessed I am that I turned out a lot like my parents, not only in my career, but also as a person. You all mean everything to me, and I am so grateful for your constant support and unconditional love.

**TABLE OF CONTENTS**

# LIST OF TABLES

# LIST OF FIGURES

**Chapter IV**

**Chapter V**

**CHAPTER I.**

**Introduction**

**Human Immunodeficiency Virus**

Human immunodeficiency virus (HIV) is one of the most prevalent infectious diseases, infecting approximately 37.9 million people worldwide as of 2018 (hiv.gov). Despite effective antiretroviral therapy, HIV continues to be a significant public health concern. In 2018, there were 1.1 million new HIV infections worldwide (hiv.gov). Although HIV most likely crossed the species barrier as early as 1930 (Korber et al. 2000), the HIV pandemic was first described in the early 1980s (Levy 2007).

HIV is a lentivirus that infects both CD4+ T lymphocytes and myeloid cells (Gonda et al. 1986; Barre-Sinoussi et al. 1983; Gallo et al. 1984). CD4+ T cell infection is one of the defining characteristics of clinical HIV disease. Without treatment, HIV causes CD4+ T lymphocyte depletion resulting in immune suppression and death approximately 8-10 years after initial infection if left untreated. Acquired immunodeficiency syndrome (AIDS), the end-stage disease of HIV infection, is defined as a CD4+ T lymphocyte count of less than 200 cells/mL of blood accompanied by an AIDS-defining opportunistic infection (Groopman and Gottlieb 1983; AIDSinfo.nih.gov).

In order for HIV to infect a cell, it first binds to the host cell CD4 and a co-receptor—either CCR5 or CXCR4 (Dalgleish et al. 1984; Choe et al. 1996). This binding leads to the fusion of the HIV envelope with the host cell membrane, releasing the viral capsid into the cytoplasm. The contents of the capsid are then released. The capsid contains the HIV genome—two single strands of RNA—and proteins required for reverse transcription (reverse transcriptase) and integration (integrase) of the HIV genome into the host DNA. Once in the cytoplasm, reverse transcriptase synthesizes complementary, double stranded DNA from the HIV RNA. This DNA is then shuttled into the nucleus with integrase where it

is integrated into the genome. Once the viral DNA is integrated into the host genome, new viral RNA and proteins are able to be synthesized by the host transcription and translation machinery (Freed 2001). Importantly, immune activation, particularly via the NF-kB pathway, is known to activate transcription of HIV genes integrated in the host genome (Duh et al. 1989). These infected cells can then generate new fully packaged virions that can be released from the host cell by another viral protein, protease. HIV protease is also essential in the maturation of the released virion; the mature virion can then infect new cells (Freed 2001).

Antiretrovirals have been successful in targeting several key points throughout infection that results in the reduction of detectable HIV in the plasma. For the initial infection of a host cell, drugs can prevent the binding of the virion to the receptors on the host cell (CCR5 antagonists), and others prevent the fusion of the viral envelope with the host cell membrane. Other antiretrovirals target reverse transcriptase (nucleoside/non-nucleoside reverse transcriptase inhibitors—N/NNRTIs), integrase, or protease. A treatment plan consisting of a combination of these antiretrovirals can successfully suppress viral replication, resulting in undetectable levels of virus in the plasma while decreasing the risk of developing resistance mutations (Pau and George 2014).

Since the development of antiretroviral therapy (ART), HIV-infected individuals are now able to live near normal lifespans (Antiretroviral Therapy Cohort 2017). However, ART is not curative. Although only a small proportion of CD4+ T cells are infected, a subset of these cells can be incredibly long-lived. HIV can readily infect activated CD4 T cells. In many cases, the infection of an activated CD4+ T cell will result in the death of the cell along with massive production of virus. However, if the virus infects an activated CD4+ T cell that

3

is in the process of transitioning to a memory cell, the virus can integrate its genome into the cell without resulting in the death of the host cell. While some virus can be produced from these cells, active viral replication is quickly shut down as the cell transitions to a quiescent memory cell. These long-lived, infected cells can remain dormant in an individual and ART cannot target these cells because ART targets active viral replication. If the cell is reactivated, it can then also activate viral replication, producing more virus to then infect other cells (Sengupta and Siliciano 2018).

Because of these characteristics, memory CD4+ T cells are considered the major cell type that makes up the latent reservoir. However, HIV also infects monocytes and tissue macrophages. Tissue macrophages can live for longer periods of time and can harbor replication competent virus in the context of ART. In a simian immunodeficiency virus (SIV)/pigtailed macaque model where animals were fully suppressed with ART for at least six months and up to 18 months, SIV DNA could be detected in macrophages isolated from the spleen and lung, as well as in peripheral blood monocytes (PBMCs). These levels of SIV DNA were comparable to those found in CD4+ T cells. Additionally, replication competent virus was isolated from macrophages taken from the spleen, lung, and blood (Abreu et al. 2019). This suggests that macrophages can serve as an additional latent reservoir.

It is clear that ART will not significantly address the issue of the latent reservoir. It is estimated that the latent reservoir in an HIV-infected individual that is fully suppressed would take approximately 74 years to be eliminated (Siliciano et al. 2003). Consequently, new therapies need to be developed that target and eliminate the latent reservoir. One cure strategy is 'latency reversal'. It is thought by treating patients with a latency reversing agent (LRA), such as a histone deacetylase (HDAC) inhibitor, viral replication can be initiated

without the activation of the infected cell. This would allow the infected cell to be recognized and eliminated by the immune system (Bashiri et al. 2018). However, LRAs have not been particularly efficient in clearing the latent reservoir. This may be due to a combination of an inability to activate virus production in all latently infected cells, off-target effects that prevent the ability of CD8+ T cells from killing infected cells, and an inability of latently-infected cells to present enough viral antigen to stimulate CD8+ T cells (Ke et al. 2018; Clutton and Jones 2018). LRAs have also been shown to cause increased inflammation in the brain of SIV-infected rhesus macaques, suggesting that LRAs could cause significant neuronal damage (Gama et al. 2017).

Therapeutic vaccines have also been considered as a potential cure. Because of HIV's high mutation rate, antibody responses to HIV have largely been ineffective. However, the discovery of broadly-neutralizing antibodies against HIV provided evidence that the development of a vaccine against HIV may be possible (Bonsignori et al. 2012). It is thought that an effective therapeutic vaccine given to an HIV-infected patient that is fully suppressed would stimulate an appropriate immune response. With subsequent activation of the viral reservoir through LRA treatment, the individual's immune system would be able to eliminate infected cells and neutralize infectious virus released from those cells (Mylvaganam et al. 2015). Although a vaccine is theoretically possible, an effective vaccine has yet to be discovered.

As the field looks toward cure strategies, it is important to consider all possible sources of HIV infection. Although there is still some debate, there is significant evidence suggesting that cells of the myeloid lineage constitute a latent reservoir for HIV (Wong et al. 2019). Additionally, chronic infection and sustained inflammation of tissue-resident

macrophages is thought to drive these chronic organ-specific diseases. It is hypothesized that as the HIV-infected population continues to age, clinicians will begin to see an increase in HIV-associated organ-specific diseases, including CNS, cardiovascular, and gastrointestinal disease (High et al. 2012). Therefore, understanding the viral dynamics of chronic HIV infection of myeloid cells is critical to not only treating chronic organ disease, but also to curing HIV infection.

**HIV-associated central nervous system (CNS) disease**

In the brain, the primary cells infected with HIV are parenchymal microglia and perivascular macrophages (Abreu et al. 2019; Wallet et al. 2019). There are several ways that HIV may establish CNS infection. HIV enters the brain either through infected CD4+ T cells or monocytes trafficking into the brain, such as CD4+ T cells or myeloid cells, via diapedesis. Free HIV virions can also enter the brain directly through the blood-brain barrier or the cerebrospinal fluid (CSF)-brain barrier via transcytosis. This process is highly dependent on pericyte responses to inflammatory cytokines (Dohgu and Banks 2013). Either of these pathways leads to direct infection of resident perivascular macrophages and microglia (Levy 2007; Williams et al. 2013). It is thought that this infection and subsequent immune responses drive CNS disease.

HIV associated neurocognitive disease (HAND) can be broken down into three clinical subsets: asymptomatic neurocognitive impairment (ANI), mild neurocognitive disorder (MND), and HIV associated dementia (HAD). ANI is characterized by decreased function in two or more neurocognitive domains that is apparent during neurocognitive testing but are asymptomatic. MND, on the other hand, is defined by neurocognitive deficits

that directly decrease quality of life. HAD presents similarly to other forms of dementia, where neurocognitive function is severely impaired (Saylor et al. 2016).

Before the introduction of ART, approximately half of HIV-infected individuals developed CNS impairment, with a significant portion of these individuals developing HAD (20%). The introduction of ART has significantly decreased the prevalence of HAD to 2% of the HIV-infected population. In spite of this reduction in severity, HAND remains a significant consequence of HIV-infection; still today, half of the HIV-infected population has neurocognitive impairment (Saylor et al. 2016). This suggests that although viral replication is a significant factor in the development of HIV CNS disease, it is not the sole cause.

There is evidence in animal models and in fully suppressed HIV-infected individuals that there is ongoing inflammation in the brain. This has been related to poorer cognitive and motor function (Saylor et al. 2016; Montoya et al. 2019). In addition to ongoing neuroinflammation, it is hypothesized that chronic HIV infection alters the homeostatic baseline of neuroimmune cells, including microglia and astrocytes. It has been shown in microglia that chronic HIV infection alters microglial metabolism, apoptosis, and immune activation (Chen et al. 2018). Consequently, microglia play an essential role in the development of HIV CNS disease.

**The role of microglia in HIV CNS disease**

Microglia are a resident immune cell in the brain and comprise approximately 10% of CNS cells. Although closely related to bone marrow-derived macrophages, microglia develop from an independent yolk-sac progenitor. These yolk sac progenitor macrophages

enter the CNS early during development, anywhere from 4 to 24 gestational weeks; in mice, this migration occurs at E9 (Menassa et al. 2018; Thion et al. 2018).

As a glial cell, microglia are essential in maintaining CNS health. During development, microglia assist in the development of neuronal networks through promoting synaptogenesis, neuronal spine pruning, and the survival of neuronal precursor cells. In adulthood, microglia continue to support neuron connections as well has assisting in the formation of new networks and the destruction of redundant pathways (Sominsky et al. 2018). Beyond directly supporting neuronal networks, microglia serve as a CNS resident immune cell. Microglia are innate immune cells, phagocytosing foreign elements including pathogens, presenting antigen to adaptive immune cells, and secreting inflammatory cytokines (Colonna and Butovsky 2017).

Microglia have been implicated in several neurodegenerative diseases, including Alzheimer's disease (AD), amyotrophic lateral sclerosis (ALS), multiple sclerosis (MS), and HIV CNS disease (Cartier et al. 2014). Considering microglia are a major immune cell in the brain and the primary CNS cell type that is infected with and can produce infection-competent HIV, microglia appear to be essential in the development of HIV CNS disease (Saylor et al. 2016; Williams et al. 2014). However, the exact mechanism of how microglia cause neurodegeneration in the context of HIV infection is not clear, especially considering that individuals continue to develop HIV CNS disease in spite of effective viral suppression.

It is hypothesized that chronic inflammation and microglial activation are major contributors to the pathogenesis of HIV CNS disease. While viral replication is inhibited, there have been reports showing that viral proteins are still released from infected cells (Ferdin et al. 2018). These proteins have the capability to stimulate immune responses, thus

resulting in chronic microglial activation (Saylor et al. 2016). Further, there is histologic evidence that in fully suppressed pigtailed macaques, microglial morphology resembles a more activated state (**Figure 2-4**). These viral proteins can also stimulate astrocytes, which release glutamate, resulting in excitotoxic neuronal damage (Saylor et al. 2016). Consequently, modulating the immune response and clearing the latent reservoirs are key components of treating HIV CNS disease.

**SIV/Pigtailed Macaque Model of HIV CNS Disease**

To study the contribution of microglia to the pathogenesis of HIV-associated CNS disease, we utilize the SIV/pigtailed macaque model of HIV CNS disease. Simian immunodeficiency virus (SIV) is a lentivirus closely related to HIV. There is evidence that a strain of SIV ($SIV_{chpz}$) crossed the species barrier to become HIV-1 in the 1930s (Korber et al. 2000). SIV naturally infects numerous African non-human primate species, including chimpanzees ($SIV_{chpz}$) and sooty mangabeys ($SIV_{smm}$). Despite active viral replication, SIV does not cause disease in these natural hosts. However, SIV is able to cause disease in non-native hosts. It is thought that $SIV_{chpz}$ crossed the species barrier and established HIV-1 infection in humans as it is most closely related to HIV-1, while $SIV_{smm}$ is closely related to HIV-2 (Hahn et al. 2000; Silvestri et al. 2007; Van Heuverswyn and Peeters 2007).

Similar to human infection, when SIV infects non-native hosts, such as Asian macaques, the disease shares many characteristics with HIV infection in humans (Hahn et al. 2000; Silvestri et al. 2007; Van Heuverswyn and Peeters 2007). Consequently, rhesus macaques (*Macaca mulatta*) and pigtailed macaques (*Macaca nemestrina*) are often utilized to study SIV infection as experimental models of HIV infection in humans.

In the SIV/pigtailed macaque model, pigtailed macaques are inoculated with two strains of SIV: SIV/DeltaB670 and SIV/17E-Fr. SIV/DeltaB670 is an immunosuppressive swarm. This virus depletes CD4+ T-cells and infects myeloid cells. SIV/17E-Fr, on the other hand, is a molecular clone with specific mutations in the *env*, *nef*, and 3'LTR regions of the viral genome that confer macrophage tropism and the ability to replicate within the CNS (Beck et al. 2017). Interestingly, this same infection paradigm in rhesus macaques, the typical animal utilized in SIV studies, does not produce the same consistent CNS presentation (Beck et al. 2015).

Peak virus can be detected in both plasma and CSF at 12 days post-infection. CSF viral loads tend to be a log lower than plasma viral loads. After acute infection, viral loads in plasma and CSF decrease, but not to the same levels seen in HIV-infected patients who are not on antiretroviral therapy. This allows for an accelerated model of HIV infection. Approximately 60% of infected pigtailed macaques will develop SIV CNS disease within 84 days of infection, the timepoint when all animals have AIDS-defining conditions (Beck et al. 2015). CNS disease is characterized by macrophage-predominant perivascular cuffs and microglial giant cells. These lesions overlap with active SIV replication in these cells (Beck et al. 2017).

An additional benefit of this model is that animals can be treated with current standard of care antiretrovirals. In our model, PMPA (9-(2-phosphonomethoxypropyl)adenine), Emtricitabine (FTC), and Dolutegravir are injected subcutaneously daily. Treatment is started 12 days post-infection and results in successful suppression, defined as plasma viral load being below 100 copies/mL of virus in both the plasma and CSF within 50 days of treatment. Animals are then held suppressed for 180 days.

In this context, we are able to study chronic SIV infection and the resultant organ-specific diseases, particularly those of the CNS under ART (Beck et al. 2017).

Beyond studying chronic suppressed SIV infection, we can also study viral rebound dynamics in this model by removing ART akin to structured treatment interruptions in HIV patients (Papasavvas et al. 2004). In this protocol, animals are released from ART and viral dynamics are monitored by tracking plasma and CSF viral loads over time. Animals are euthanized when they reach viral set-point with three consecutive measurements of plasma viral load within one log of each other. We can then identify tissue and cellular sites that the virus replicates to study the immunologic impacts of rebound active viral replication.

**Project Overview**

For my dissertation, I characterized chronic microglial activation in the context of HIV CNS infection in the SIV/pigtailed macaque ART model.

In chapter II, I characterized colony stimulating factor 1 (CSF1R) and its two ligands, colony stimulating factor 1 (CSF1) and IL34 in the SIV/pigtailed macaque model. Colony stimulating factor 1 receptor (CSF1R) is a classic tyrosine kinase receptor constitutively expressed on cells of the myeloid lineage. In the brain, the primary cells expressing this receptor are microglia (Stanley and Chitu 2014). CSF1R signaling is essential for the survival, proliferation, and activation of microglia; if CSF1R receptor signaling is prevented either with a small molecule inhibitor or by knocking out the gene, microglia are depleted (**Figure 1-2**; Elmore et al. 2014; Erblich et al. 2011). Increased CSF1R expression has been seen in multiple neurodegenerative diseases, including AD, ALS, and prion diseases (Akiyama et al. 1994; Gomez-Nicola et al. 2013). I found that *CSF1* is significantly

increased in both grey and white matter in SIV-infected pigtailed macaque frontal cortex after 84 days of infection whereas *IL34* expression did not change (**Figure 2-2**). CSF1R protein levels were also significantly increased in the white matter of these same animals as shown by immunohistochemistry (**Figure 2-4**) and ELISA (**Figure 2-5**). Interestingly, CSF1R protein remained elevated in fully suppressed SIV-infected pigtailed macaque frontal cortex. As microgliosis does not occur in fully suppressed SIV-infected pigtailed macaques, this increase in CSF1R is not thought to be due to an increase in microglial number. Rather, the increase in CSF1R protein is likely due to an increase at the single-cell level. This suggests that although SIV replication is inhibited, microglia are in a different state of immune activation. This could represent microglial priming or a continued activated state.

In chapter III, I characterized triggering receptor expressed on myeloid cells 2 (TREM2) mRNA and protein expression in this same model. TREM2, much like CSF1R, is constitutively expressed on cells of the myeloid lineage, and in the brain is primarily expressed on microglia. TREM2 has many of the same downstream effects as CSF1R: cell activation, survival, and proliferation (**Figure 1-3**; Yeh et al. 2017). In spite of this, we found that while TREM2 and CSF1R mRNA expression are highly correlated in this model (**Figure 3-2**), they are not correlated at the protein level (**Figure 3-4**). Additionally, after animals were released from antiretroviral treatment to study viral rebound, TREM2 protein remained at baseline, while CSF1R protein remained elevated from baseline with several animals expressing much higher levels of CSF1R than in fully suppressed animals (**Figure 3-6**). While both TREM2 and CSF1R protein increase with SIV encephalitis, we hypothesize that the increase in TREM2 protein is due to an increase in microglial cell number. This is supported by TREM2 protein levels returning to baseline in fully suppressed SIV-infected

12

pigtailed macaques. However, CSF1R protein levels remain elevated in these animals, suggesting that this increase is happening at the single-cell level (**Figure 1-4**). Consequently, we hypothesize that CSF1R may be a marker of microglial priming, wherein after initial responses, microglia are more easily activated and have stronger responses upon secondary stimulation (Perry and Holmes 2014).

Finally, in chapter IV, I determined the efficacy of the CSF1R small molecule inhibitor, PLX3397 in our SIV/pigtailed macaque model. *In vitro*, PLX3397 effectively killed primary pigtailed macaque microglia (**Figure 4-3**). *In vivo*, 165mg/kg of PLX3397 prevented viral rebound in the cerebrospinal fluid in one of two animals, while it had no effect on viral rebound in plasma (**Figure 4-5**). Additionally, microglia isolated at necropsy from this animal did not release detectable virus *ex vivo* by quantitative PCR. Therefore, PLX3397 treatment may be effective at eliminating or suppressing the CNS SIV reservoir.
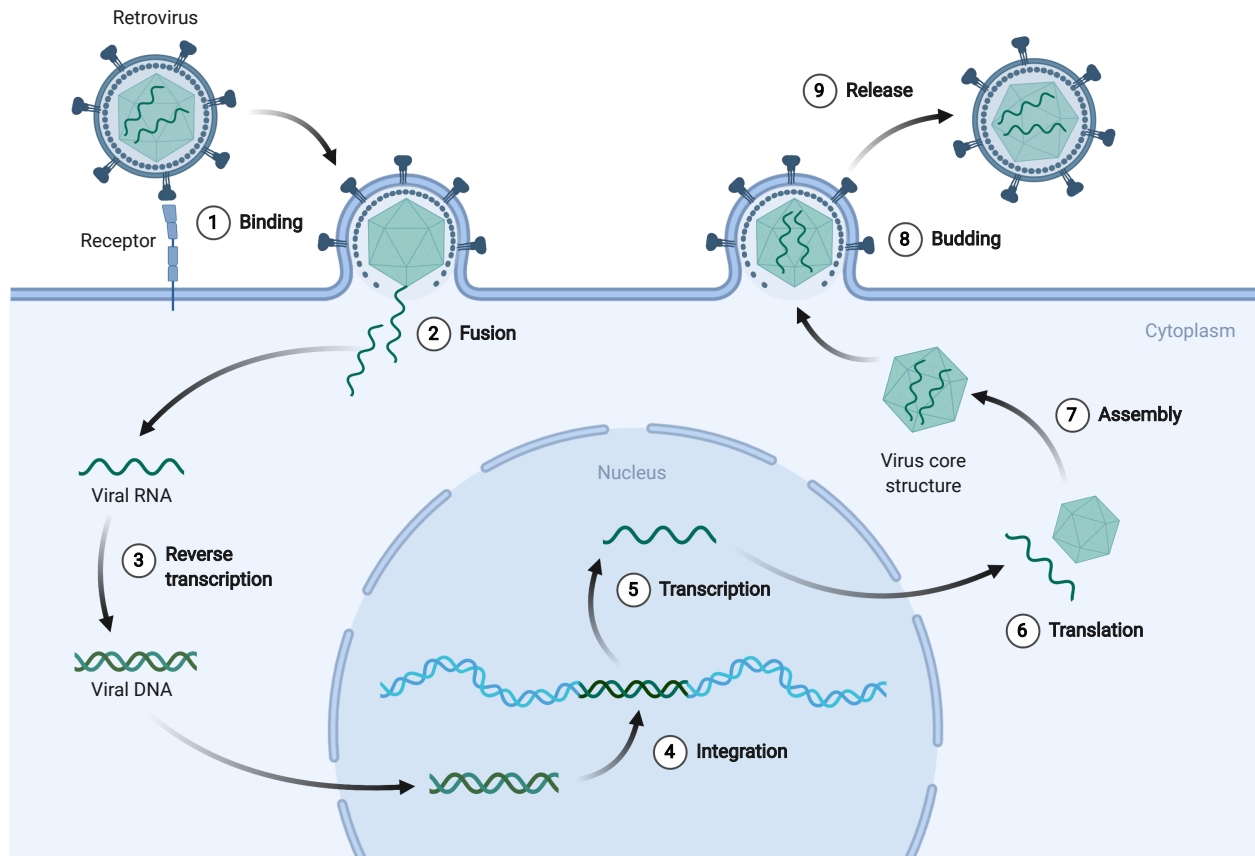
**Figure 1-1. Overview of the HIV infection lifecycle.** (1) HIV initially binds to the host cell via receptors. This triggers (2) fusion and the release of viral RNA. Once in the cytoplasm, (3) reverse transcription of viral RNA to double-stranded DNA occurs. This is then shuttled to the nucleus and is (4) integrated into the host genome. Once integrated, (5) transcription of viral RNA is possible. (6) Translation of viral proteins is followed shortly thereafter by (7) virion assembly. The virion is then able to (8) bud off from the host cell and is (9) released. After release, the virion undergoes further maturation. The mature virion is then capable of infecting another cell. Figure provided by BioRender.
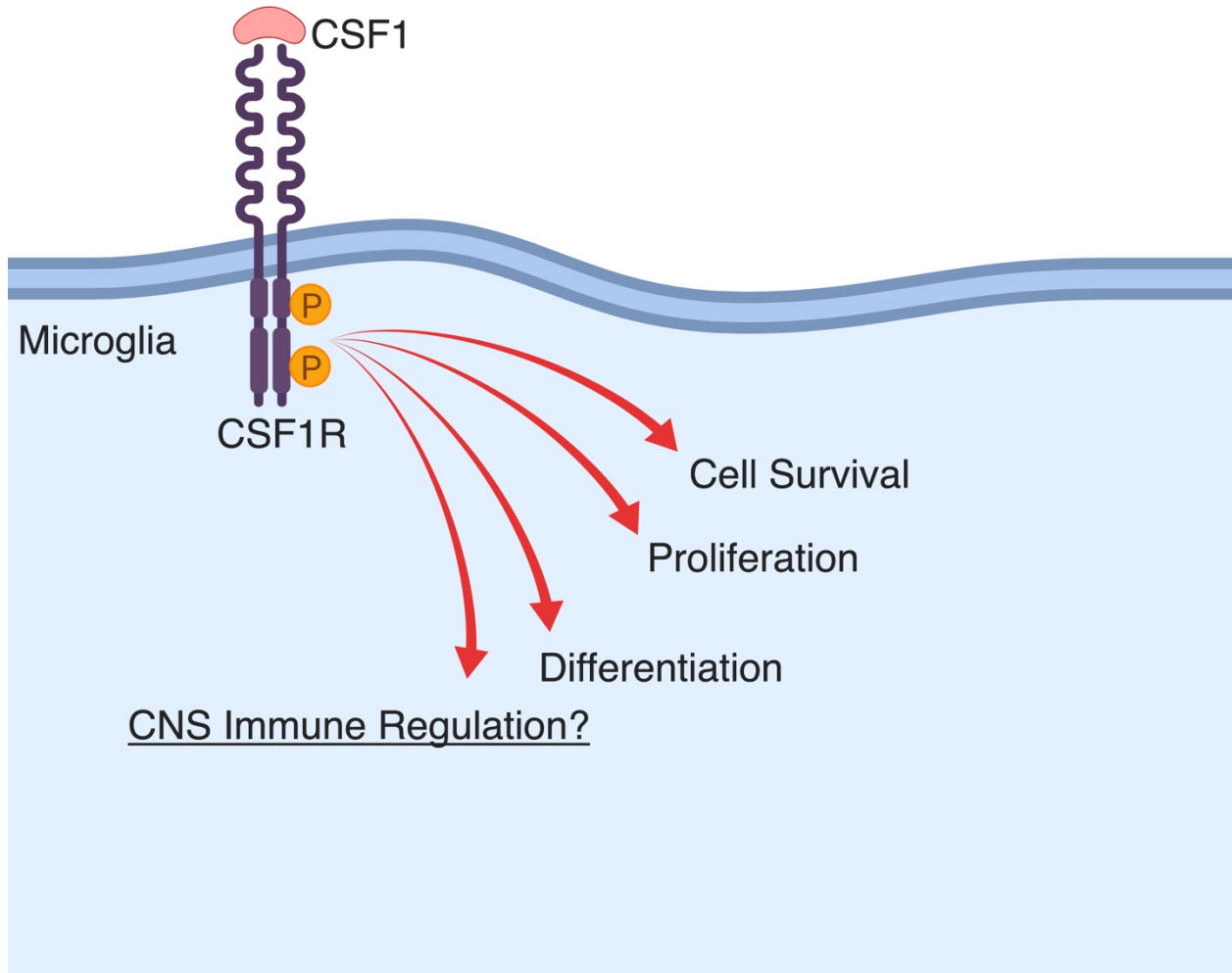
**Figure 1-2. CSF1R signaling in microglia.** After the binding of one of its ligands (CSF1 pictured), CSF1R undergoes autophosphorylation. This signaling results in cell survival, proliferation, and differentiation. We hypothesize that CSF1R signaling may also impact CNS immune regulation. Figure made with BioRender.
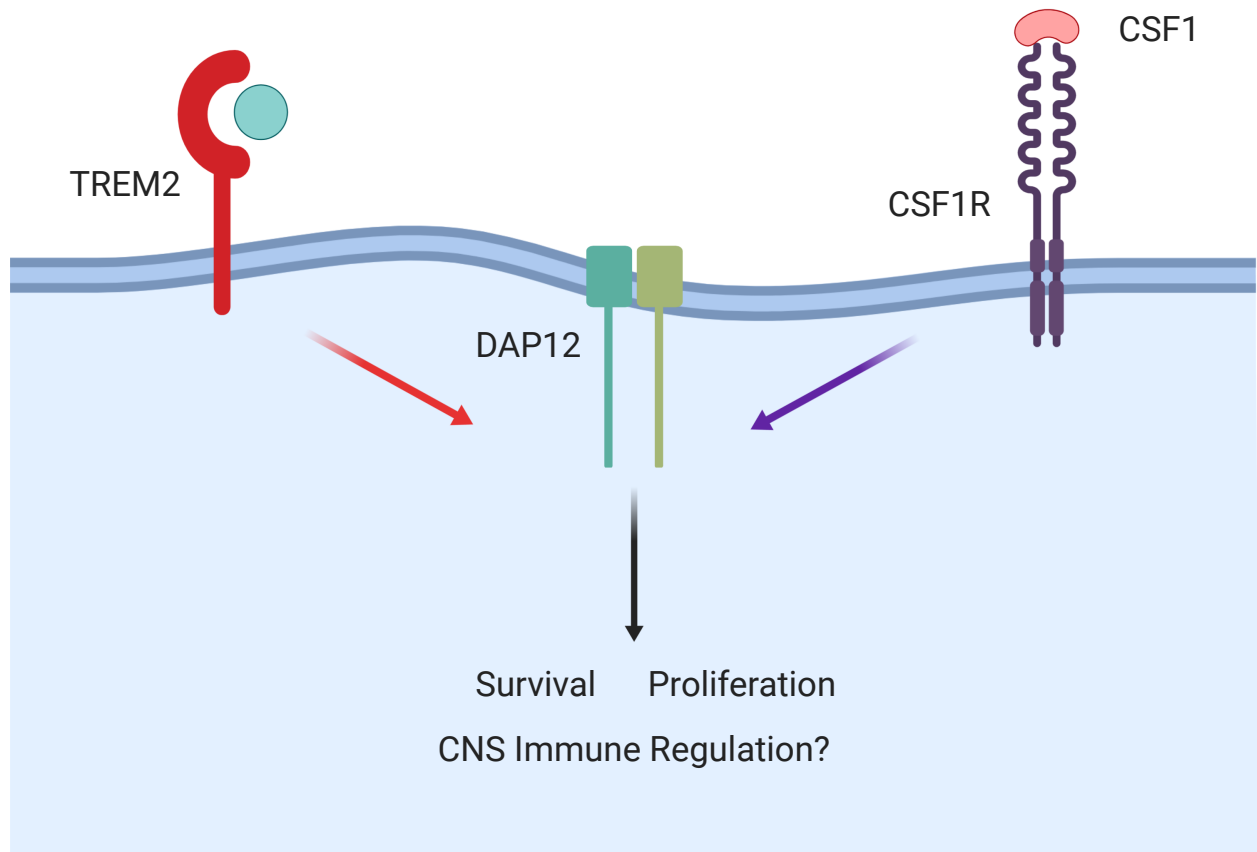
**Figure 1-3. TREM2 and CSF1R signaling interact via DAP12 in microglia.** TREM2 and

CSF1R signaling intersect at the signal transduction receptor DNAX-activating protein of 12

kDa (DAP12). Consequently, there is significant overlap between the downstream signaling

effects of TREM2 and CSF1R including microglial survival and proliferation. We

hypothesized that TREM2 and CSF1R signaling would also affect CNS immune regulation

in the context of SIV infection. Figure made with BioRender.
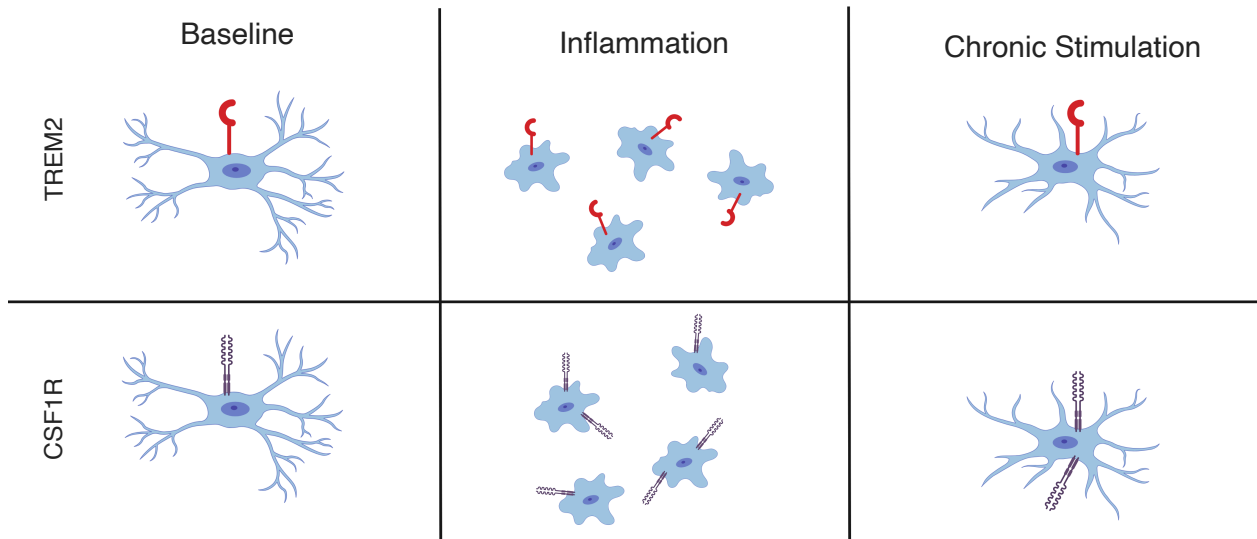
**Figure 1-4. Summary of the effect of chronic immune stimulation on TREM2 and CSF1R during SIV infection.** TREM2 and CSF1R protein increases with inflammation and microgliosis. With chronic immune stimulation, where microglial number returns to baseline, TREM2 protein levels return to baseline. However, CSF1R protein levels remain elevated even with suppressive ART. Figure made with BioRender.

**CHAPTER II.**

**Increased Microglial CSF1R Expression in the SIV/Macaque Model of HIV CNS**

**Disease**

This chapter has been accepted for publication in the *Journal of Neuropathology and Experimental Neurology*

**Abstract**

Chronic microglial activation and associated neuroinflammation are key factors in neurodegenerative diseases including HIV-associated neurocognitive disorders. Colony stimulating factor 1 receptor (CSF1R)-mediated signaling is constitutive in cells of the myeloid lineage, including microglia, promoting cell survival, proliferation, and differentiation. In amyotrophic lateral sclerosis and Alzheimer's disease, CSF1R is upregulated. Inhibiting CSF1R signaling in animal models of these diseases improved disease outcomes. In our studies, CNS expression of the CSF1R ligand, colony stimulating factor 1 (CSF1) was significantly increased in an SIV/macaque model of HIV CNS disease. Using a Nanostring nCounter immune panel, we found *CSF1* overexpression was strongly correlated with upregulation of microglial genes involved in antiviral and oxidative stress responses. Using *in situ* hybridization, we found that *CSF1R* mRNA was only present in IBA1 positive microglia. By ELISA and immunostaining with image analysis, SIV-infected macaques had significantly higher CSF1R levels in frontal cortex than uninfected macaques (P = 0.018 and P = 0.02, respectively). SIV-infected macaques treated with suppressive ART also had persistently elevated CSF1R similar to untreated SIV-infected macaques. Coordinate upregulation of CSF1 and CSF1R expression implicates this signaling pathway in progressive HIV CNS disease.

**Introduction**

Microglia, comprising parenchymal microglia and perivascular macrophages in the CNS, play a central role in multiple chronic neurodegenerative diseases including Alzheimer's disease (AD), amyotrophic lateral sclerosis (ALS), and HIV-Associated Neurocognitive Disorder (HAND) (Lall and Baloh 2017; Ransohoff and El Khoury 2015; Saylor et al. 2016; Williams et al. 2014). In these diseases, immune activation of microglia may be pivotal in regulating neuroinflammation, a process likely dependent on disease stage (Dheen, Kaur, and Ling 2007).

Knockout and inhibition studies in rodent models have shown that colony stimulating factor 1 receptor (CSF1R) signaling is essential for microglial survival, proliferation, and differentiation (Elmore et al. 2014; Erblich et al. 2011; Sherr 1990; Stanley and Chitu 2014). Upregulation of CSF1R by microglia has been identified in AD, ALS, and other neuroinflammatory diseases including prion diseases (Akiyama et al. 1994; Gomez-Nicola et al. 2013; Mitrasinovic and Murphy 2003). Of particular note, CSF1R blockade improved disease outcomes in mouse models of late-stage AD and ALS (Dagher et al. 2015; Martinez-Muriana et al. 2015), demonstrating that microglial immune responses can be either beneficial or harmful depending on context.

CSF1R has two known ligands: colony stimulating factor 1 (CSF1) and IL34. Both ligands are expressed in the CNS, but IL34 appears to be more essential to homeostatic regulation in specific areas of the brain, including the cerebral cortex, basal ganglia, and hippocampus (Zelante and Ricciardi-Castagnoli 2012). Interestingly, previous work suggests that CSF1 is more inducible than IL34 in neurodegenerative diseases (Martinez-Muriana et

al. 2016; Gerngross and Fischer 2015) and therefore may be the more important CSF1R ligand in chronic neurodegeneration (De et al. 2014).

Persistent CNS inflammation including microglial immune activation is thought to drive the pathogenesis of HAND (Saylor et al. 2016; Spudich 2016). HIV can infect cells of the myeloid lineage, including microglia, thereby stimulating or dysregulating the neuroimmune response in HAND (Saylor et al. 2016; Williams et al. 2014). Previous work in a rhesus macaque SIVmac251 model of HIV CNS infection has shown that increased CSF1 expression occurs in CD163+ cells (Gerngross et al. 2015), cells that accumulate in perivascular cuffs and microglial nodules in SIV encephalitis (Gerngross and Fischer 2015).

In this report, we show that *CSF1* expression increased in the SIV/pigtailed macaque model of HIV CNS disease whereas *IL34* expression did not change with SIV infection. CSF1 overexpression was significantly correlated with microglial genes involved in the anti-viral response to SIV, and in response to oxidative stress. In addition to upregulation of the ligand CSF1, CSF1R expression in microglia also increased with infection, implicating the CSF1-CSF1R signaling pathway in HIV CNS disease.

**Materials and Methods**

<u>Animals</u>

      All experiments were performed on samples collected at necropsy from male juvenile pigtailed macaques (*Macaca nemestrina*). Samples were stored at -80°C prior to use. Animals were either (1) mock inoculated with Lactated Ringers Solution (LRS), (2) inoculated intravenously with the neurovirulent molecular clone SIV/17E-Fr and the immunosuppressive swarm SIV/DeltaB670 (SIV), or (3) SIV inoculated and treated with an ART regimen (SIV + ART) (Beck, Kelly et al. 2015; Beck et al. 2017; Beck, Queen et al. 2015). Untreated SIV-infected animals were euthanized at 21 days post-infection (p.i.), or 84 days p.i. unless the animal began showing symptoms of AIDS before the end point of the respective study. SIV-infected animals that were treated with ART (n=7) were fully suppressed in CSF and plasma by 56 days p.i., and were euthanized 180 days p.i., after approximately 120 days of ART suppression. SIV+ART animals were treated daily with a subcutaneous injection of 2.5 mg/kg Dolutegravir (ViiV Healthcare US, Raleigh, NC), 20 mg/kg PMPA, and 40 mg/kg FTC (Gilead, Foster City, CA). Four of the seven treated animals were also given 20 mg of oral Maraviroc (ViiV Healthcare US, Raleigh, NC) daily. This difference in treatment regimen did not cause a significant difference in time to suppression in either CSF or plasma; there was also no significant difference in the CNS-specific measures performed for this study. As this study was conducted retrospectively, all samples were not available for each animal, hence minor variation in animal group size in different experiments.

      At necropsy, all animals were perfused with phosphate-buffered saline. Brains were harvested and sectioned coronally at necropsy. All samples were either immersion fixed in

10% neutral buffered formalin (NBF), Streck tissue fixative (STF), or flash-frozen. Both basal ganglia and frontal cortex sections were utilized in this study. All animal studies were approved by the Johns Hopkins Animal Care and Use Committee.


RNA measurements

The Nanostring nCounter gene expression panel used for analysis included 249 genes of interest (Meulendyke et al. 2014). The geometric means of four housekeeping genes were used to normalize counts. mRNA counts of genes of interest were then normalized to the geometric mean of the four housekeeping genes (*GAPDH, RPL13A, SDHA*, and *TBP*), as well as the geometric mean of spike-in controls. The limit of detection was determined by taking the mean of three negative controls plus two standard deviations as detailed previously (Meulendyke et al. 2014). RNA for this panel was isolated from basal ganglia sections harvested at necropsy from uninfected and SIV-infected (84 days p.i.) macaques as described previously (Meulendyke et al. 2014). 100ng of RNA was used for input. 100ng of MS2 phage RNA (Roche, Basel, Switzerland) run in triplicate served as a negative control.

For quantitative RT-PCR, RNA was isolated from grey and white matter frontal cortex flash frozen at -80°C. Tissue was placed in Fast RNA tubes with lysing matrix D (MP Bio, Solon, OH) and RNA STAT-60. Each tube was homogenized for 30 seconds using the Fast Prep-24 homogenizer (MP Bio, Solon, OH). Tubes were then incubated at room temperature for 5 minutes. 200µL of chloroform was added. Tubes were then shaken for 15 seconds and incubated at room temperature for three minutes. Samples were then centrifuged at 14,000 rpm for 15 minutes at 4°C. The aqueous portion was then added to a fresh tube with 500µL of ice-cold 2-isopropanol and vortexed. After an overnight incubation at -20°C,

tubes were centrifuged at 14,000 rpm for 15 minutes at 4°C and the isopropanol was

removed. The pellet was then washed in ice-cold 70% ethanol. Tubes were centrifuged at

10,000 rpm for 5 minutes at 4°C and the ethanol was removed. The pellet was then allowed

to air dry for approximately 15 minutes at room temperature. RNA isolation was completed

using the Qiagen RNeasy kit (Qiagen, Frederick, MD) according to the manufacturer's

protocol. Quality and concentration of the isolated RNA was determined using Nanodrop.

One microgram of RNA was added to each RT reaction. The High Capacity cDNA

reverse transcription kit was used (Applied Biosystems, Carlsbad, CA) with samples run in

duplicate with a no reverse transcriptase control for each as well as no template controls.

Reverse transcription was performed with the PTC-200 (MJ Research, Port Republic, NJ).

The samples were held at 25°C for 10 minutes to anneal, then 37°C for 120 minutes for

reverse transcription, and finally 85°C for 5 minutes to inactivate the reverse transcriptase.

Samples were held at 4°C overnight before being stored at -20°C.  4μL of cDNA was used

for qPCR per sample. Each was run in duplicate with no template controls and no reverse

transcriptase controls. The TaqMan ® Universal Master Mix II or the Gene Expression

Master Mix was used (Applied Biosystems, Carlsbad, CA) with CSF1 (cat.

Rh02621778_m1) and IL34 (cat. Rh01050928_m1) probes (Biosystems, Carlsbad, CA); all

counts were normalized to 18S ribosomal RNA and reported as $\Delta\Delta Ct$ (cycle threshold).

CSF1R cellular localization and measurements

*CSF1R* RNA was visualized in cells by *in situ* hybridization. Combined CSF1R

ISH—Iba-1 IHC double-staining was performed on frontal cortex using the Leica Bond RX

automated system (Leica Biosystems, Richmond, IL). Tissue was fixed in 10% NBF for 24

hours and embedded in paraffin before sectioning at 5 μM. A CSF1R probe (cat. 310818, Advanced Cell Diagnostics, Newark, NJ) was used with the RNAScope® 2.5 LS Assay-RED Kit according to manufacturer's protocol. Epitope retrieval was performed by heating to 95°C for 20 minutes in EDTA-based ER2 buffer (Leica Biosystems, Richmond, IL). Anti-Iba-1 antibody (cat. 019-19741, Wako, Richmond, VA) was diluted 1:500. Slides were counterstained with hematoxylin.

CSF1R IHC was performed using indirect, alkaline phosphatase-based immunostaining on STF fixed frontal cortex sections using the Bond RX automated system with the Bond Polymer Refine Red kit (Leica Biosystems, Richmond, IL). Each slide was heated to 95°C for 20 minutes in EDTA-based ER2 buffer for heat-induced epitope retrieval. Anti-CSF1R (Santa Cruz Technologies, cat. sc-692, Santa Cruz, CA) was used as the primary antibody (1:50 dilution). Positive immunoreactivity was visualized by labeling with the Bond Polymer Refine Red kit (alkaline phosphatase) (Leica Biosystems, Richmond, IL). Slides were counterstained with hematoxylin. Image acquisition and analysis to measure CSF1R was performed with Nikon Elements software (Nikon, Melville, NY) by generating composite images composed of 3X12 200X high power fields encompassing both grey and white matter. A threshold for positive staining was established using a set of blinded images and applied to all images to calculate the area fraction (%ROI) representing positive staining. Regions of interest (ROIs) were drawn around grey and white matter separately. The median size of the areas analyzed for grey and white matter were $2.6 \times 10^6$ μm$^2$ and $8.6 \times 10^5$ μm$^2$ respectively.

CSF1R ELISAs were performed on frontal cortex homogenates prepared from 50 mg of tissue placed in 200μL of 1X cell lysis buffer (Cell Signaling and Technologies, Danvers,

MA) with added protease and phosphatase inhibitors (Roche, Basel, Switzerland) and homogenized with a hand-held homogenizer. 300μL of 1X cell lysis buffer was then added for a total of 500μL. Samples were then sonicated using a cup sonicator five times for 20 seconds with 15 second breaks. Tubes were then rotated at 4°C for two hours and pelleted at 4°C for 5 minutes at 14K rpm. Supernatant was collected and used. Protein concentrations of these homogenates were determined using the Qubit™ protein assay kit according to manufacturer's protocol (Invitrogen, Carlsbad, CA). These concentrations were validated by running 5μg of protein of each sample on a Criterion Stain Free™ Tris-HCL 4-20% separation gel and read using the Gel Doc EZ Imager™ (Bio Rad, Hercules, CA). The Biomatik Human MCSFR ELISA kit (Biomatik, Wilmington, DE) was used per manufacturer's protocol. 30μg of protein from each sample were added in duplicate to antibody pre-coated wells. TMB solution was allowed to develop for 15 minutes at room temperature. Wells were read at 450nm immediately after the addition of stop solution.

Statistical Analysis

Prism was used to calculate all statistics except the Benjamini-Hochberg correction, which was applied using the p.adjust function in R. The Benjamini-Hochberg false discovery rate was set to 0.05. Non-parametric statistical tests were used (Mann-Whitney and Spearman correlation). Statistical significance was attributed to P values less than or equal to 0.05.

**Results**

*CSF1 expression increased in SIV-infected pigtailed macaques.*

Alterations in expression of both CSF1R ligands CSF1 and IL34 have been reported *in vivo* in an SIVmac251/rhesus macaque model and with HIV infection *in vitro* (Gerngross and Fischer 2015; De et al. 2014; Gruber et al. 1995; Kalter et al. 1991). To evaluate *CSF1* expression in the SIV/pigtailed macaque model of HIV CNS disease, we analyzed a Nanostring nCounter dataset including 123 genes above the limit of detection (**Supplemental Table 1**) obtained using RNA isolated from basal ganglia from SIV-infected macaques sacrificed 21 days p.i. (n = 6) or 84 days p.i. (n = 13). Uninfected pigtailed macaques (n = 10) served as controls (Meulendyke et al. 2014). *CSF1* mRNA levels were significantly increased in SIV-infected pigtailed macaques at 84 days p.i. compared to uninfected controls (P = 0.003, Mann-Whitney, **Figure 1**). To determine whether development of SIV encephalitis was related to *CSF1* expression levels, the 84 day p.i. SIV-infected group was subdivided into SIV-infected animals with (n = 8) or without SIV encephalitis (n = 5). *CSF1* mRNA expression was significantly increased in the animals with SIV encephalitis versus those without encephalitis (P = 0.002, Mann-Whitney, **Figure 1**).

To determine whether *CSF1* expression was altered during the asymptomatic phase of infection, *CSF1* mRNA counts in basal ganglia of SIV-infected pigtails euthanized at 21 days p.i. were compared with uninfected and 84 day groups. The asymptomatic SIV group had higher *CSF1* expression than uninfected controls (P = 0.09, Mann-Whitney; median = 196.5 mRNA copies) comparable to the terminal SIV-infected animals without encephalitis sacrificed at 84 days p.i. (median = 122 mRNA copies). This intermediary level of *CSF1*

expression suggests that *CSF1* alterations develop early in the course of disease; analysis of larger groups is needed to confirm this finding.

Further analysis of the Nanostring nCounter dataset revealed differential expression of 44 additional genes in the basal ganglia of SIV-infected pigtailed macaques sacrificed 84 days p.i. (n =13) compared to uninfected controls (n = 10). Fold change in expression was calculated by dividing the median expression of the SIV 84 day p.i. mRNA counts by that of the uninfected controls. In cases of downregulation, the value of uninfected median counts divided by the SIV-infected counts was a negative number. Statistical significance was calculated by Mann-Whitney with a Benjamini-Hochberg adjustment (P ≤ 0.05). If any gene had mRNA counts below the limit of detection, their values were set at the limit of detection for use in Mann-Whitney tests. These values were also used to identify strength of correlations between differentially expressed genes and *CSF1* RNA levels. 29 of the 45 genes found to be differentially expressed with SIV were highly correlated with *CSF1* mRNA expression levels. A subset of these genes grouped functionally is represented in **Table 1**; the complete list of genes above the limit of detection is listed in **Supplemental Table 1**. Correlation was determined using Spearman's rank analysis with a Benjamini-Hochberg adjustment (P ≤ 0.05). *CSF1* mRNA levels were significantly positively correlated with genes involved in receptor tyrosine kinase signaling, including *STAT3*. As CSF1R is the only known receptor of CSF1, the correlation between *CSF1* RNA with RTK genes indicates that increased CSF1 promotes CSF1R signaling. *CSF1* expression was also positively correlated with microglial markers. Of particular interest, *CD163* and *CD68* expression on microglia have been associated with immune activation and phagocytosis (Sasaki 2017). *CSF1* mRNA levels were also strongly correlated with *ALOX5AP*, a microglial protein essential in the

production of leukotrienes that serves as a positive regulator of inflammation. As such, *ALOX5AP* activity has been shown to increase neuronal damage *in vitro* (Klergeris and McGeer 2003). These correlations taken together suggest a regulatory relationship between CSF1R signaling and regulation of microglial immune responses in SIV infection.

Given these correlations between *CSF1* and microglial immune activation, the finding that *CSF1* mRNA expression also highly correlated with genes essential in immune signaling, particularly those involved in the anti-viral response such as *CCL2* and *Mx1*, was also consistent with a pro-inflammatory environment in the CNS. Correlations with *CSF1* also extended to genes associated with oxidative stress including *SOD2*, further supporting a relationship between CSF1R signaling and a functional immune response in the CNS.


*CSF1 and IL34 mRNA expression in SIV-infected pigtailed macaque frontal cortex.*

To validate the finding of increased *CSF1* expression from the Nanostring nCounter analyses and to expand measurements to include both CSF1R ligands in grey and white matter, qRT-PCR was performed to quantify *CSF1* and *IL34* expression using samples from frontal cortex (**Figure 2**). *CSF1* expression was increased in both grey and white matter frontal cortex samples (**Figure 2, upper row**). In contrast, *IL34*, did not change with SIV infection in either grey or white matter (**Figure 2 , lower row**). This ligand-specific difference has been reported in multiple CNS inflammation models (Martinez-Muriana et al. 2016; Gerngross and Fischer 2015) and implies that *CSF1* is selectively induced during chronic neuroinflammation whereas *IL34* expression is not altered.

*CSF1R expression is increased in frontal cortex white matter of SIV-infected pigtailed macaques.*

Given upregulation of CNS *CSF1* in our SIV/macaque model of HIV CNS disease, we next evaluated the CSF1 receptor, CSF1R, in the CNS. To identify the cell populations expressing CSF1R, *in situ* hybridization to detect *CSF1R* RNA was performed on macaque brain sections (**Figure 3**). *CSF1R* mRNA was present in both Iba-1 positive perivascular macrophages and parenchymal microglia (**Figure 3B, C**). *CSF1R*-IBA1 double-positive cells were distributed across both grey and white matter, including perivascular and subpial locales, suggesting that both resident and infiltrating myeloid cells express *CSF1R*. Of particular interest, highest numbers of *CSF1R*-IBA1 double-positive cells were present in perivascular cuffs and microglial nodules.

As upregulated CSF1R protein expression has been associated with several neuroinflammatory conditions, we visualized CSF1R protein using immunohistochemical staining. CSF1R immunostaining was markedly upregulated in white matter compared to uninfected controls (**Figure 4A, B**). This increase was most pronounced within perivascular cuffs composed of macrophages that are characteristic of SIV encephalitis (**Figure 4B inset**). Increased CSF1R staining was associated with a change in microglial morphology. In the SIV and SIV + ART groups, microglia were larger with broad processes as compared to uninfected animals (**Figure 4B, C**). CSF1R immunostaining was significantly increased in white matter of SIV-infected macaques compared to uninfected animals (P = 0.02, Mann-Whitney; median %ROI positive for CSF1R in SIV = 0.87 (n= 8 animals) versus 0.50 in uninfected macaques (n=7 animals)). CSF1R immunostaining was also increased in grey matter of SIV-infected macaques compared to uninfected animals (P = 0.054, Mann-

Whitney; median %ROI positive for CSF1R in SIV = 0.99 versus 0.53 in uninfected macaques).  In previous studies, changes in the white matter have been the most predictive of HAND development in HIV-infected patients (Cardenas et al. 2009). This further suggests a role for CSF1R expression and its signaling in the pathogenesis of neurologic disease in SIV infection.

Immunostaining results for CSF1R expression were confirmed by performing ELISA measurements on frontal cortex white matter homogenates. CSF1R protein levels were significantly increased in SIV-infected pigtailed macaques compared to uninfected macaques (P = 0.018, Mann-Whitney, **Figure 5**). Additionally, there was no difference in CSF1R protein levels between the SIV and the SIV + ART groups (P > 0.999, Mann-Whitney). Collectively, these data demonstrate that CNS CSF1R expression by microglia is upregulated in SIV-infected macaques corresponding with increases in its ligand CSF1.

**Discussion**

In this study based in the SIV/pigtailed macaque model of HIV CNS disease, we found that CSF1 expression is significantly increased in the CNS in both grey and white matter with SIV infection. This increase was most pronounced in SIV-infected animals that developed SIV encephalitis. CSF1 mRNA levels in the brain were strongly correlated with upregulation of immune activation and oxidative stress genes. The increase in CSF1 expression in our pigtailed macaque model of HIV CNS disease is in contrast to the work done in the rhesus macaque model of HIV CNS disease where a decrease in *CSF1* expression was observed (Gerngross and Fischer 2015).

Interestingly, although IL34, the other ligand that binds CSF1R, is primarily expressed in the CNS (Zelante and Ricciardi-Castagnoli 2012), IL34 mRNA expression did not change with SIV infection. Similarly, a lack of a change in IL34 expression has been shown in other models of neurodegenerative diseases including SIV infection of rhesus macaques (Martinez-Muriana et al. 2016; Gerngross and Fisher 2015). Other groups have also noted that high concentrations of IL34 in media promotes ramified microglial morphology *in vitro,* suggesting that IL34 promotes a resting state (Muffat et al. 2016). Together, these findings suggest that induction of CSF1 rather than IL34 is the key driver of increased CSF1R signaling during neuroinflammatory processes including HIV-induced CNS inflammation. This is further supported by the strong correlation between CSF1 and receptor tyrosine kinase signaling in the SIV/pigtailed macaque model.

Both CSF1 and IL34 have been evaluated in a SIV rhesus macaque model, but CSF1R has not been examined in detail. CSF1R is expressed by microglia, including parenchymal microglia and perivascular macrophages (Elmore et al. 2014; Sherr 1990;

Stanley and Chitu 2014). Like the ligand CSF1, CSF1R protein levels were significantly

increased in the CNS of SIV-infected pigtailed macaques. Surprisingly, CSF1R expression

by microglia also remained elevated in ART-treated SIV-infected pigtailed macaques despite

sustained suppressive therapy. The significant increase in CSF1R expression shown by both

CSF1R ELISA and digital image analysis of CSF1R immunostaining may represent

sustained microglial immune activation, increased trophic demand from stressed microglia,

or a combination of these. Together, these findings suggest that CSF1 and CSF1R may also

remain upregulated in the CNS of HIV-infected patients treated with ART and could

contribute to the sustained CNS inflammation suspected to underpin HAND.

Although it has been suggested that CSF1R is an M2 marker (Ohashi et al. 2017), the

M1/M2 polarization paradigm may not be applicable to microglia (Ransohoff 2016). As

*CSF1* expression correlates with both M1 and M2 markers, notably CD14 and CD68

respectively, as well as genes associated with driving M1 and M2 polarization (Martinez and

Gordon 2014), it follows that CSF1R is not representative of either M1 or M2

immunophenotypes. This activation axis is a fluid spectrum, and it is likely that any given

microglial cell can behave in an equally fluid manner in response to insult. It is possible that

CSF1R signaling plays an anti-inflammatory role, in which case coordinate upregulation of

CSF1 and its receptor, CSF1R, could represent a CNS response to mitigate the strong pro-

inflammatory response to SIV. An alternate possibility is that CSF1R signaling indirectly

promotes the pro-inflammatory environment by increasing the survival and proliferation of

microglia. In light of studies showing damage by removing CSF1R-expressing microglia at

the beginning of disease progression (Jin et al. 2017) and others showing the opposite effect

later on in disease (Elmore et al. 2014; Dagher et al. 2015; Martinez-Muriana et al. 2016), it

is possible that CSF1R signaling may be protective at the initiation of disease, but becomes damaging with persistent sustained immune stimulation.

Evidence of a relationship between CSF1R over-expression, increased signaling through CSF1R, and the pathogenesis of neurodegenerative diseases such as Alzheimer's Disease and amyotrophic lateral sclerosis in mouse models (Elmore et al. 2014; Dagher et al. 2015; Martinez-Muriana et al. 2016) suggests that this CSF1R immunoregulatory role extends beyond HIV to chronic CNS immune activation in general. However, considering the strong correlations between CSF1 expression and the genes associated with the anti-viral response in particular, upregulation of CSF1R in SIV-infected macaques may also be linked to SIV replication within the CNS. Whether upregulation of CSF1R represents a direct immune response to virus, an enhanced demand for trophic support by damaged microglia, or a combination of these remains to be determined.

Given these findings and our study results, inhibiting CSF1R signaling may prove to be an effective therapy for chronic inflammation in the CNS, such as that seen in HAND. Future studies testing the ability of CSF1 receptor blockade to deplete microglia in SIV-infected macaques receiving suppressive ART will enable us to determine whether microglia depletion alters persistent immune activation present in SIV-infected macaques receiving ART to model HIV CNS disease. Moreover, CSF1R blockade to target and selectively deplete brain macrophage populations harboring latent, replication competent HIV will be a novel approach to decrease or eradicate HIV CNS reservoirs.

**Acknowledgments**

**Table 2-1**

| | Gene | Uninfected vs SIV mRNA Counts | | | Correlation with CSF1 mRNA | |
|---|---|---|---|---|---|---|
| | | Fold Change | SEM | P value | Spearman R | P Value |
| RTK Signaling | STAT1 | 7.9 | U: 20.49 S: 468.6 | 0.002 | 0.60 | 0.051 |
| | STAT3 | 2.1 | U: 24.88 S: 110.4 | 0.05 | 0.96 | 0.002 |
| | STAT5a | 2.1 | U: 7.42 S: 19.36 | 0.01 | 0.82 | 0.005 |
| | TYK2 | 1.3 | U: 8.67 S: 20.24 | 0.04 | 0.63 | 0.04 |
| Mφ/Microglia | CD14 | 4.2 | U: 10.64 S: 82.75 | 0.002 | 0.87 | 0.003 |
| | CD16* | 6.9 | U: 0.70 S: 13.49 | *0.002 | 0.71 | 0.016 |
| | CD68* | 9.0 | U: 4.05 S: 82.22 | *0.009 | 0.80 | 0.006 |
| | CD163 | 13.8 | U: 8.80 S: 316 | 0.004 | 0.72 | 0.01 |
| | ALOX5AP | 3.1 | U: 11.78 S: 85.05 | 0.009 | 0.75 | 0.01 |
| Immune Activation | CCL2 | 50.6 | U: 2.78 S: 288.3 | 0.002 | 0.84 | 0.004 |
| | IRF1 | 17.7 | U: 3.33 S: 137.3 | 0.002 | 0.92 | 0.02 |
| | IRF3 | 1.2 | U: 41.34 S: 47.8 | 0.04 | 0.72 | 0.02 |
| | MX1 | 48.9 | U: 42.88 S: 1957 | 0.002 | 0.74 | 0.01 |
| Oxidative Stress | SOD2 | 7.2 | U: 112.2 S: 5744 | 0.009 | 0.91 | 0.002 |
| | GPX1 | 2.2 | U: 104.4 S: 191.3 | 0.006 | 0.74 | 0.005 |
| | GSTZ1 | 1.4 | U: 12.59 S: 12.16 | 0.054 | 0.82 | 0.004 |

**Table 2-1. With SIV infection, a subset of genes expressed in the brain was significantly correlated with CSF1 mRNA counts.** Uninfected versus SIV P values were calculated using normalized mRNA counts (Mann-Whitney). Correlations were calculated only using SIV mRNA counts. All P values were adjusted using Benjamini-Hochberg correction. *Values below the limit of detection were set at the limit of detection to calculate the conservative P value.
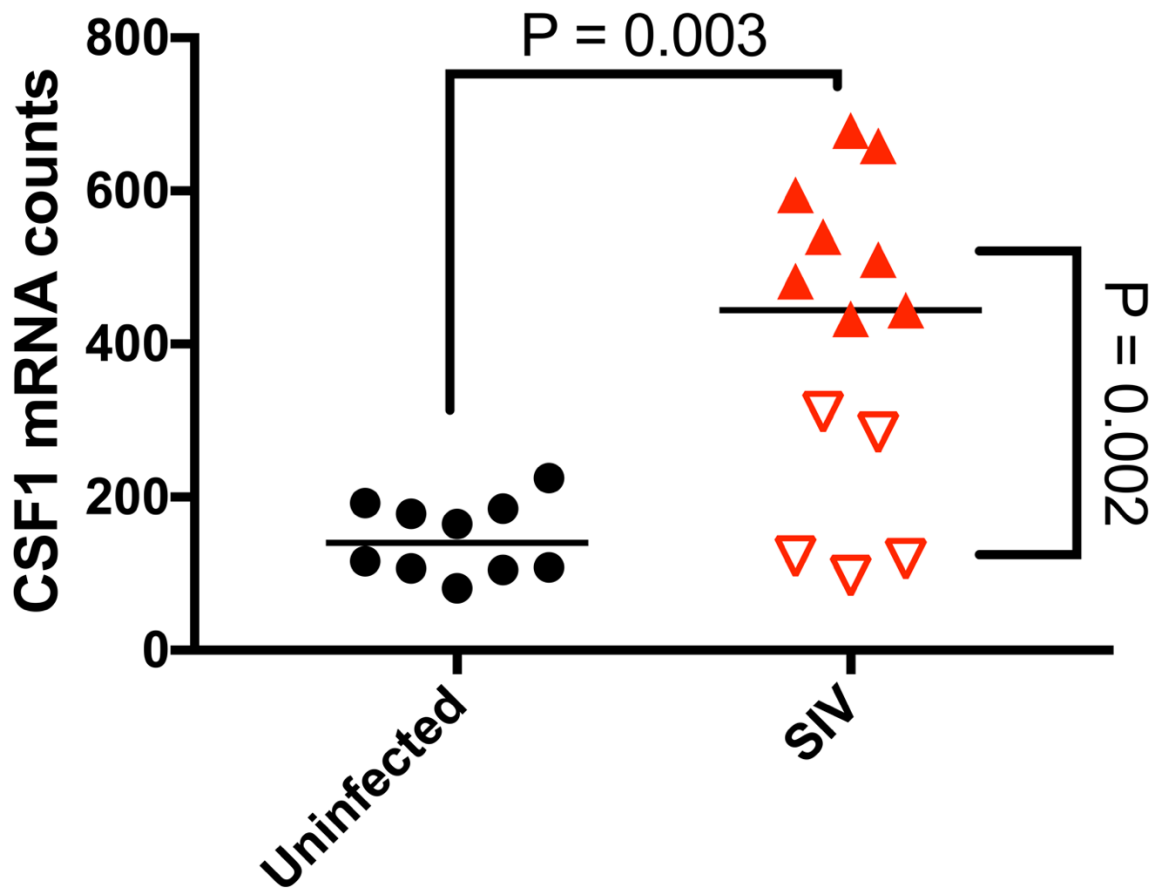
**Figure 2-1. Nanostring analysis of CSF1 mRNA expression in SIV-infected pigtailed macaques.** CSF1 mRNA counts in basal ganglia of SIV-infected macaques were significantly increased versus uninfected animals. CSF mRNA expression was also significantly higher in animals with SIV encephalitis compared to SIV-infected animals without encephalitis (encephalitis = ▲; no encephalitis = ▽).
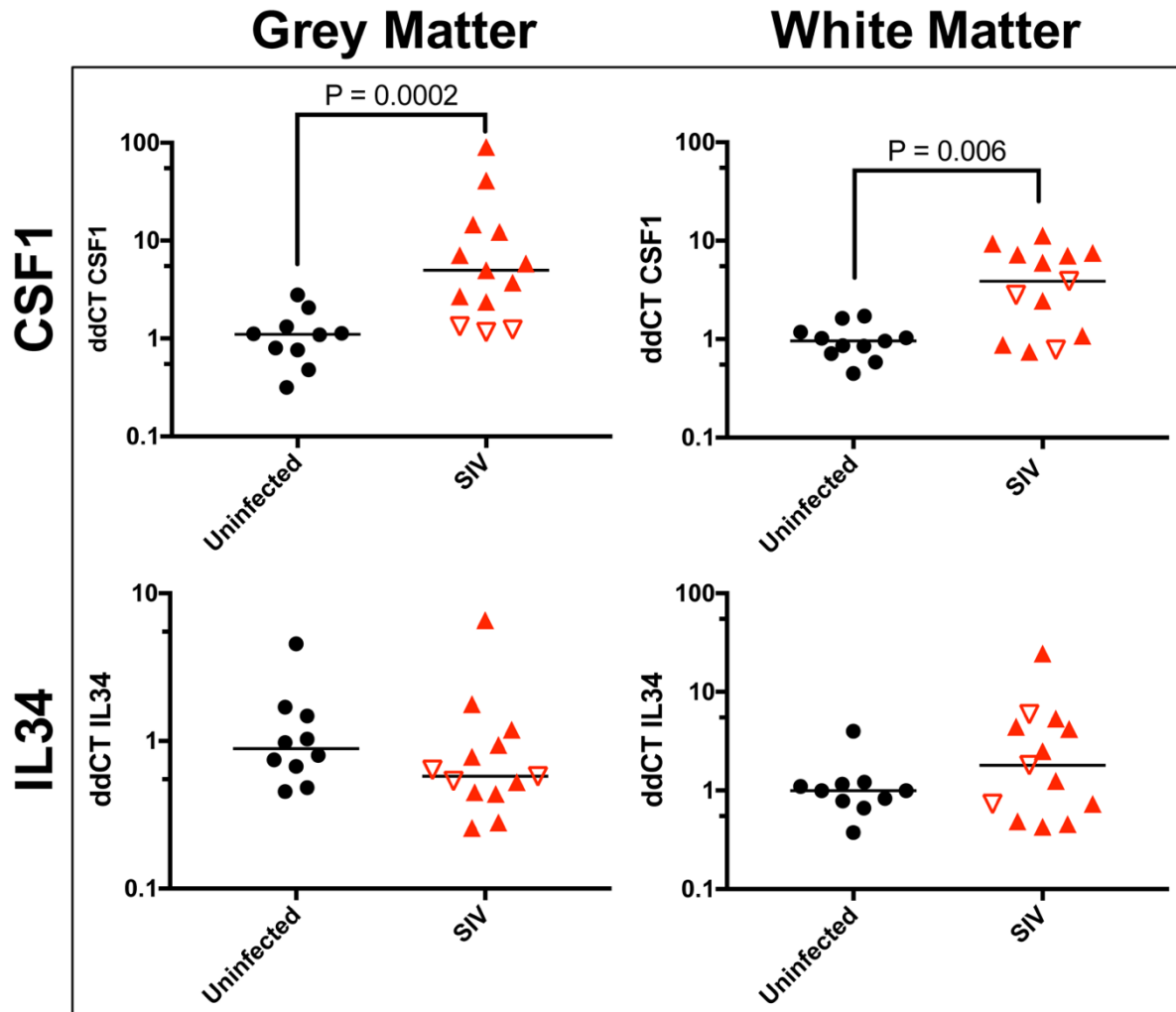
**Figure 2-2. CSF1 mRNA significantly increased with SIV infection.** CSF1 mRNA expression measured by qRT-PCR significantly increased in SIV-infected macaques (frontal cortex) compared to uninfected animals in both grey and white matter (top row). In contrast, there was no significant difference in IL34 expression in either grey or white matter. (No encephalitis = ▽; Encephalitis = ▲).
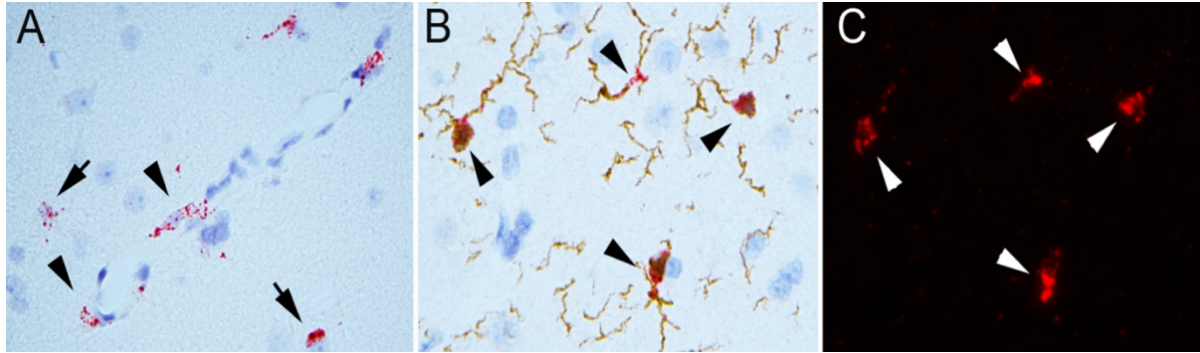
**Figure 2-3. Constitutive and induced CSF1R expression was restricted to microglia.** (A)
CSF1R ISH bright-field shows positive staining (red) in both parenchymal microglia
(arrows) and perivascular macrophages (arrowheads). (B) CSF1R RNA (red) co-localizes
with Iba1-positive microglia (brown). Double stained cells are denoted by arrowheads. (C)
Overlaid CSF1R ISH fluorescence image of (B) confirmed localization of CSF1R RNA
(arrowheads, red) specifically to microglia.
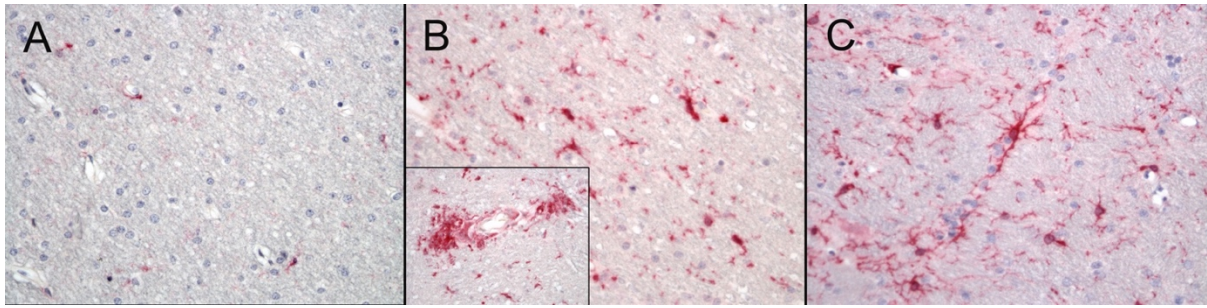
**Figure 2-4. Elevated CSF1R protein in both untreated and ART-treated SIV-infected pigtailed macaques.** (A) Constitutive CSF1R staining in the frontal cortex of an uninfected untreated macaque. Both perivascular macrophages and parenchymal microglia were positively immunostained for CSF1R (red). (B) A marked increase in CSF1R immunostaining developed with SIV infection. Inset: Perivascular cuff of macrophages with high CSF1R expression. (C) CSF1R immunostaining remained elevated in microglia in SIV-infected macaques receiving suppressive ART (frontal cortex; 400X).
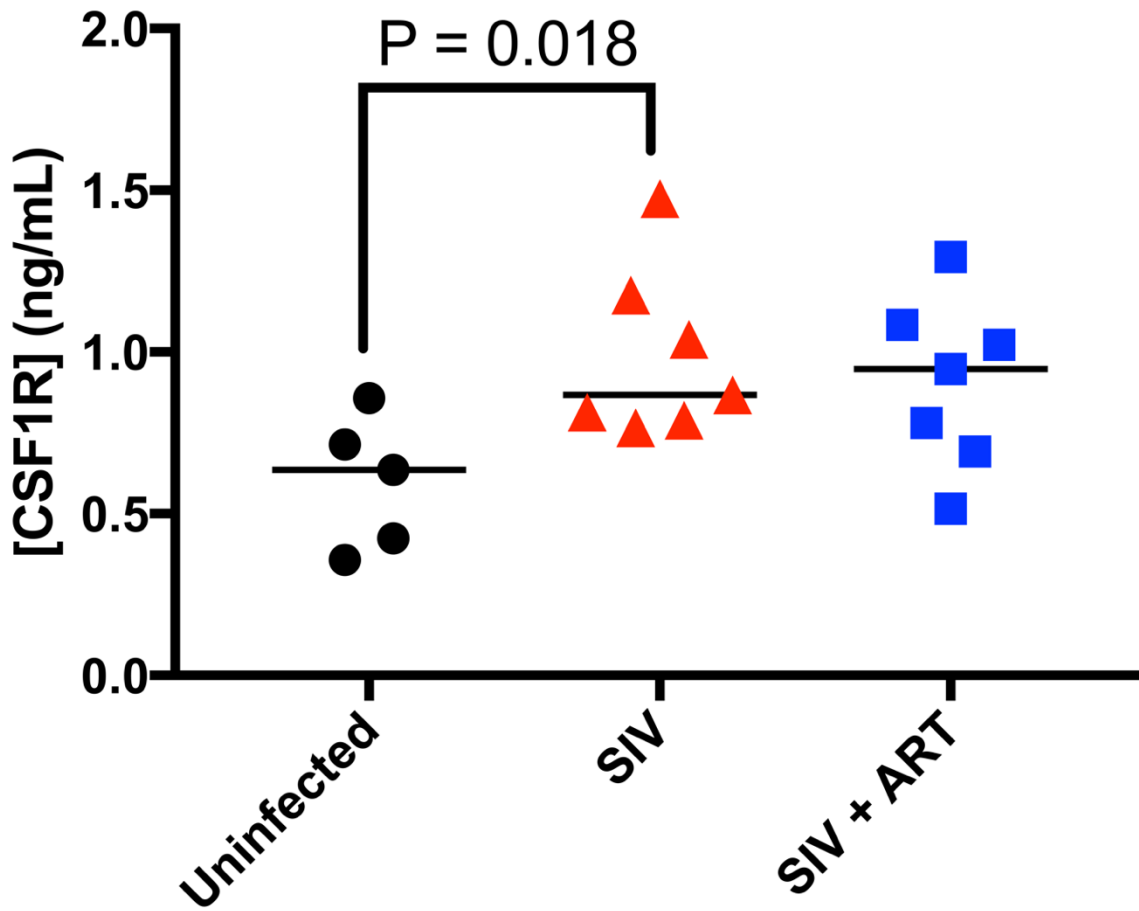
**Figure 2-5. Elevated CNS CSF1R Expression in SIV and SIV+ART.** Measurements of CSF1R protein levels in frontal cortex by ELISA showed a significant increase in CSF1R concentration in the SIV-infected group (Mann-Whitney). With suppressive ART, CSF1R levels in frontal cortex remained elevated. (Uninfected = ●; SIV encephalitis = ▲; SIV + ART = ■)

## Supplemental Table 2-1

| Gene | Fold Change | Mean & SEM | Median | Mann-Whitney p (BH) | Spearman R | Spearman p (BH) |
|---|---|---|---|---|---|---|
| | | Uninfected vs SIV mRNA counts | | | Correlation with CSF1 mRNA | |
| CSF1 | 3.16 | 146.2 +/- 15.29 | 140.5 | 0.01 | 1 | N/A* |
| | | 405.8 +/- 56.24 | 444 | | | |
| AADAT | -1.33 | 161.9 +/- 6.31 | 168.5 | 0.009 | -0.1458 | 0.662127907 |
| | | 128 +/- 6.06 | 127 | | | |
| AGER | 1.26 | 25.3 +/- 3.56 | 21.5 | 0.23 | N/A | N/A |
| | | 28.85 +/- 2.39 | 27 | | | |
| ALOX5AP | 3.06 | 148 +/- 11.78 | 134 | 0.002 | 0.75 | 0.011117647 |
| | | 477.9 +/- 85.05 | 410 | | | |
| APP | -1.27 | 11694 +/- 350.2 | 11925 | 0.002 | -0.3846 | 0.23777027 |
| | | 9110 +/- 450.3 | 9360 | | | |
| ARG2 | -1.24 | 216.7 +/- 20 | 233 | 0.45 | N/A | N/A |
| | | 189.4 +/- 14.69 | 188 | | | |
| CAMK2A | -1.11 | 3200 +/- 708.7 | 2468 | 0.29 | N/A | N/A |
| | | 2009 +/- 304.2 | 2220 | | | |
| CAMK2B | -1.18 | 1510 +/- 219.2 | 1354 | 0.43 | N/A | N/A |
| | | 1124 +/- 182.4 | 1146 | | | |
| CAMK2D | -1.09 | 742 +/- 171.9 | 568.5 | 0.68 | N/A | N/A |
| | | 519.2 +/- 72.61 | 522 | | | |
| CAMK2G | -1.70 | 1037 +/- 140.4 | 986 | 0.04 | 0.4066 | 0.211875 |
| | | 655 +/- 65.12 | 579 | | | |
| CAT | 1.47 | 246.8 +/- 24.92 | 237 | 0.2 | N/A | N/A |
| | | 335.3 +/- 36.6 | 348 | | | |
| CCBL1 | 1.07 | 204 +/- 9.6 | 199 | 0.97 | N/A | N/A |
| | | 199.5 +/- 15.54 | 213 | | | |
| CCBL2 | 1.03 | 850.3 +/- 42.66 | 861 | 0.43 | N/A | N/A |
| | | 944.5 +/- 62.28 | 888 | | | |
| CCL2 | 50.55 | 21.9 +/- 2.78 | 20 | 0.002 | 0.8352 | 0.0045 |
| | | 1119 +/- 288.3 | 1011 | | | |
| CCR1 | 1.88 | 85.8 +/- 9.221 | 82.5 | 0.0053 | 0.4835 | 0.132409091 |
| | | 165.5 +/- 17.46 | 155 | | | |
| CCS | -1.17 | 152.7 +/-6.57 | 151 | 0.15 | N/A | N/A |
| | | 127.1 +/- 9.46 | 129 | | | |

| | | | | | | |
|---|---|---|---|---|---|---|
| CD14 | 4.24 | 116.8 +/- 10.64 | 117 | 0.002 | 0.8681 | 0.003375 |
| | | 477.7 +/- 82.75 | 496 | | | |
| CD16 | 6.90 | 11.31 +/- 0.70 | 10 | 0.002 | 0.7088 | 0.016125 |
| | | 69.15 +/- 13.49 | 69 | | | |
| CD163 | 9.01 | 78.5 +/- 8.80 | 79.5 | 0.004 | 0.7198 | 0.014282609 |
| | | 1207+/- 316 | 1095 | | | |
| CD68 | 13.77 | 50.6 +/- 4.05 | 49.5 | 0.01 | 0.8006 | 0.006230769 |
| | | 420.8 +/- 82.22 | 473 | | | |
| CHRNA7 | -1.01 | 88.1 +/- 8.34 | 83 | 0.8 | N/A | N/A |
| | | 82 +/- 3.40 | 82 | | | |
| CHRNB2 | -1.48 | 501.8 +/- 49.07 | 513.5 | 0.025 | -0.8088 | 0.00525 |
| | | 313.2 +/- 40.62 | 347 | | | |
| CNOT8 | -1.31 | 563.8 +/- 18.47 | 586 | 0.002 | -0.3077 | 0.3445875 |
| | | 448.8 +/- 13.03 | 447 | | | |
| CNTF | 1.35 | 61.6 +/- 6.07 | 54 | 0.45 | N/A | N/A |
| | | 71.54 +/- 7.25 | 73 | | | |
| COMT | 1.14 | 302.3 +/- 17.16 | 316 | 0.07 | N/A | N/A |
| | | 434.2 +/- 41.58 | 359 | | | |
| CX3CL1 | -1.26 | 2168 +/- 207.2 | 2279 | 0.6 | N/A | N/A |
| | | 1992 +/- 171.9 | 1803 | | | |
| CX3CR1 | -1.10 | 614.5 +/- 60.37 | 543 | 0.29 | N/A | N/A |
| | | 495.5 +/- 114.4 | 492 | | | |
| CXCL12 | 1.53 | 255.7 +/- 20.39 | 241 | 0.02 | 0.1209 | 0.711818182 |
| | | 388.8 +/- 31.97 | 369 | | | |
| CXCR4 | 1.92 | 41.4 +/- 6.39 | 38.5 | 0.054 | N/A | N/A |
| | | 68.69 +/- 8.12 | 74 | | | |
| CYBA | 1.97 | 102.4 +/- 12.91 | 108 | 0.006 | 0.3571 | 0.267230769 |
| | | 219.8 +/- 21.94 | 213 | | | |
| DGCR8 | 1.07 | 234.6 +/- 9.46 | 232 | 0.68 | N/A | N/A |
| | | 243.7 +/- 9.57 | 248 | | | |
| DICER | -1.16 | 421 +/- 15.92 | 427.5 | 0.07 | N/A | N/A |
| | | 366 +/- 15.39 | 368 | | | |
| DLG4 | -1.37 | 3834 +/- 433.2 | 4162 | 0.33 | N/A | N/A |
| | | 2983 +/- 427.2 | 3036 | | | |
| DROSHA | -1.15 | 775.3 +/- 40.14 | 785 | 0.16 | N/A | N/A |
| | | 668 +/- 40.64 | 690 | | | |

| | | | | | | |
|---|---|---|---|---|---|---|
| EDN1 | 1.74 | 72.1 +/- 7.25 | 78 | 0.026 | 0.2198 | 0.503892857 |
| | | 151 +/- 19.85 | 136 | | | |
| EIF2C1 | -1.11 | 560.2 +/- 17.34 | 563.5 | 0.14 | N/A | N/A |
| | | 492.5 +/- 27.54 | 507 | | | |
| EIF2C2 | -1.02 | 738.3 +/- 32.76 | 758 | 0.84 | N/A | N/A |
| | | 737.1 +/- 17.97 | 744 | | | |
| ENO2 | -1.28 | 4701 +/- 227.9 | 4701 | 0.04 | -0.6703 | 0.0245 |
| | | 3627 +/- 269.1 | 3669 | | | |
| GFAP | 3.00 | 2109 +/- 5414 | 17993 | 0.07 | N/A | N/A |
| | | 54809 +/- 9645 | 53960 | | | |
| GLRX | 1.63 | 335.1 +/- 15.68 | 342.5 | 0.14 | N/A | N/A |
| | | 546.4 +/- 70.36 | 558 | | | |
| GLS | -1.50 | 2058 +/- 203.1 | 1848 | 0.005 | -0.7912 | 0.006428571 |
| | | 1234 +/- 131.8 | 1235 | | | |
| GLS2 | -1.14 | 110.8 +/- 12.42 | 107.5 | 0.7 | N/A | N/A |
| | | 97.08 +/- 11.41 | 94 | | | |
| GLUD1 | -1.13 | 2917 +/- 155.4 | 2865 | 0.2 | N/A | N/A |
| | | 2574 +/- 120.5 | 2532 | | | |
| GLUL | 1.12 | 6412 +/- 520.3 | 6520 | 0.24 | N/A | N/A |
| | | 7820 +/- 640.6 | 7328 | | | |
| GOT1 | -1.32 | 886.1 +/- 32.31 | 865.5 | 0.002 | -0.8297 | 0.0045 |
| | | 659.4 +/- 35.14 | 657 | | | |
| GOT2 | -1.20 | 1026 +/-51.39 | 1023 | 0.015 | 0.03297 | 0.9205 |
| | | 840 +/- 30.62 | 849 | | | |
| GPX1 | 2.19 | 751.7 +/- 104.4 | 840 | 0.006 | 0.7363 | 0.0126 |
| | | 1691 +/- 191.3 | 1842 | | | |
| GPX3 | 1.22 | 349.7 +/- 79 | 251 | 0.89 | N/A | N/A |
| | | 414.3 +/- 103 | 305 | | | |
| GPX4 | -1.12 | 1445 +/- 43.67 | 1479 | 0.22 | N/A | N/A |
| | | 1328 +/- 58.92 | 1338 | | | |
| GPX7 | 1.52 | 61.2 +/- 2.95 | 58.5 | 0.01 | 0.2198 | 0.503892857 |
| | | 86.46 +/- 6.14 | 89 | | | |
| GSR | 1.17 | 450.5 +/- 13.73 | 428 | 0.15 | N/A | N/A |
| | | 500.2 +/- 21.34 | 502 | | | |
| GSS | 1.07 | 199.2 +/- 19.64 | 176 | 0.92 | N/A | N/A |
| | | 2009 +/- 16.59 | 188 | | | |
| GSTZ1 | 1.43 | 137.1 +/- 12.59 | 126 | 0.055 | 0.8242 | 0.0045 |

| | | | | | | |
|---|---|---|---|---|---|---|
| | | 182.8 +/- 12.16 | 180 | | | |
| HAAO | -1.04 | 80.1 +/- 7.11 | 78 | 0.68 | N/A | N/A |
| | | 74 +/- 7.50 | 75 | | | |
| IFNaR | 1.02 | 599.1 +/- 21.41 | 602 | 0.68 | N/A | N/A |
| | | 605.8 +/- 18.25 | 616 | | | |
| IL18 | 1.40 | 230 +/- 22.52 | 215.5 | 0.07 | N/A | N/A |
| | | 352.2 +/- 49.95 | 301 | | | |
| IL18BP | 4.00 | 106.3 +/- 4.83 | 104.5 | 0.01 | 0.7857 | 0.0066 |
| | | 383 +/- 66.58 | 418 | | | |
| IRF1 | 17.74 | 41 +/- 3.33 | 42 | 0.002 | 0.9231 | 0.0015 |
| | | 627.8 +/- 137.3 | 745 | | | |
| IRF3 | 1.22 | 639.9 +/- 41.34 | 643 | 0.04 | 0.7235 | 0.014282609 |
| | | 816.3 +/- 47.8 | 785 | | | |
| ITGAM | 1.08 | 109.6 +/- 10.07 | 108.5 | 0.9999 | N/A | N/A |
| | | 106.2 +/- 10.72 | 117 | | | |
| MAOA | 1.10 | 451 +/- 46.36 | 436 | 0.64 | N/A | N/A |
| | | 629.5 +/- 120.3 | 481 | | | |
| MAOB | 1.28 | 1503 +/- 175.9 | 1537 | 0.14 | N/A | N/A |
| | | 2285 +/- 275.7 | 1973 | | | |
| MAP2 | -1.10 | 5855 +/- 356.7 | 5823 | 0.13 | N/A | N/A |
| | | 4775 +/- 430.1 | 5275 | | | |
| MBP | -1.41 | 28939 +/- 6191 | 28731 | 0.33 | N/A | N/A |
| | | 21579 +/- 4218 | 20428 | | | |
| MPV17 | 1.12 | 206.7 +/- 7.21 | 205 | 0.14 | N/A | N/A |
| | | 229.4 +/- 9.37 | 230 | | | |
| Mx1 | 48.92 | 266.4 +/- 42.88 | 221 | 0.002 | 0.7418 | 0.012078947 |
| | | 9663 +/- 1957 | 10812 | | | |
| OGT | 1.18 | 1576 +/- 103.1 | 1529 | 0.33 | N/A | N/A |
| | | 1817 +/- 176.7 | 1802 | | | |
| PCNA | 1.27 | 377.5 +/- 13.94 | 378 | 0.15 | N/A | N/A |
| | | 503.5 +/- 39.56 | 481 | | | |
| PDGFA | -1.32 | 272.2 +/- 31.62 | 314 | 0.56 | N/A | N/A |
| | | 305.9 +/- 38.49 | 238 | | | |
| PDGFB | 1.13 | 65.4 +/- 3.77 | 63 | 0.24 | N/A | N/A |
| | | 77.85 +/- 6.37 | 71 | | | |
| PDGFC | 1.19 | 91.1 +/- 9.39 | 79.5 | 0.76 | N/A | N/A |
| | | 95.92 +/- 9.03 | 95 | | | |

| | | | | | | |
|---|---|---|---|---|---|---|
| PDLIM1 | 1.32 | 37.6 +/- 3.37 | 37 | 0.08 | N/A | N/A |
| | | 85.69 +/- 15.57 | 49 | | | |
| PECAM1 | 2.50 | 264.9 +/- 12.12 | 268 | 0.002 | 0.7802 | 0.00703125 |
| | | 626.8 +/- 69.23 | 670 | | | |
| PRDX1 | 1.70 | 1365 +/- 149.5 | 1240 | 0.055 | N/A | N/A |
| | | 2079 +/- 221.2 | 2111 | | | |
| PRDX2 | -1.09 | 1043 +/- 38.11 | 1014 | 0.33 | N/A | N/A |
| | | 920.2 +/- 56.01 | 927 | | | |
| PRDX3 | 1.12 | 1918 +/- 116.5 | 1848 | 0.68 | N/A | N/A |
| | | 1976 +/- 90.82 | 2069 | | | |
| PRDX4 | 1.35 | 178.9 +/- 9.96 | 174.5 | 0.3 | N/A | N/A |
| | | 218 +/- 18.66 | 236 | | | |
| PRDX6 | 1.21 | 2152 +/- 156.8 | 2128 | 0.14 | N/A | N/A |
| | | 2565 +/- 159.6 | 2571 | | | |
| PRNP | -1.09 | 4450 +/- 252.4 | 4387 | 0.3 | N/A | N/A |
| | | 3976 +/- 251.7 | 3920 | | | |
| PTGDS | -1.17 | 5493 +/- 904.4 | 5360 | 0.8 | N/A | N/A |
| | | 4766 +/- 467.3 | 4571 | | | |
| PTGES2 | 1.03 | 299.6 +/- 22.46 | 283 | 0.97 | N/A | N/A |
| | | 280.3 +/- 22.08 | 297 | | | |
| RBFOX3 | -1.47 | 1816 +/- 269 | 2084 | 0.15 | N/A | N/A |
| | | 1210 +/- 190.1 | 1419 | | | |
| SAMHD1 | 3.67 | 167 +/- 11.71 | 166 | 0.002 | 0.8571 | 0.0036 |
| | | 566.8 +/- 82.64 | 609 | | | |
| SLC1A2 | -1.64 | 17290 +/- 1854 | 17499 | 0.1 | N/A | N/A |
| | | 11382 +/- 1790 | 10690 | | | |
| SLC1A3 | 1.19 | 10185 +/- 395.4 | 10149 | 0.1 | N/A | N/A |
| | | 13630 +/- 1278 | 12077 | | | |
| SLC2A1 | 1.16 | 91.1 +/- 5.02 | 95 | 0.054 | N/A | N/A |
| | | 108.7 +/- 4.29 | 110 | | | |
| SNAP25 | -1.34 | 16027 +/- 1647 | 16054 | 0.2 | N/A | N/A |
| | | 11669 +/- 1280 | 12023 | | | |
| SOD1 | 1.07 | 5444 +/- 122.9 | 5463 | 0.5 | N/A | N/A |
| | | 5761 +/- 261.9 | 5848 | | | |
| SOD2 | 7.17 | 3608 +/- 112.2 | 3667 | 0.01 | 0.9066 | 0.0015 |
| | | 23509 +/- 5744 | 26304 | | | |
| SOD3 | 5.47 | 105.5 +/- 9.86 | 102 | 0.002 | 0.4725 | 0.139897059 |

| | | 605.6 +/- 138.6 | 558 | | | |
|---|---|---|---|---|---|---|
| SRXN1 | 1.05 | 383.1 +/- 43.17 | 370 | 0.2 | N/A | N/A |
| | | 469.8 +/- 49.11 | 388 | | | |
| STAT1 | 7.90 | 427.7 +/- 20.49 | 429.5 | 0.002 | 0.5989 | 0.051 |
| | | 3031 +/- 468.6 | 3401 | | | |
| STAT2 | 5.13 | 152.8 +/- 8.89 | 146.5 | 0.004 | 0.7473 | 0.0115 |
| | | 578.8 +/- 91.36 | 752 | | | |
| STAT3 | 2.14 | 427.4 +/- 24.88 | 421 | 0.049 | 0.956 | 0.0015 |
| | | 851.2 +/- 110.4 | 901 | | | |
| STAT5A | 2.09 | 110.7 +/- 7.42 | 111 | 0.01 | 0.8187 | 0.00495 |
| | | 205.8 +/- 19.36 | 232 | | | |
| STAT5B | 1.00 | 343.2 +/- 12.28 | 346.5 | 0.9 | N/A | N/A |
| | | 347.1 +/- 14.93 | 346 | | | |
| STK25 | -1.15 | 1039 +/- 78.52 | 1149 | 0.63 | N/A | N/A |
| | | 947.9 +/- 82.13 | 1000 | | | |
| SYP | -1.50 | 3478 +/- 604.4 | 2960 | 0.049 | -0.6758 | 0.023711 538 |
| | | 2086 +/- 173.4 | 1969 | | | |
| TARBP2 | 1.04 | 121 +/- 7.81 | 119 | 0.97 | N/A | N/A |
| | | 120.6 +/- 7.58 | 124 | | | |
| TGFA | 1.08 | 66.1 +/- 8.37 | 55.5 | 0.68 | N/A | N/A |
| | | 61.54 +/- 6.69 | 60 | | | |
| TGFB1 | -1.19 | 285.4 +/- 19.01 | 265 | 0.04 | 0.4066 | 0.211875 |
| | | 424.3 +/- 49.36 | 384 | | | |
| TGFB2 | 1.98 | 417.6 +/- 38.64 | 395 | 0.015 | 0.8407 | 0.0045 |
| | | 796.8 +/- 97.44 | 783 | | | |
| TGFB3 | 1.23 | 242.8 +/- 12.33 | 239 | 0.41 | N/A | N/A |
| | | 297.8 +/- 31.39 | 294 | | | |
| TJP1 | -1.10 | 1683 +/- 105.5 | 1813 | 0.52 | N/A | N/A |
| | | 1611 +/- 71.37 | 1644 | | | |
| TJP2 | 1.16 | 256.5 +/- 33.77 | 225.5 | 0.6 | N/A | N/A |
| | | 311.5 +/- 37.53 | 262 | | | |
| TLR1 | 1.47 | 111.5 +/- 9.42 | 104 | 0.005 | 0.4842 | 0.132409 091 |
| | | 188.2 +/- 17.41 | 153 | | | |
| TLR3 | 2.87 | 78.5 +/- 9.86 | 86 | 0.002 | 0.7033 | 0.01674 |
| | | 201.5 +/- 26.05 | 195 | | | |
| TLR4 | 2.20 | 157.2 +/- 24.79 | 143.5 | 0.002 | 0.533 | 0.093193 548 |
| | | 363.9 +/- 40.77 | 316 | | | |

| Gene | Fold | Mean +/- SEM | Median | p-value | Col6 | Col7 |
|---|---|---|---|---|---|---|
| TLR5 | 1.49 | 32.6 +/- 4.89 | 27.5 | 0.18 | N/A | N/A |
| | | 42.38 +/- 3.74 | 41 | | | |
| TLR6 | 1.41 | 101.8 +/- 7.26 | 100.5 | 0.015 | 0.3681 | 0.256618 421 |
| | | 147.5 +/- 11.62 | 142 | | | |
| TLR7 | 1.36 | 68.9 +/- 6.817 | 60.5 | 0.45 | N/A | N/A |
| | | 91.38 +/- 14.73 | 82 | | | |
| TNFRSF10A | 2.10 | 32.6 +/- 4.72 | 29.5 | 0.002 | 0.8077 | 0.00525 |
| | | 71.54 +/- 9.98 | 62 | | | |
| TNRC6A | -1.03 | 577.1 +/- 19.88 | 563.5 | 0.77 | N/A | N/A |
| | | 558.1 +/- 21.97 | 548 | | | |
| TP53 | 2.10 | 50 +/- 2.91 | 50.5 | 0.01 | 0.7198 | 0.014282 609 |
| | | 94.62 +/- 10.32 | 106 | | | |
| TRIM32 | -1.08 | 287 +/- 10.67 | 294 | 0.6 | N/A | N/A |
| | | 273.2 +/- 19.85 | 272 | | | |
| TSPAN7 | -1.39 | 14302 +/- 942.4 | 14992 | 0.18 | N/A | N/A |
| | | 10986 +/- 1221 | 10810 | | | |
| TUBB3 | -1.39 | 1954 +/- 265 | 1942 | 0.24 | N/A | N/A |
| | | 1464 +/- 133.6 | 1397 | | | |
| TXN | 1.04 | 4156 +/- 258.6 | 3959 | 0.88 | N/A | N/A |
| | | 4235 +/- 208 | 4101 | | | |
| TXNRD1 | 1.16 | 971.1 +/- 39.36 | 984 | 0.02 | 0.6044 | 0.049655 172 |
| | | 1184 +/- 49.63 | 1140 | | | |
| TXNRD2 | -1.19 | 237 +/- 16.46 | 245 | 0.3 | N/A | N/A |
| | | 210.8 +/- 13.66 | 206 | | | |
| TYK2 | 1.26 | 244.6 +/- 8.67 | 238 | 0.04 | 0.6319 | 0.037928 571 |
| | | 309.5 +/- 20.24 | 301 | | | |
| VEGFA | 1.07 | 236.6 +/- 12.71 | 229.5 | 0.81 | N/A | N/A |
| | | 241.2 +/- 16.63 | 245 | | | |
| VEGFB | -1.19 | 351.4 +/- 20.78 | 360.5 | 0.5 | N/A | N/A |
| | | 327.7 +/- 30.17 | 302 | | | |

**Supplemental Table 2-1. Genes above the limit of detection that were significantly changed after 84 days of SIV infection in the basal ganglia and their correlation scores with CSF1 mRNA expression.**

# CHAPTER III.

# Differential Regulation of TREM2 and CSF1R in CNS Macrophages in an

# SIV/Macaque Model of HIV CNS Disease

This chapter has been accepted with minor revisions for publication in the *Journal of NeuroVirology*.

**Abstract**

HIV-associated neuroinflammation is primarily driven by CNS macrophages including microglia. Regulation of these immune responses, however, remains to be characterized in detail. Using the SIV/macaque model of HIV, we evaluated CNS expression of Triggering Receptor Expressed on Myeloid cells 2 (TREM2) which is constitutively expressed by microglia and contributes to cell survival, proliferation, and differentiation. Loss-of-function mutations in TREM2 are recognized risk factors for neurodegenerative diseases including Alzheimer's disease (AD), amyotrophic lateral sclerosis (ALS), and Nasu-Hakola disease (NHD); recent reports have also indicated a role for TREM2 in HIV-associated neuroinflammation. Using *in situ* hybridization (ISH) and qRT-PCR, TREM2 mRNA levels were found to be significantly elevated in frontal cortex of macaques with SIV encephalitis compared to uninfected controls ($P = 0.02$). TREM2 protein levels were also elevated as measured by ELISA of frontal cortex tissue homogenates in these animals. Previously, we characterized the expression of CSF1R (colony stimulating factor 1 receptor) in this model; the TREM2 and CSF1R promoters both contain a PU.1 binding site. While TREM2 and CSF1R mRNA levels in frontal cortex were highly correlated (Spearman R = 0.79, $P < 0.001$), protein levels were not well correlated. In SIV-infected macaques released from ART to study viral rebound, neither TREM2 nor CSF1R mRNA increased with rebound viremia. However, CSF1R protein levels remained significantly elevated unlike TREM2 ($P = 0.02$). This differential expression suggests that TREM2 and CSF1R play unique, distinct roles in the pathogenesis of HIV CNS disease.

**Introduction**

Triggering Receptor Expressed on Myeloid cells 2 (TREM2) is an immunoglobulin-like receptor expressed on cells of the myeloid lineage. Within the brain, TREM2 is primarily expressed by parenchymal microglia and perivascular macrophages. TREM2 signaling promotes survival and proliferation of these cells. It has also been suggested that TREM2 plays a role in immune regulation and activation (Konishi and Kiyama 2018).

TREM2 loss-of-function mutations in humans are associated with several neurodegenerative diseases. In particular, loss-of-function mutations in humans have been linked to the development of Alzheimer's disease (AD) (Jonsson et al. 2013; Guerreiro et al. 2013), Nasu-Hakola disease (NHD) (Dardiotis et al. 2017), and frontotemporal dementia (FTD) (Thelen et al. 2014). This highlights the clinical significance of TREM2 in neurodegeneration.

The potential role of TREM2 in the development of AD was further characterized in murine model systems, which ultimately showed that increased TREM2 signaling from baseline can be protective at the onset of disease but then detrimental at later stages of the disease (Yeh et al. 2017). It has also been shown in mice that TREM2-expressing microglia surround amyloid beta plaques, further suggesting a sequestering and protective role of these cells (Wang et al. 2016). This shows that increased TREM2 activation is beneficial and protective at the onset of neurodegenerative disease. However, long-term activation of TREM2 can also contribute to neurodegenerative diseases, suggesting that the role of TREM2 signaling in neurodegeneration is time dependent (Jay et al. 2015). Therefore, it is important to maintain a homeostatic balance of TREM2 signaling to maintain CNS health. Along these same lines, altered TREM2-APOE signaling has been shown to be important in

the pathogenesis amyotrophic lateral sclerosis (ALS) and multiple sclerosis (MS) in a mouse model (Krasemann et al. 2017).

Much like TREM2, increased expression of colony stimulating factor 1 receptor (CSF1R) has been linked to many of these same neurodegenerative diseases including AD (Akiyama et al. 1994). TREM2 and CSF1R are both highly expressed within the CNS by microglia (Chitu et al. 2016). Additionally, TREM2 and CSF1R share the transcription factor PU.1 (Satoh et al. 2014). We have previously shown that CSF1R is upregulated within the CNS of SIV-infected pigtailed macaques, demonstrating a role for CSF1R in promoting HIV CNS disease (Knight et al. 2018). Similar findings were reported for HIV (Irons et al. 2019). Recent reports also described altered TREM2 expression in HIV-infected individuals with HIV-associated neurocognitive disorder (HAND) (Fields et al. 2018; Gisslén et al. 2018).

As HAND is thought to be due to sustained CNS inflammation even with suppressive anti-retroviral therapy, microglia likely play an essential role in its pathogenesis (Saylor et al. 2016). In particular, we hypothesized that chronic activation of TREM2 and CSF1R signaling contributes to the pathogenesis of HIV CNS disease. It has been previously established that TREM2 signaling is linked to CSF1R-related downstream affects in macrophages (Otero et al. 2009). Other studies have further shown a coordinated effect of TREM2 and CSF1R signaling via the accessory protein DNAX activating protein 12 (DAP12) resulting in sensory nerve damage due to microglial proinflammatory activity (Guan et al. 2016; Kobayashi et al. 2016). However, it is yet to be established whether TREM2 and CSF1R signaling are directly linked and causative in HIV CNS disease or other neurodegenerative diseases. We therefore hypothesized that upregulation of TREM2 would

55

be associated with SIV CNS disease in our SIV/pigtailed macaque model in parallel with

CSF1R alterations. (Knight et al. 2018).

**Methods**

Animals

Samples from juvenile male pigtailed macaques (*Macaca nemestrina*) were used for these studies dependent on sample availability. All animals were specific pathogen free for *Macacine herpesvirus* 1 (B virus), simian immunodeficiency virus (SIV), simian T-cell leukemia virus (STLV-1), and simian retrovirus (SRV). At necropsy, all animals were perfused with phosphate buffered saline. When collected, brains were sectioned coronally and either immersion fixed in 10% neutral buffered formalin (NBF) or Streck tissue fixative (STF), or snap-frozen in liquid nitrogen. All flash-frozen samples were stored at -80°C from the time of initial collection at necropsy until use.

Samples from five groups of juvenile male pigtailed macaques (*Macaca nemestrina*) were evaluated as available: 1) uninfected controls that were mock inoculated with Lactated Ringers Solution (LRS) (n = 9), 2) SIV-infected animals that were intravenously inoculated with both the immunosuppressive swarm SIV/DeltaB670 and the molecular clone SIV/17E-Fr and euthanized 42 days post infection (dpi; n = 6), 3) SIV-infected animals that were intravenously inoculated with SIV/DeltaB670 and SIV/17E-Fr and euthanized 84 dpi unless the animal developed AIDS-defining criteria, in which case the animal was euthanized at that time (n = 9), 4) SIV-infected animals treated with a suppressive ART regimen (SIV + ART) beginning 12 days post-SIV inoculation (n = 7) (Beck SE et al. 2015; Beck SE et al. 2017; Beck SE et al. 2015), and 5) SIV-infected animals treated with ART and then released from their ART-regimen after 120 days of suppression of SIV (n = 10) (Supplemental Table 1). SIV + ART animals were treated with a combination injectable regimen of 2.5 mg/kg Dolutegravir (ViiV Healthcare US, Raleigh, NC), 20 mg/kg PMPA, and 40 mg/kg FTC

(Gilead, Foster City, CA) administered daily subcutaneously. Four of the seven SIV + ART

animals also received an oral dose of 20 mg of maraviroc (ViiV Healthcare, US, Raleigh,

NC) daily. SIV + ART animals were suppressed in both plasma and CSF by 56 days p.i. and

were euthanized 180 days p.i. Animals that were released from treatment were given the

same ART regimen as listed above. Six of the 12 animals released from treatment received

maraviroc. Release animals were euthanized at a viral set point in plasma, defined as three

consecutive time points with viral loads within one log. Maraviroc did not have an effect on

time to suppression, time to rebound, or any macrophage/microglial markers and thus were

included to increase group size (Knight et al. 2018). All animal studies were approved by the

Johns Hopkins Animal Care and Use Committee.


## *In situ* hybridization to detect TREM2 RNA

*In situ* hybridization (ISH) was performed on 5μm thick sections of frontal cortex

after immersion fixation in 10% NBF followed by paraffin embedding. Staining was

performed using the Leica Bond RX automated system (Leica Biosystems, Richmond, IL).

The TREM2 probe (cat. 432238, Advanced Cell Diagnostics, Newark, NJ) was used with the

Leica RNAScope 2.5 LS Assay-RED kit and a hematoxylin counterstain (Leica Biosystems,

Richmond, IL). Slides were treated in protease (Advanced Cell Diagnostics, Newark, NJ) for

15 minutes and probes hybridized to RNA for 1 minute.


## TREM2 ISH and IBA1 IHC dual staining

TREM2 ISH was combined with IBA1 immunostaining performed on frontal cortex

sections from an SIV infected animal. TREM2 ISH was performed as described above. The

first heat-induced epitope retrieval was conducted by heating slides to 95°C in EDTA-based

ER2 buffer for 15 minutes (Leica Biosystems, Richmond, IL). Slides were then stained with

anti-IBA1 antibody (cat. 01919741, Wako, Richmond, VA) at a dilution of 1:500. IHC was

performed using the Bond RX automated system (Leica Biosystems, Richmond, IL). A

second heat-induced epitope retrieval was conducted by heating slides to 95°C for 20

minutes in sodium citrate-based ER1 buffer (Leica Biosystems, Richmond, IL). Positive

immunostaining was visualized using DAB, and slides were counterstained with

hematoxylin.

## PU.1 Immunohistochemistry and image analysis

Streck tissue fixative-fixed frontal cortex sections of uninfected, 84d SIV-infected,

SIV + ART, and release pigtailed macaques were stained with anti-PU.1 antibody (cat.

PA517505, Invitrogen, Carlsbad, CA) at a dilution of 1:100. Heat-induced epitope retrieval

was conducted by heating slides to 95°C for 20 minutes in sodium citrate-based ER1 buffer

(Leica Biosystems, Richmond, IL). Nikon Elements software (Nikon, Melville, NY) was

utilized for image acquisition and positive object count analysis. Images were composed of

36 contiguous 200X fields covering cortical grey and white matter. A threshold was set to

determine positive staining to perform object count analysis that counted PU.1-

immunopositive cells.

## Quantitative RT-PCR

RNA was isolated from flash-frozen white matter frontal cortex or parietal cortex as

previously described (Knight et al. 2018). The High Capacity cDNA Reverse Transcriptase

kit (Applied Biosystems, Carlsbad, CA) was used for both reverse transcriptase (RT) and no

reverse transcriptase (NRT) reactions. RT reactions were run in duplicate. One microgram of

RNA was added to each reaction. RT step was performed using the PTC 200 (MJ Research,

Port Republic, NJ) as previously described (Knight et al. 2018). Four microliters of cDNA

from these reactions were then added to qPCR reactions. Each reaction contained the

TaqMan ® Universal Master Mix II or the Gene Expression Master Mix (Applied

Biosystems, Carlsbad, CA) with one of two multiplexed probe mixes. The TREM2 probe

(cat. Hs00219132_m1, ThermoFisher Scientific, Waltham, MA) was multiplexed with the

18S probe, while the CSF1R probe (cat. Hs00911250_m1, ThermoFisher Scientific) was

multiplexed with the CSF1 probe (cat. Rh02621778_m1, ThermoFisher Scientific) probe. As

TREM2 and CSF1R probes were not available for the macaque genes, human probes were

used. There is significant homology between the human and macaque TREM2 and CSF1R

genes (96% and 92% homology respectively). Both multiplexed reactions were run in

parallel, and each sample was run in duplicate. qPCR was performed using the C1000 Touch

thermal cycler and the CFX96 Real-Time PCR Detection System (Bio Rad, Hercules, CA) as

previously described (Knight et al. 2018). All RNA counts were normalized to 18S ribosomal

RNA counts and reported as *ΔΔCt* (cycle threshold).


ELISAs

TREM2 and CSF1R ELISAs were performed using protein homogenates from frontal

cortex sections. A total of 34 animals were included based on availability of samples. 4 mm

biopsy punches were taken from white matter and placed in RIPA cell lysis buffer (Cell

Signaling Technology, Danvers, MA). A hand-held homogenizer was used to grind the

tissue. Samples were then sonicated. The protein concentration of each sample was measured using either Qubit or BCA (ThermoFisher, Waltham, MA) and validated visually using Criterion™ TGX Stain-Free 10% protein separation gels. The gel was imaged using the Gel Doc EZ-Imager (Bio-Rad, Hercules, CA). The Biomatik (Cambridge, Ontario, CA) human MCSFR (cat. EKU09066) and human TREM2 (cat. EKU07882) kits were used according to the manufacturer's protocol. 30 ug of protein were added to the pre-coated wells in duplicate and positive immunoreactivity was read at 450 nm using a TMB solution. Results from SIV + ART for CSF1R protein levels were previously published (Knight et al. 2018) and included in this study to determine differences between suppression and release.

Statistical Analysis

All statistical analysis was performed using Prism 7 or 8 GraphPad Software (GraphPad Software, La Jolla, CA). Non-parametric analyses included Mann-Whitney tests and Kruskal-Wallis tests with Dunn's multiple comparisons. Significance was determined at a P value of less than or equal to 0.05.

**Results**

*TREM2 mRNA expression in SIV-infected pigtailed macaque frontal cortex.*

TREM2 is constitutively expressed on cells of the myeloid lineage, specifically perivascular macrophages and parenchymal microglia within the CNS (Schmid et al. 2002). Upregulation of TREM2 has been reported in several models of CNS inflammation and neurodegenerative diseases (Yeh et al. 2017). To confirm this cell-specific expression pattern of TREM2 in the SIV/pigtailed macaque model of HIV CNS disease, *in situ* hybridization (ISH) was performed on sections of macaque frontal cortex. In uninfected pigtail macaque frontal cortex, low-level constitutive TREM2 positive staining could be observed in parenchymal microglia (**Figure 1A, inset**). TREM2 mRNA expression was markedly increased 42 days post-SIV infection. Increased TREM2 positive staining could be seen in both parenchymal microglia and in perivascular macrophages (**Figure 1B**). Localization of TREM2 RNA to CNS macrophages was confirmed by dual TREM2 ISH and IBA1 IHC staining (**Supplemental Figure 1**).

In SIV-infected macaques with encephalitis, TREM2 positive staining was also localized to both perivascular macrophages (**Figure 1C**) and parenchymal microglia (**Figure 1D**). This pattern of TREM2 staining is consistent with that reported in human brain (Yeh et al. 2017). These findings were confirmed by qRT-PCR (**Figure 2A**). TREM2 mRNA expression increased, but not significantly ($P = 0.1$), at 42 days post-SIV infection in the frontal cortex compared to uninfected controls. At 84 days post infection, the increase in TREM2 mRNA was significant ($P = 0.02$). TREM2 mRNA returned to baseline with suppressive ART treatment (uninfected v SIV + ART $P > 0.999$). This same trend was seen in CSF1R mRNA qRT-PCR data (**Figure 2B**). Considering TREM2 and CSF1R expression

are both controlled, at least in part, by the transcription factor PU.1 (Satoh et al. 2014), we determined whether or not TREM2 and CSF1R mRNA expression were correlated in this model. With SIV infection, TREM2 mRNA expression was highly correlated with both CSF1R expression (**Figure 2C**, Spearman R = 0.79, P = 0.0008), and the CSF1R ligand, CSF1 (**Figure 2D**, Spearman R = 0.84, P = 0.0002). These results suggest coordinated increase in TREM2, CSF1R, and CSF1 transcripts in the frontal cortex in response to SIV infection.

To validate these findings, we used immunohistochemistry and quantitative image analysis to characterize PU.1, the transcription factor common to both TREM2 and CSF1R. PU.1 protein significantly increased after 84 days of SIV infection in frontal cortex compared to uninfected controls (**Figure 3** uninfected vs 84d SIV, P = 0.03). With ART suppression, PU.1 returned to baseline levels (**Figure 3** uninfected vs SIV + ART, P > 0.999). This pattern closely parallels both TREM2 and CSF1R mRNA level alterations that develop with SIV infection, which is consistent with a regulatory role for PU.1.

*TREM2 and CSF1R protein levels differ despite mRNA similarities*

Given the mRNA findings described above, we hypothesized that TREM2 protein levels would reflect what we previously described with CSF1R protein levels in our SIV/macaque model (Knight et al. 2018). To explore this possibility, we measured TREM2 protein in frontal cortex homogenates by ELISA in samples from uninfected controls, untreated SIV infected pigtailed macaques euthanized 42 days and 84 days post-infection, and fully suppressed ART treated SIV-infected macaques. While we did not see a significant increase in TREM2 protein in any of the four groups compared to uninfected controls, the

wide range of TREM2 protein concentrations present in the uninfected frontal cortices limited the statistical power of these comparisons (**Figure 4A**). Although not significant (P = 0.55), levels of TREM2 protein in SIV-infected pigtailed macaques with encephalitis were moderately increased. Additionally, TREM2 protein levels returned to baseline with suppressive ART compared to levels seen in the 84-day post-infection group (Uninfected vs SIV + ART P > 0.999; 84d SIV vs SIV + ART P = 0.2).

These findings of TREM2 protein in the brain returning to baseline with suppressive ART contrast sharply with CSF1R protein levels in these same animals; CSF1R protein levels remained elevated in fully suppressed animals (Knight et al. 2018). TREM2 protein and CSF1R protein levels were not strongly correlated despite the observed significant correlation in mRNA expression (**Figure 4B**, Spearman R = 0.4, P = 0.03).

*TREM2 and CSF1R expression upon release from suppressive ART therapy.*

To explore the potential differential roles of TREM2 and CSF1R in HIV CNS disease during viral rebound after treatment interruption, we measured both mRNA and protein expression in SIV-infected pigtailed macaques that were released from suppressive ART after approximately 120 days of suppression (titled 'release group'). TREM2 and CSF1R mRNA expression measured by qRT-PCR in this release group was equivalent to uninfected controls (**Figure 5A, B**, uninfected v TREM2 and CSF1R P = 0.9). The number of cells expressing PU.1 protein was also not significantly different during the early phases of viral rebound compared to uninfected animals (**Figure 5C**, P = 0.6).

TREM2 and CSF1R protein levels were also measured in frontal cortex of the release group. In this group, TREM2 protein levels were not significantly higher than those of SIV + ART animals (**Figure 6A**; P = 0.86) in agreement with the mRNA expression levels. CSF1R protein expression, on the other hand, was higher than SIV + ART animals upon release from ART (**Figure 6B**; P = 0.14). Again, the protein levels of CSF1R diverged from its mRNA expression. The median fold increase from uninfected baseline of CSF1R, however, was significantly higher than TREM2 (**Figure 6C,** P = 0.02).

**Discussion**

In these studies, we tracked SIV-induced alterations in both TREM2 mRNA and protein expression in the brain using the SIV/pigtailed macaque model of HIV-induced neurologic disease (Beck et al. 2015; Laast et al. 2011). As reported in humans, TREM2 was expressed constitutively at low levels by macrophages within the macaque brain including both perivascular macrophages and parenchymal microglia (Yeh et al. 2017). TREM2 mRNA expression significantly increased with SIV infection as shown by both *in situ* hybridization and qRT-PCR measurements. TREM2 protein levels were moderately higher in the frontal cortex with SIV infection; this increase was not significant, however, when compared to the wide range of TREM2 levels seen in uninfected control animals. The reason for the variation in range of TREM2 protein in uninfected specific pathogen-free macaques is not known but may reflect unidentified subclinical infections or systemic immune responses conveyed across the blood-brain barrier. It has been reported that common, short-lived gastroenteritis can affect the mucosal barrier of the gut, resulting in the translocation of intestinal microbiota or LPS. This may cause low-levels of systemic inflammation, which can affect the neuroinflammatory state (Brenchley and Douek 2012; Yarandi et al. 2016). This could potentially explain an increase in TREM2 in certain animals in the absence of overt disease.

In general, the pattern of increased expression of TREM2 with SIV infection independent of ART parallels our previous report of CSF1R expression increases seen within the same SIV model (Knight et al. 2018). Our finding that TREM2 RNA levels were strongly correlated with both CSF1R and its ligand CSF1 RNA levels is consistent with previous reports demonstrating that TREM2 and CSF1R share PU.1 as a common transcription factor

66

and also interact with the same adapter protein, DAP12, for downstream signaling (Satoh et al. 2014; Guan et al. 2016; Kobayashi et al. 2016).

Of note, treating SIV-infected pigtailed macaques with suppressive ART reduced brain TREM2 RNA and protein levels to baseline pre-infection values in contrast with the sustained elevated CSF1R protein levels that we have reported with ART (Knight et al. 2018). This suggests that TREM2 may not play a key immunoregulatory role in the ART era in contrast with previous studies (Fields et al. 2018; Gisslén et al. 2019). This finding also suggests that post-transcriptional regulation differentiates TREM2 from CSF1R with respect to duration of expression on macrophages. This difference likely represents the different functional roles that these receptors play, including both trophic and immunoregulatory functions. The sustained increase in CSF1R protein levels with ART may represent reduced degradation or elevated cytosolic stores of CSF1R that are key for maintaining high CSF1R levels in the face of cellular stress. Additionally, slower processing of the immature CSF1R protein may result in a more consistently elevated level of mature CSF1R at the cell membrane (Uden, Morley, and Dibb 1999). This may also explain why CSF1R protein remains elevated without a concordant increase in CSF1R mRNA.

We extended these findings to examine whether stopping ART treatment in SIV-infected macaques induced expression of TREM2 during early viral rebound when SIV emerges from latency. Since we did not have access to acute timepoints to measure TREM2 mRNA and protein at the earliest stage of SIV rebound, we sampled terminal timepoints in SIV-infected macaques released from ART. We hypothesized that TREM2 could be an early regulator of CNS macrophage immune activation and potentially related to viral load at post-ART setpoints. We did not find TREM2 alterations during rebound despite detecting

abundant SIV RNA in both plasma and CSF.  In contrast, we did find significantly higher levels of CSF1R protein in the frontal cortex during rebound similar to the sustained elevation of CSF1R present under long-term ART. As this rebound was relatively short (approximately 20 days post ART release), it is possible that TREM2 mRNA and protein would increase with longer reactivation.

CSF1R signaling is essential for microglial survival and also may regulate microglial immune function during chronic neurodegeneration like that seen in HIV CNS disease. Therefore, microglia may have developed mechanisms to maintain CSF1R protein without activating transcription.  It is possible that herein lies the key difference in TREM2 and CSF1R protein levels in this model of HIV CNS disease. We hypothesize that TREM2 is a marker of microglial cell number that does not change at the single cell level with infection. CSF1R, on the other hand, may be a marker of microglial priming as CSF1R protein remains elevated in fully suppressed macaques after initial SIV infection. It has previously been shown in rodent models of acute and chronic neuroinflammation that TREM2 is a marker of bulk microglia whereas CSF1 correlates primarily with chronic microglial activation and priming, and secondarily with acute microglial immune responses (Holtman et al. 2015). Maintaining CSF1R protein after initial infection may allow the cell to be more prepared for a subsequent insult. This ultimately suggests that although both TREM2 and CSF1R are closely related proteins in both mRNA expression control and downstream function in microglia (Yeh et al. 2017; Chitu et al. 2016; Stanley and Chitu 2014), CSF1R may play a more significant role in the pathogenesis of HAND.

**Acknowledgments**
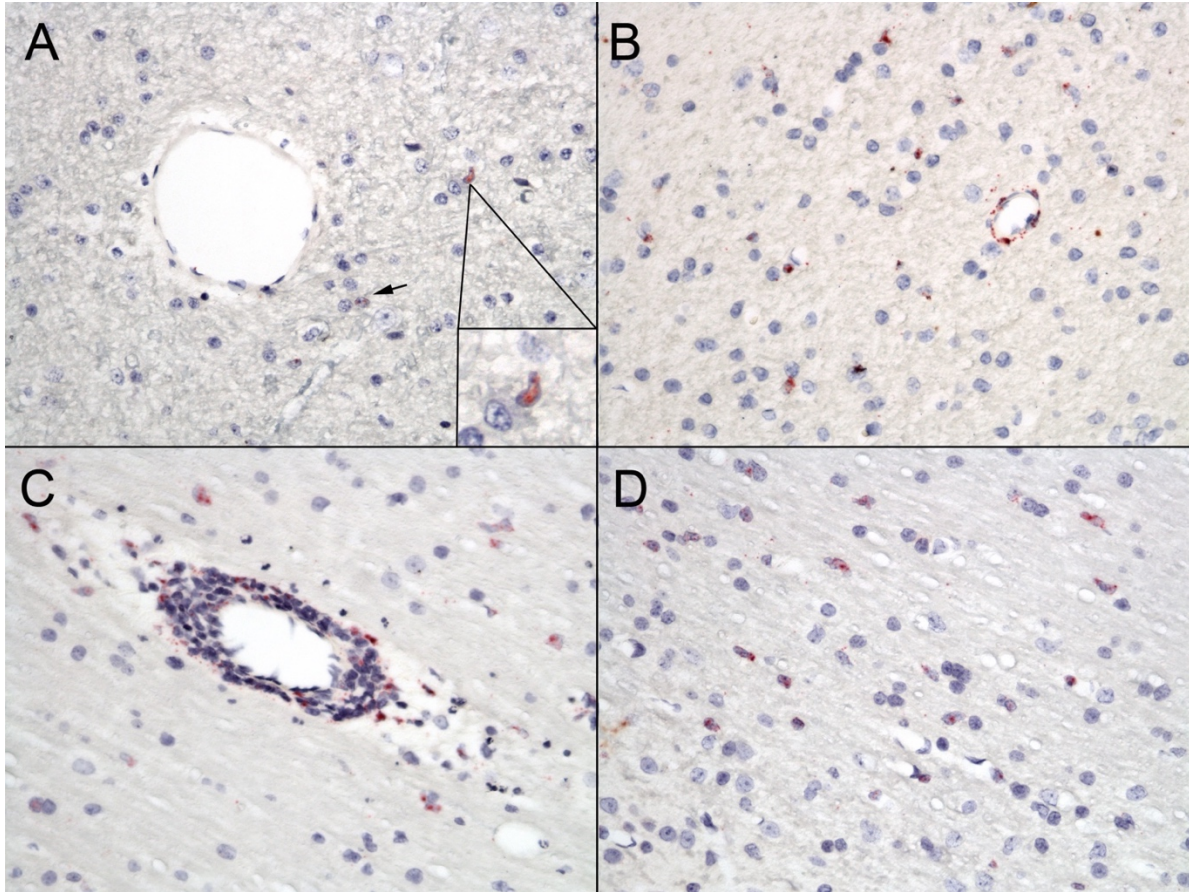
**Figure 3-1. TREM2 mRNA localizes to microglia and perivascular macrophages in pigtailed macaques.** (A) TREM2 RNA in frontal cortex parenchyma in an uninfected pigtailed macaque. (B) TREM2 RNA increased after 42 days of SIV infection. (C) TREM2 RNA present in a perivascular cuff of macrophages in a macaque with encephalitis. (D) TREM2 RNA in parenchymal microglia of a macaque with encephalitis.
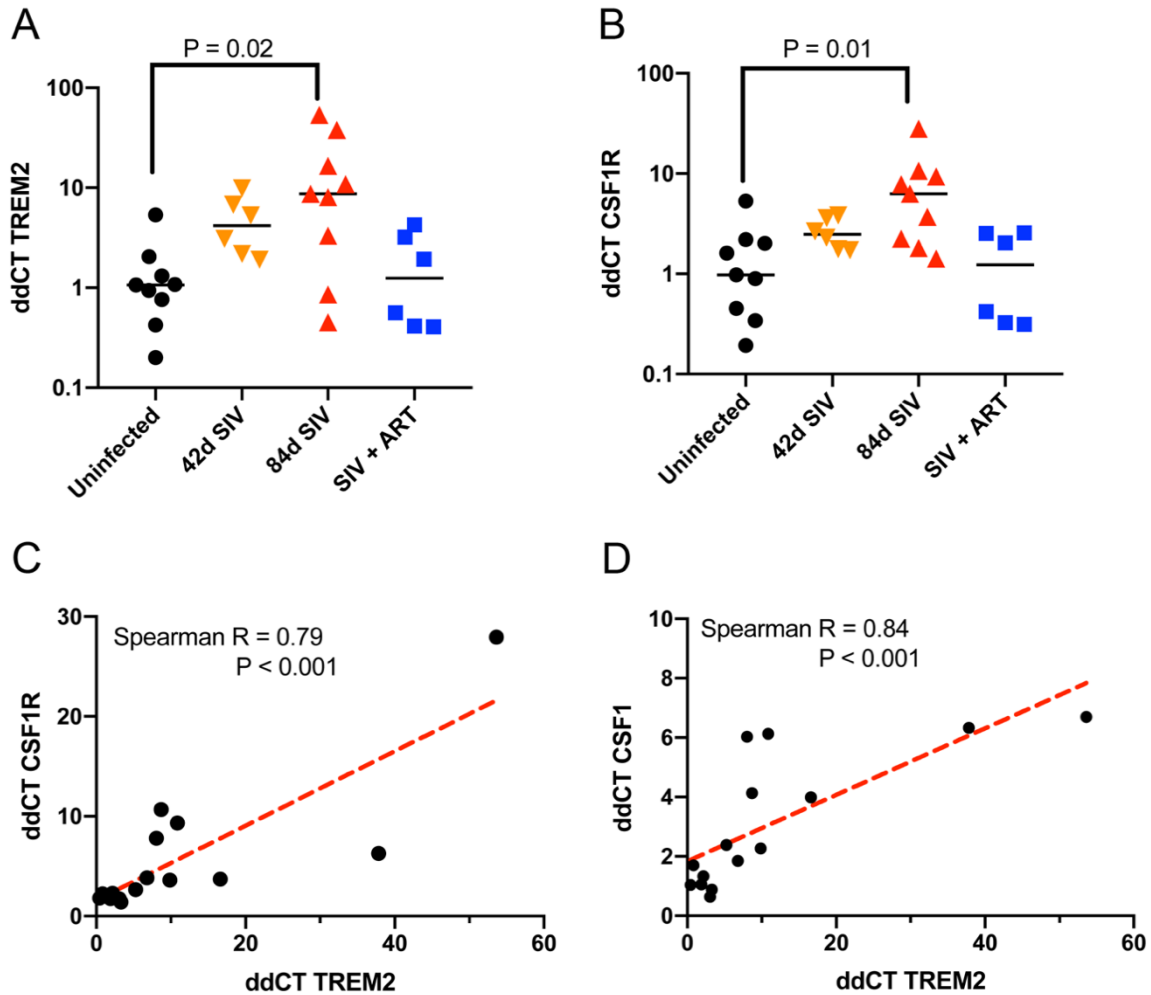
**Figure 3-2. mRNA expression of TREM2 and CSF1R increase with SIV encephalitis and are positively correlated with each other** (A) TREM2 mRNA and (B) CSF1R mRNA were significantly increased in SIV-infected pigtailed macaques with encephalitis and returned to baseline levels with suppressive ART. Kruskal-Wallis tests with Dunn's multiple comparisons were performed to determine significance. (C) TREM2 mRNA was significantly correlated with CSF1R and (D) CSF1 mRNA in SIV-infected macaques without ART. (Uninfected = ● n = 9; 42d SIV = ▼ n = 6; 84d SIV = ▲ n = 9; SIV + ART =■ n = 6).
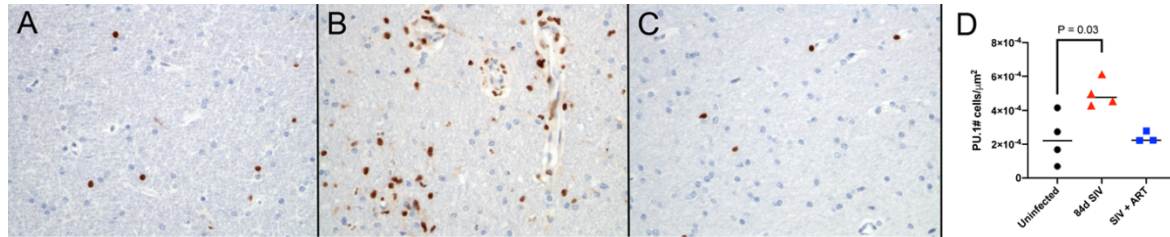
**Figure 3. PU.1 protein, a transcription factor shared by TREM2 and CSF1R, increased with SIV and returned to baseline with suppressive ART, in agreement with TREM2 and CSF1R mRNA expression.** (A) In uninfected macaque frontal cortex, PU.1 positive staining was localized to the nuclei of parenchymal microglia and perivascular macrophages. (B) After 84 days of SIV infection (84d SIV), there was a marked increase in the number of PU.1+ cells (P = 0.03). (C) PU.1+ cell numbers then returned to baseline with ART. IHC quantification results are shown in D.
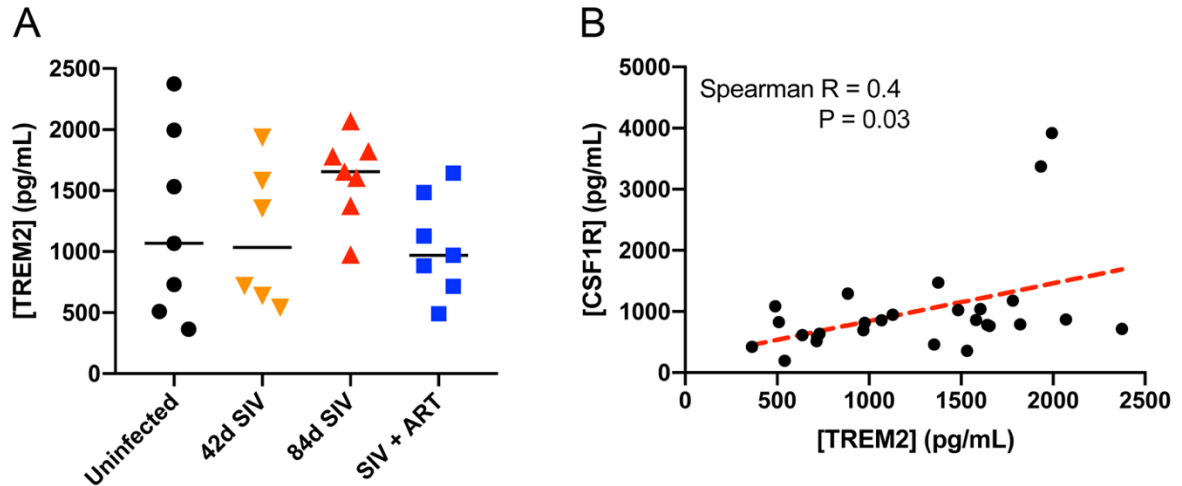
**Figure 3-4. TREM2 and CSF1R protein levels were discordant in SIV infected pigtailed macaques.** (A) TREM2 protein levels were not significantly higher in SIV infected macaques with or without ART treatment (Kruskal-Wallis with multiple comparisons P = 0.09) (B) Despite correlation of mRNA levels, TREM2 and CSF1R protein concentrations in frontal cortex of SIV infected pigtailed macaques did not correlate. All protein levels were used to evaluate the correlation between TREM2 and CSF1R protein expression (n = 26) (Uninfected = ● n = 7; 42d SIV = ▼ n = 6; 84d SIV = ▲ n = 7; SIV + ART = ■ n = 7).
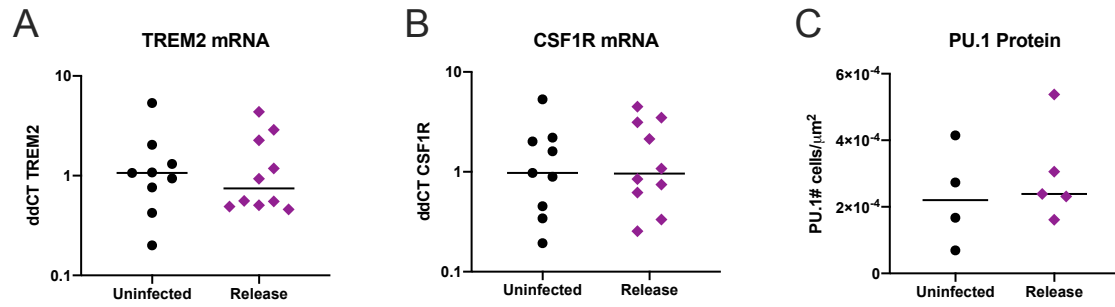
**Figure 3-5. TREM2 and CSF1R mRNA did not increase after release from suppressive ART.** TREM2 mRNA (A, Mann-Whitney P = 0.9) and CSF1R (B, Mann-Whitney P = 0.9) remained at baseline after release from suppressive treatment by qPCR. PU.1 IHC quantification supported this finding (C). PU.1 protein did not increase with release from ART (Mann-Whitney P = 0.6) (A and B: Uninfected = ● n = 7; TREM2 and CSF1R Release = ◆ n = 10; C: Uninfected = ● n = 4, Release = ◆ n = 5).
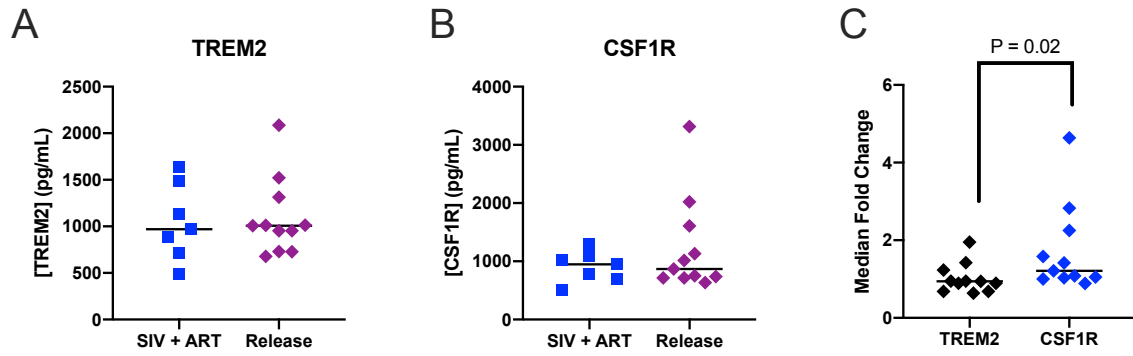
**Figure 3-6. TREM2 and CSF1R protein expression after release from antiretroviral treatment.** Like mRNA, TREM2 protein levels did not increase upon release from suppressive ART (A). However, CSF1R protein was higher under these conditions (B). The median fold change from baseline was significantly higher for CSF1R protein than TREM2 protein (C). (A and B. SIV + ART = ■ n =7; Release = ◆ n = 11; C. TREM2 release = ◆ n = 11; CSF1R Release = ◆ n = 11).

**Supplemental Table 3-1**

| Animal ID | Age at Euthanasia (yrs) | Inoculation Status | Treatment | Length of SIV infection (wks) |
|---|---|---|---|---|
| PT247 | 3.5 | Mock | None | - |
| PT248 | 2.9 | Mock | None | - |
| PT249 | 3.1 | Mock | None | - |
| PT290 | 2.5 | Mock | None | - |
| PT293 | 2.3 | Mock | None | - |
| PT332 | 5.0 | Mock | None | - |
| PT334 | 5.1 | Mock | None | - |
| PT373 | 3.5 | Mock | None | - |
| PT374 | 3.5 | Mock | None | - |
| PT437 | 3.2 | SIV | None | 6 |
| PT439 | 3.1 | SIV | None | 6 |
| PT438 | 3.1 | SIV | None | 6 |
| PT441 | 2.4 | SIV | None | 6 |
| PT440 | 2.9 | SIV | None | 6 |
| PT442 | 2.2 | SIV | None | 6 |
| PT300 | 3.2 | SIV | None | 11 |
| PT265 | 4.7 | SIV | None | 6 |
| PT353 | 5.3 | SIV | None | 12 |
| PT298 | 3.1 | SIV | None | 13 |
| PT291 | 2.5 | SIV | None | 12 |
| PT203 | 9.5 | SIV | None | 9 |
| PT320 | 3.6 | SIV | None | 9 |
| PT297 | 2.5 | SIV | None | 11 |
| PT274 | 6.2 | SIV | None | 7 |
| PT394 | 3.8 | SIV | ART* | 26 |
| PT400 | 4.3 | SIV | ART* | 26 |
| PT390 | 4.1 | SIV | ART* | 26 |
| PT401 | 3.6 | SIV | ART* | 26 |
| PT391 | 3.3 | SIV | ART | 26 |
| PT392 | 3.2 | SIV | ART | 26 |
| PT409 | 3.7 | SIV | ART*/Release | 28 |
| PT410 | 3.4 | SIV | ART*/ Release | 28 |
| PT411 | 3.4 | SIV | ART*/ Release | 27 |
| PT412 | 3.2 | SIV | ART*/ Release | 27 |
| PT413 | 3.1 | SIV | ART*/ Release | 26 |
| PT414 | 2.9 | SIV | ART*/ Release | 26 |
| PT422 | 3.1 | SIV | ART/ Release | 26 |
| PT423 | 3.0 | SIV | ART/ Release | 26 |

| PT425 | 2.8 | SIV | ART/ Release | 27 |
| PT424 | 2.8 | SIV | ART/ Release | 28 |

ART* denotes animals receiving ART+MVC

**Supplemental Table 3-1. Study Animals.** Description of animals from which samples were taken for the studies described in this paper.
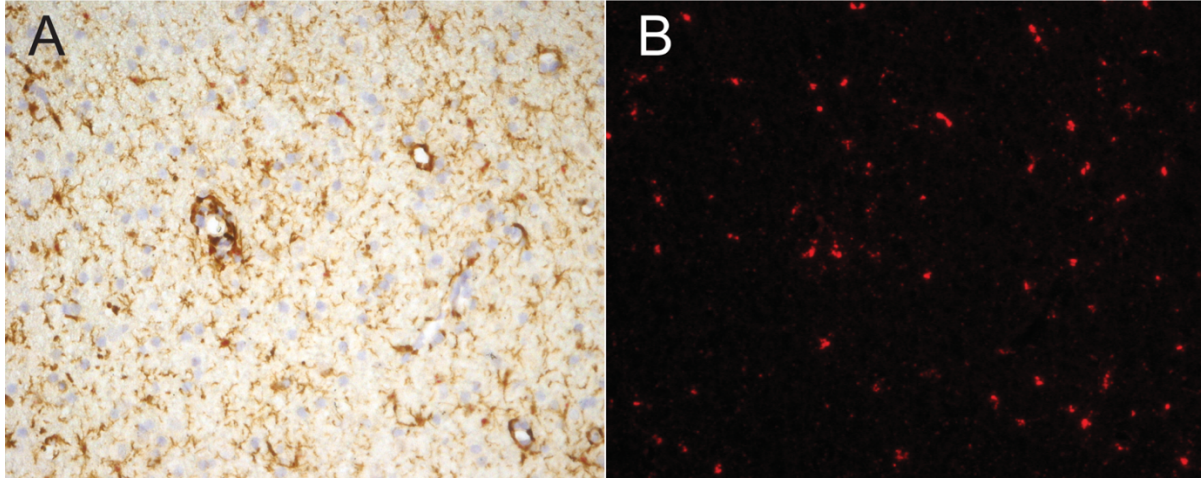
**Supplemental Figure 1: TREM2 ISH colocalizes with IBA1+ CNS macrophages.** (A)

The double IHC-ISH staining showed that TREM2 ISH (red) colocalizes with IBA1+ cells

(brown) in an SIV infected pigtailed macaque with encephalitis. (B) Fluorescence was used

to highlight TREM2 ISH staining (red channel).

# CHAPTER IV.

## CSF1R Inhibition Targets CNS Macrophages in an SIV/Macaque Model of HIV CNS Disease

## Abstract

CNS macrophages, including microglia, serve as a latent HIV cellular reservoir. Colony stimulating factor 1 receptor (CSF1R) is expressed exclusively on cells of myeloid lineage and is essential for microglial survival. We have previously shown that CSF1R protein levels increase with SIV infection and remain elevated in the CNS despite suppressive ART. Other groups have described the same pattern of CSF1R protein expression with HIV infection. Consequently, CSF1R is a potential drug target to reduce the CNS latent reservoir. PLX3397 (Pexidartinib) is an FDA-approved, small-molecule inhibitor of CSF1R and has been shown to effectively eliminate microglia in rodent models *in vivo*. To determine whether CSF1R inhibition in primates would result in microglia depletion, we cultured primary brain and spinal cord microglia and then treated cells with 10μM PLX3397 for three days. Microglial viability was significantly reduced as observed by calcein (live) and ethidium (dead) staining, as well as interferon-beta qPCR (Two-Way ANOVA P < 0.0001). Following *in vitro* treatment, *in vivo* studies were conducted using daily oral treatment of 165mg/kg PLX3397 in ART-suppressed SIV-infected pigtailed macaques (N = 2). Two weeks after the start of PLX3397 treatment, ART was stopped while PLX3397 treatment continued for an additional 16 days. Drug treatment was well tolerated; animals did not show side-effects such as monocytopenia. PLX3397 treatment did not significantly affect plasma viral rebound kinetics. However, CSF viral rebound did not develop in one animal. In addition, neither SIV RNA nor DNA was detected in cultured primary microglia from this animal. In the second animal, viral RNA was isolated from CNS macrophages cultured from both brain and spinal cord. These studies showed that PLX3397 reduced CNS macrophage viability *in vitro*, demonstrating that targeting CSF1R may reduce CNS macrophages,

including those harboring HIV. Treatment of SIV-infected macaques on ART was associated

with a lack of SIV rebound from the CNS and a decrease in IBA1+ CNS macrophages in one

of two animals after stopping ART. These studies demonstrate the potential of targeting

CSF1R to reduce the HIV latent reservoir in the CNS.

**Introduction**

Central nervous system macrophages, including microglia, have been associated with the development of several neurodegenerative diseases, including HIV associated CNS disease (Cartier et al. 2014; Saylor et al. 2016; Williams et al. 2014). In HIV CNS disease, microglia are chronically activated, even in the context of full viral suppression using antiretroviral therapy (ART). This chronic immune activation is thought to drive neuronal damage and consequently CNS impairment (Saylor et al. 2016; Williams et al. 2014). Beyond the effects of chronic immune activation, microglia are also essential in the development of the viral reservoir within the brain. In the brain, microglia are the main cell infected by HIV that harbor and produce infection-competent virus (Abreu et al. 2019; Wallet et al. 2019). Consequently, targeting microglia is important not only for the potential treatment of HIV-induced neurologic disease, but also for eliminating HIV from the CNS to achieve cure.

Colony stimulating factor 1 receptor is a classic tyrosine kinase receptor constitutively expressed on cells of the myeloid lineage. In the central nervous system, it is exclusively expressed on microglia and perivascular macrophages (Chitu et al. 2016). CSF1R signaling is essential for microglial survival and proliferation (Elmore et al. 2014; Stanley and Chitu 2014). Previous evidence suggests that CSF1R signaling may impact microglial immune responses as well (Coleman et al. 2020). Increased levels of CSF1R have been reported in several neurodegenerative diseases, including Alzheimer's disease (AD), amyotrophic lateral sclerosis (ALS), and other neuroinflammatory diseases such as prion disease (Akiyama et al. 1994; Gomez-Nicola et al. 2013; Mitrasinovic and Murphy 2003). Specifically in AD, CSF1R expressing-microglia surround amyloid-beta plaques in mouse

models of AD and in post-mortem human brain samples (Akiyama et al. 1994; Dagher et al. 2015). A recent GWAS study identified a mutation in *CSF1R* that led to increased basal levels that increased the risk of developing early-onset AD (Sassi et al. 2018). Beyond AD, we have shown that CSF1R expression increases in an SIV/macaque model of HIV CNS disease during SIV encephalitis and remains elevated when animals are suppressed with ART (Knight et al. 2018). Because of the association between increased CSF1R expression and neurodegenerative disease, targeting this receptor is of particular interest.

PLX3397 is a small molecule inhibitor of CSF1R that has recently received FDA approval for the treatment of tenosynovial giant-cell tumors (Lamb 2019). PLX3397 treatment effectively kills CSF1R-expressing tumor associated macrophages (TAMs) in these tumors (Tap et al. 2015). These cells are thought to promote tumorigenesis (Cannarile et al. 2017). However, in other cancers there is some debate as to whether PLX3397 depletes TAMs or alters the phenotype of these cells (Dammeijer et al. 2017; Ao et al. 2017). CSF1R inhibitors, including PLX3397, have also been used in multiple rodent models of neurodegenerative diseases, including AD, ALS, and MS (Mancuso et al. 2019; Olmos-Alonso et al. 2016; Spangenberg et al. 2016; Dagher et al. 2015;  Martinez-Muriana et al. 2016; Tahmasebi et al. 2019; Beckmann et al. 2018; Nissen et al. 2018). In mouse models, CSF1R inhibition depletes microglia to varying degrees (Han et al. 2017). PLX3397 is the most effective of these inhibitors, depleting at least 90% of microglia (Han et al. 2017; Elmore et al. 2015; Jin et al. 2017; Li et al. 2017; Szalay et al. 2016).

Because of its efficacy, FDA approval, and ability to penetrate the blood-brain barrier (BBB), we evaluated the ability of PLX3397 to inhibit CSF1R signaling in our SIV/pigtailed macaque model of CNS disease. We hypothesized that CSF1R inhibition would significantly

reduce the number of microglia *in vitro* and *in vivo* in this model by blocking a vital trophic signaling pathway. Consequently, we proposed that by reducing the number of microglia, the SIV latent reservoir in the CNS would also be reduced. Here, we show that CSF1R inhibition quickly depleted primary pigtailed macaque microglia *in vitro*. However, PLX3397 treatment did not significantly deplete microglia *in vivo*. Interestingly, PLX3397 did prevent viral rebound in a PLX3397-treated animal after it was released from ART. This suggests that when activated, nonhuman primate microglia require CSF1R signaling for survival; in resting or primed microglia, inhibiting CSF1R signaling may alter the immunophenotype of these cells rather than killing the cell. These findings also reflect that maximal dosing was not achieved in this study. Also, CSF1R inhibition may be an effective way to reduce, and potentially eliminate, the latent CNS viral reservoir in HIV.

**Methods**

<u>Animals</u>

Male juvenile specific-pathogen-free pigtailed macaques (*Macaca nemestrina*) were included in this study. Animals were screened for *Macacine herpesvirus 1* (B virus), simian immunodeficiency virus (SIV), simian T-cell leukemia virus (STLV-1), and simian retrovirus (SRV). At necropsy, animals were perfused with phosphate-buffered saline. Sections of the brain were serially sectioned and were flash-frozen or fixed in Streck tissue fixative (STF). Remaining brain tissue was used to isolate microglia.

For PLX3397 *in vitro* experiments, microglia were isolated from three uninfected pigtailed macaques. These animals were mock inoculated with Lactated Ringers Solution (LRS) and euthanized 84 days after mock inoculation.

Eight animals were intravenously infected with two strains of SIV: SIV/17E-Fr and SIV/DeltaB670. SIV/17E-Fr is a neurovirulent molecular clone, while SIV/DeltaB670 is an immunosuppressive swarm. At 12 days post-infection (dpi), animals were treated daily with a subcutaneous injection of a combination of 2.5 mg/kg Dolutegravir (ViiV Healthcare US, Raleigh, NC), 20 mg/kg PMPA, and 40 mg/kg FTC (Gilead, Foster City, CA). They were also treated with a daily oral dose of 20 mg of Maraviroc (ViiV Healthcare US, Raleigh, NC). Animals were fully suppressed for 120 days. At this time, they were released from ART and euthanized at viral set point (Release group). This was defined as three cumulative plasma viral loads within one log of each other. Typically, this point was reached within 20 days post-release. Plasma and CSF were collected every four days post-ART release to measure SIV RNA levels.

Two of the 8 animals were also given a daily 165 mg/kg oral dose of PLX3397 starting two weeks prior to ART release (PLX3397-treated group). Dosing was based upon previously published pharmacokinetic studies (Tap et al. 2015). PLX3397 treatment continued for two weeks after ART was removed, at which time the animals were euthanized (**Figure 1**). One animal, PLX2, was euthanized 16 days post ART release when it developed significant weight loss.

All animal studies were approved by the Johns Hopkins Animal Care and Use Committee.

Microglia isolation

Microglia were isolated from the brains of two PLX3397-treated animals, 2 uninfected, untreated animals, and 1 SIV-infected, untreated animal euthanized 84 days post-infection. After sectioning, remaining pieces encompassing every section of the brain were used. Meninges were removed from CNS tissue. Tissue was minced and then centrifuged twice in PBS for 3 minutes at 400xg at room temperature. The tissue was then incubated in Dulbecco's modified Eagle (DMEM) media (Life Technologies, Carlsbad, CA) supplemented with 0.25% trypsin, 50μM DNase/mL and 50μg gentamicin/mL solution at 37°C for 30 minutes. Fifteen minutes into the incubation, the slurry was briefly agitated and then returned to the water bath. This slurry was then filtered through a 183μM pore filter and then a 100μM pore mesh in DMEM supplemented with fetal bovine serum (FBS), at a final concentration of 10%, to remove undigested tissue fragments. This filtrate was centrifuged for 10 minutes at 400xg at room temperature. The resultant cell pellet was resuspended in PBS and centrifuged on a 9mL Percoll gradient in a 50mL conical at 411,000xg for 30

minutes at room temperature. The supernatant below the myelin cap was then removed and spun down for 10 minutes at 400xg at room temperature to isolate the cell pellet free from myelin. Cells were then plated at in DMEM supplemented with FBS at a 10% concentration. After 24 hours, wells were washed with DMEM 10 to remove unattached cells and the remaining adherent cells were then cultured in microglia media composed of DMEM (Life Technologies, Carlsbad, CA) supplemented with 50µg gentamycin/mL (Life Technologies, Carlsbad, CA), 1mM sodium pyruvate, 10% volume of 100% FBS (ThermoFisher Scientific, Waltham, MA), and 10% volume of giant cell tumor conditioned medium(Fisher Scientific, Hampton, NH) (Alvalos et al. 2017).

SIV RNA quantification

SIV RNA was quantified in plasma and CSF by qRT-PCR and ddPCR as previously described (Abreu et al. 2019; Barber et al. 2004; Beck et al. 2015; Witwer et al. 2009).

SIV RNA levels in cell culture supernatants were quantified by qRT-PCR as previously reported (Abreu et al. 2019). Cells were left in culture for seven days before supernatant collection began. Half-volume supernatants were then collected every two days; the amount of microglia media sampled was then replaced after sampling. SIV was isolated from supernatants using QIAmp MinElute Virus Spin Kit according to manufacturer's protocol (Qiagen, Frederick, MD).

Because early timepoints for microglia isolated from PLX2 were negative for SIV RNA, cells were stimulated with 10ng/mL of TNF-α (ProSpec, East Brunswick, NJ) for 48 hours before the last timepoint was collected (Alvalos et al. 2016).

<u>PLX3397 *in vitro* treatment</u>

Microglia from the brains of two uninfected pigtailed macaques and one untreated SIV-infected pigtailed macaque euthanized 84 dpi were utilized for these experiments. After isolation, adherent cells were left in culture for seven days before treatment. Cells were then treated once daily with 10μM PLX3397 in DMSO or vehicle alone (DMSO). For each experiment, four wells of microglia were used. The first well was collected before treatment to determine the baseline number of cells. Each subsequent well was collected at 24, 48, and 72 hours post-PLX3397 treatment (**Supplemental Figure 4-1**). Lysates were collected in RLT+ buffer (Qiagen, Frederick, MD) and stored at -80°C for cell count analysis. Brightfield images were taken at 100X and 200X at each timepoint using the Nikon H600L inverted microscope.

DNA was then isolated from cell lysates to determine total cell number in each well. The number of cells remaining in the well at each timepoint was determined by interferon beta qPCR as previously described (Abreu et al. 2019), enabling quantitative assessments that complemented visual comparisons of microglia density with and without PLX3397 treatment.

<u>Cell viability immunofluorescence</u>

Live versus dead cell staining was performed at each timepoint. Each timepoint represents a different well as represented in **Supplemental Figure 4-1**. Live cells were labeled with calcein and dead cells labeled with ethidium as previously described (Bohlen et al. 2017). Images were colorized and background was subtracted in ImageJ (Schneider et al. 2012).

IBA1 Immunohistochemistry

        Frontal cortex, occipital cortex, and parietal cortex sections immersion fixed in Streck tissue fixative from PLX3997-treated and release groups were stained with anti-IBA1 antibody (cat. 019-19741, Wako, Richmond, VA) at a dilution of 1:500. Slides were counterstained with hematoxylin. All slides were stained using the Leica Bond RX automated system with the Bond Polymer Refine Red kit (Leica Biosystems, Richmond, IL). Heat-induced epitope retrieval was performed at 100°C for 20 minutes in sodium citrate-based ER1 buffer (Leica Biosystems, Richmond, IL). Images were acquired using Nikon Elements software (Nikon, Melville, NY).

**Results**

*PLX3397 treatment kills pigtailed macaque microglia in vitro*

Previous reports have shown that PLX3397 treatment effectively kills human macrophages *in vitro* (Ao et al. 2017; Cunyat et al. 2016). However, the effects of PLX3397 on nonhuman primate microglia have not been determined *in vitro*. Based on the previously published report of PLX3397 treatment on human macrophages infected with HIV, we treated primary microglia isolated from uninfected pigtailed macaques with 10μM PLX3397 in DMSO or vehicle alone once daily over the course of 72 hours (Cunyat et al. 2016). At 24 hours, there was a clear decrease in the number of microglia in the treated group (**Figure 4-2A**). The number of microglia continued to decline at 48 hours (**Figure 4-2A**). Depletion was maximal after 72 hours of treatment with loss of 84% of microglia from baseline. This decrease was statistically significant (**Figure 4-2B**; $P = 0.03$ Sidak's multiple comparisons) Two-way ANOVA revealed that time and treatment were driving this decline in microglia from baseline ($P < 0.0001$).

This was further confirmed using fluorescent live/dead staining. Live cells were stained with calcein (green) and dead cells were labeled with ethidium (red). At 48 hours post-treatment, there were no dead cells in the vehicle treated well (**Figure 4-3A**). However, there were detectable dead cells in the PLX3397 treated well (**Figure 4-3B, red arrowheads**). The live cell staining also highlighted the clear difference in cell morphology in the PLX3397 treated cells compared to the vehicle treated cells. PLX3397 treatment resulted in smaller cell size and it causes microglia to cluster and bind together, characteristic of dying microglia. Interestingly, there were occasional double-positive cells for both calcein

and ethidium (**Figure 4-3B, yellow arrowhead**). These cells were likely in the process of dying.

*The effects of PLX3397 treatment on SIV viral rebound kinetics in plasma and CSF*

It has been previously reported that PLX3397 treatment eliminated over 90% of microglia in the rodent brain (Elmore et al. 2015; Jin et al. 2017; Li et al. 2017; Szalay et al. 2016). However, studies of PLX3397 in nonhuman primates have been limited to drug tolerance and $P_K/P_D$ characterization (Tap et al. 2015). Here, we evaluated the effects of PLX3397 in SIV-infected pigtailed macaques. We treated fully-suppressed pigtailed macaques with 165 mg/kg of oral PLX3397 once daily for two weeks. We then released these two animals from their ART regimen but maintained PLX3397 treatment (**Figure 4-1**). Paired plasma and CSF samples were collected every 4 days post-release from ART to characterize the viral rebound kinetics.

The drug dose was well-tolerated by the animals with no side-effects noted. Additionally, no monocytopenia developed in either animal (data not shown). After release from ART, SIV RNA was detected in the plasma of both animals and the rebound trajectory was not different from PLX3397-naive animals released from ART (**Figure 4-4A**). In animal PLX1, viral rebound in the cerebrospinal fluid (CSF) was detected 12 days post-ART release, and the rebound trajectory matched the PLX3397-naïve animals. However, PLX2 had no detectable virus in CSF at any timepoint before euthanasia at 16 days post-release from ART (**Figure 4-4B**). This suggests that PLX3397 has the potential to suppress viral rebound specifically in the CSF.

*PLX3397 prevented viral outgrowth in the primary microglia isolated from one animal*

Since microglia are thought to be a significant contributor to SIV viral load in the CSF, we isolated primary microglia from PLX3397-treated animals to determine if SIV RNA was detectable. In both animals, approximately half of the number of microglia were isolated compared to uninfected control pigtailed macaques (data not included). These microglia were cultured, and cell culture supernatants were sampled for SIV RNA. Microglia cell culture supernatant was sampled for 12 days. In PLX1, virus was detectable by qRT-PCR at the first sampled timepoint after 7 days in culture (**Figure 4-5**). Virus remained detectable until the termination of sampling at day 14. However, SIV RNA was not detected in microglia cell culture supernatants isolated from PLX2 after 12 days in culture (**Figure 4-5**). This shows the potential for PLX3397 treatment to reduce the CNS SIV reservoir.

*PLX3397 treatment affected microglial morphology* in vivo

PLX3397 significantly reduced the number of microglia in brains of mice (Han et al. 2017; Elmore et al. 2015; Jin et al. 2017; Li et al. 2017; Szalay et al. 2016). To determine whether PLX3397 treatment affected microglial numbers in nonhuman primates similarly, IBA1 immunohistochemistry was performed on frontal cortex, occipital cortex, and parietal cortex of PLX3397 treated animals and release animals. In both PLX1 and PLX2, there were clearly detectable IBA1+ microglia in grey and white matter sections in all brain regions stained. However, there were visually fewer microglia in these sections compared to release animals.

In frontal cortex white matter especially, there was a clear reduction in microglia in PLX2, and to a lesser extent in PLX1, compared to the ART-release group (**Figure 4-6**). In

addition to this visual reduction in microglial number, there was a clear difference in microglial morphology in PLX3397-treated animals compared to release animals. The microglia in the ART-release animal frontal cortex show a more ameboid morphology, representing an activated state. However, the microglia in both PLX3397-treated animals had clear, long, ramified projections, which are characteristic of a surveilling or resting immunophenotype (**Figure 4-6**; Hanisch and Kettenmann 2007; Kreutzberg 1996). This suggests that PLX3397 had an effect on nonhuman primates *in vivo*, as evidenced by reduced microglial number and changed microglial immunophenotypes.

**Discussion**

We described the effects of PLX3397 on pigtailed macaque microglia both *in vitro* and *in vivo*. As previously reported with human macrophages, we showed that PLX3397 effectively kills pigtailed macaque microglia *in vitro* at a concentration of 10μM (Cunyat et al. 2016). Approximately 84% of microglia were depleted *in vitro* after 72 hours. It is possible that with more time, the percent depletion would reach that seen in mice *in vivo* (Han et al. 2017; Elmore et al. 2015; Jin et al. 2017; Li et al. 2017; Szalay et al. 2016).

While PLX3397 did not deplete microglia in pigtailed macaques to the extent seen in mice, it did reduce microglial number in SIV-infected pigtailed macaques. The lack of total depletion of microglia in PLX3397-treated pigtailed macaques may be due to a lack of efficient and maximal drug penetrance. The dosage selected for this pilot trial was based on a single preclinical study conducted in a cynomolgus macaque (Tap et al. 2015). In this previously published study, there were high concentrations of drug in both plasma and CSF, showing efficient drug absorption from oral dosing. However, it is not clear whether the pigtailed macaques in this study reached similar drug concentrations. Further $P_K/P_D$ studies will need to be conducted to determine the proper drug dosing strategy.

Beyond a lack of drug penetration, this lack of total depletion of microglia may be specific to primates. The effect of PLX3397 on primate microglia has not been evaluated outside of this study. Recent reports show that rodent microglia are significantly different in function compared to primate microglia (Geirsdottir et al. 2019). Consequently, primate microglia may not be as reliant on CSF1R signaling for survival as rodent microglia.

Despite this lack of depletion, it is clear that PLX3397 did have an effect on pigtailed macaque microglia *in vivo*. In this study, there was a clear change in microglial morphology.

This change in morphology may represent a change in microglial phenotype (Hanisch and Kettenmann 2007; Kreutzberg 1996). Previously, we hypothesized that microglia in our fully suppressed animals may be primed from previous exposure to replicating SIV or continued exposure to viral proteins. We also hypothesized that CSF1R signaling may be important in this primed state (**Chapter III; Figure 1-4**). Consequently, this return to a resting morphology in PLX3397-treated animals may be a result of inhibiting CSF1R signaling and subsequently changing in microglial phenotype. A previous study did note that CSF1R inhibition resulted in the resetting of primed microglia to a resting state (Coleman et al. 2016). Further single-cell sequencing studies of these microglia will be necessary to confirm this in our model.

Interestingly, although released from ART, there was no evidence of viral rebound in the CSF of PLX2. This may be due to a reduction in the viral reservoir in the CNS. Although not significant, there was a reduction in the number of microglia that was more apparent in PLX2 than in PLX1. It is possible that if this study were extended, PLX2 would eventually rebound in the CSF. However, this delay is important to note, as it may represent a reduction in the latent reservoir. It is also interesting to note that PLX3397 treatment had no effect on plasma viral rebound. This shows that PLX3397 may target the CNS reservoir rather than in other tissues.

Overall, PLX3397 treatment was more effective in PLX2 than in PLX1. One possible explanation for this difference is that PLX2 had a lower body fat content than PLX1, enhancing drug distribution to the CNS in this animal. Measuring drug concentration in both body fat and in the brain will be required to examine this difference in future studies. Treating additional animals with PLX3397 will elucidate whether this drug is consistently

effective at reducing the SIV viral reservoir in the brain. PLX3397 may be an effective

treatment to reduce the viral reservoir in the CNS and also reset primed microglia to a resting

state to reduce the chronic inflammation in the CNS that accompanies HIV infection.
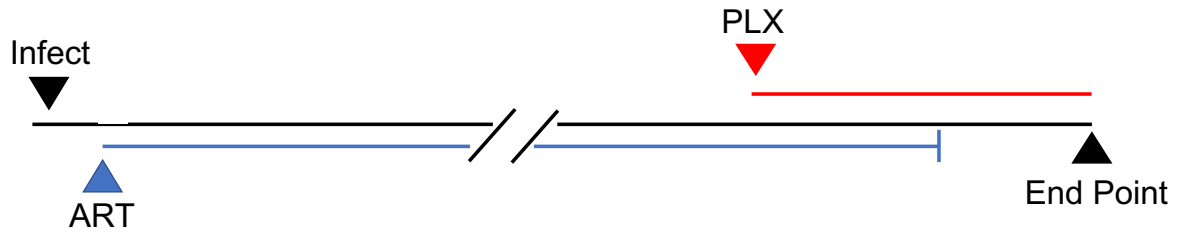
**Figure 4-1. *In vivo* treatment protocol.** Animals were IV inoculated with SIV/17EFr and SIV/DeltaB670. Infected animals were then treated with ART as described. Two weeks preceding withdrawal from ART regimen, animals PLX1 and PLX2 were treated with 165mg/kg PLX3397. PLX3397 was maintained until the animals were euthanized post ART withdrawal at end point.

**Figure 4-2**
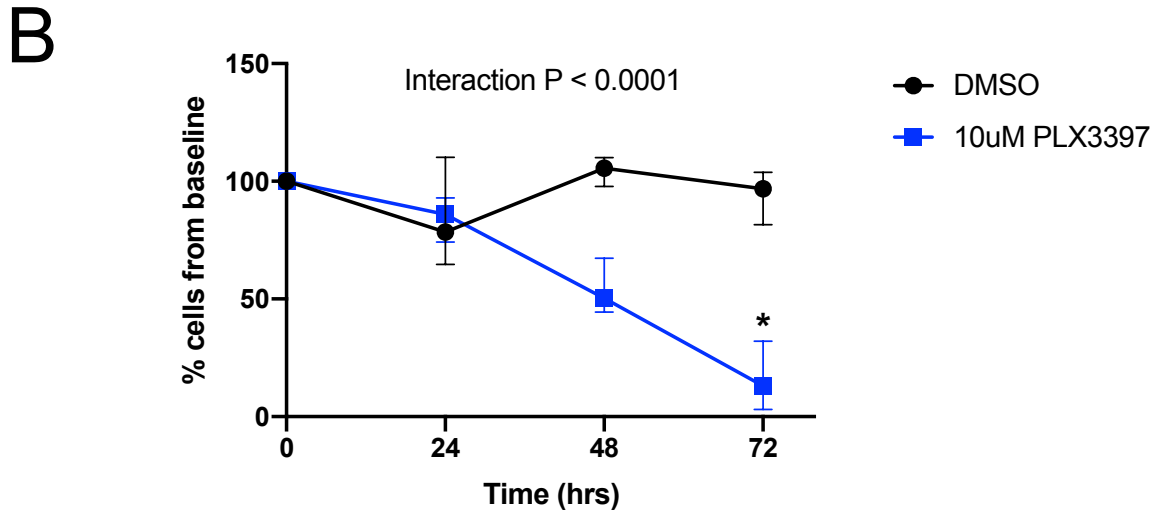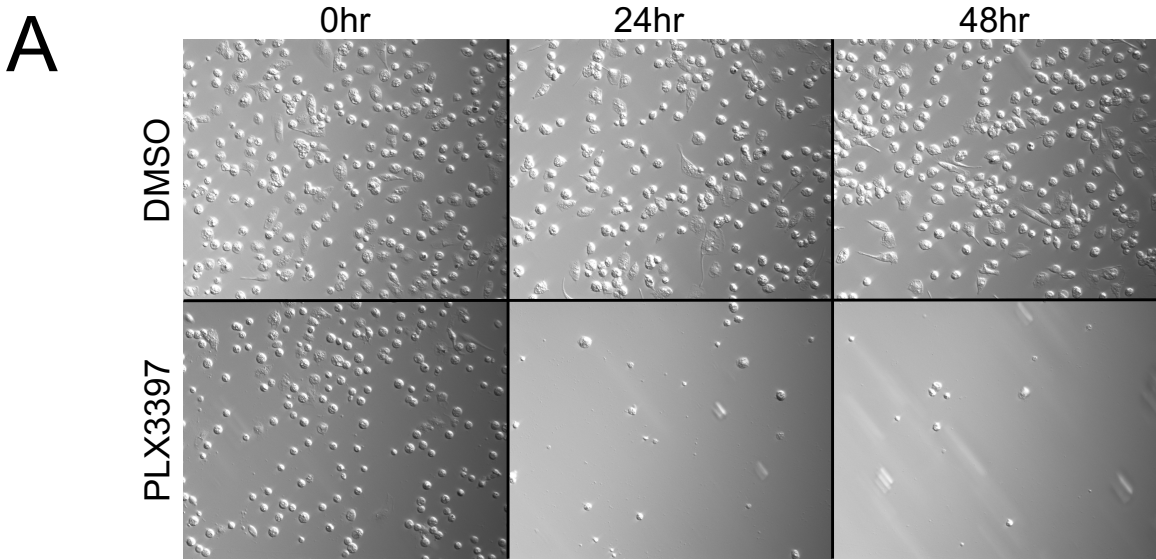
**Figure 4-2: 72 hours of PLX3397 treatment depletes microglia *in vitro*.** Uninfected

pigtailed macaque microglia were treated daily with 10μM PLX3397 in DMSO or with

vehicle (DMSO) alone. (A) Phase microscopy showed a visible decrease in cell number over

48 hours of PLX3397 treatment compared to vehicle control. (B) Cell counts were

determined with interferon-beta qPCR. After 72 hours of PLX3397 treatment, microglia cell

number decreased approximately 84% from baseline. This decrease was significant (P =

0.03, Sidak's multiple comparisons test) and was due to PLX3397 treatment over time (Two-

way ANOVA P < 0.0001).
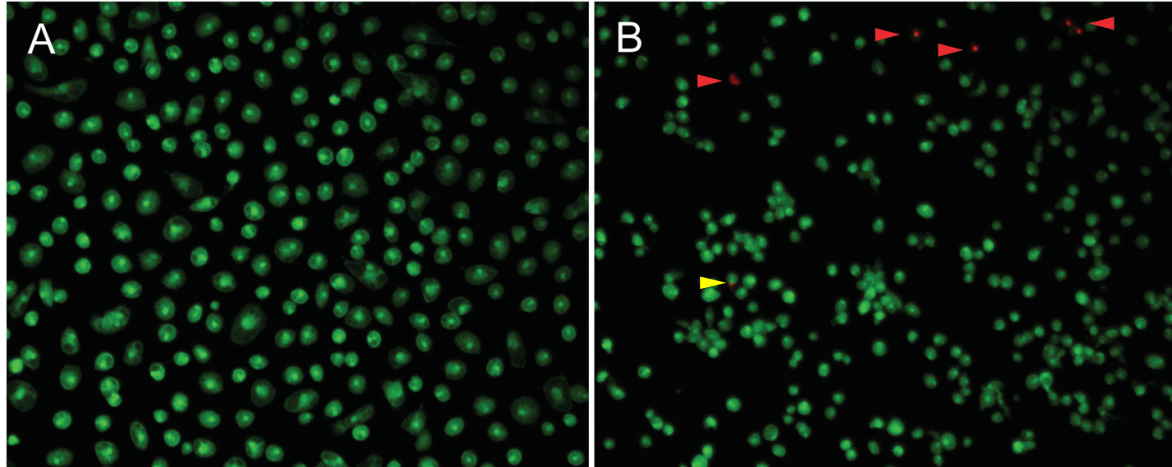
**Figure 4-3. PLX3397 kills primary pigtailed macaque microglia *in vitro*.** Primary

microglia isolated from an uninfected pigtailed macaque were treated for 48 hours with

vehicle (DMSO) (A) or 10μM PLX3397 (B). Live microglia were identified with the uptake

of calcein (green), and dead cells were identified with the uptake of ethidium homodimer

(red). PLX3397 treatment (B) killed cells, and the remaining live cells were smaller and

arranged in clusters.
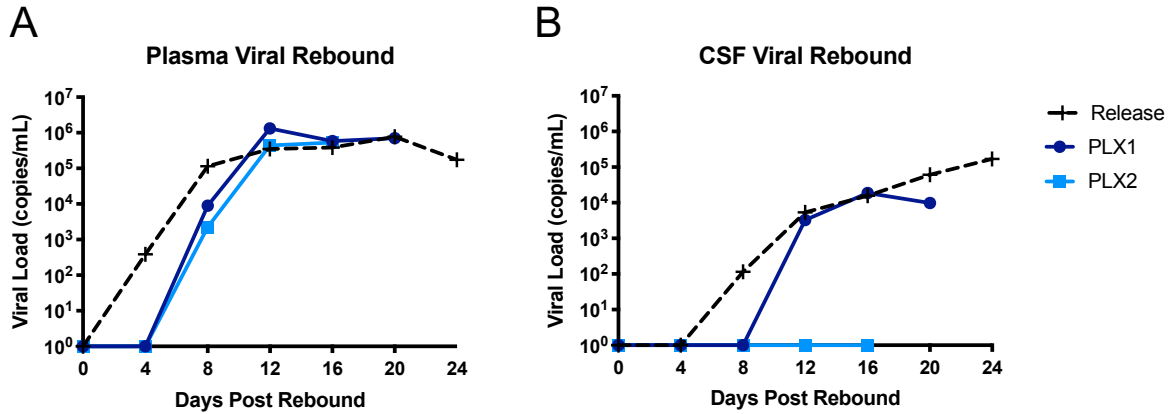
**Figure 4-4. The effect of PLX3397 on plasma and CSF viral rebound kinetics in SIV-infected macaques released from ART.** (A) The kinetics of viral rebound in the plasma of PLX3397 treated animals was no different compared to procedural control animals (Release). (B) While the viral rebound kinetics in the CSF was not affected in PLX1, CSF viral rebound did not occur in PLX2 16 days post-release from ART.
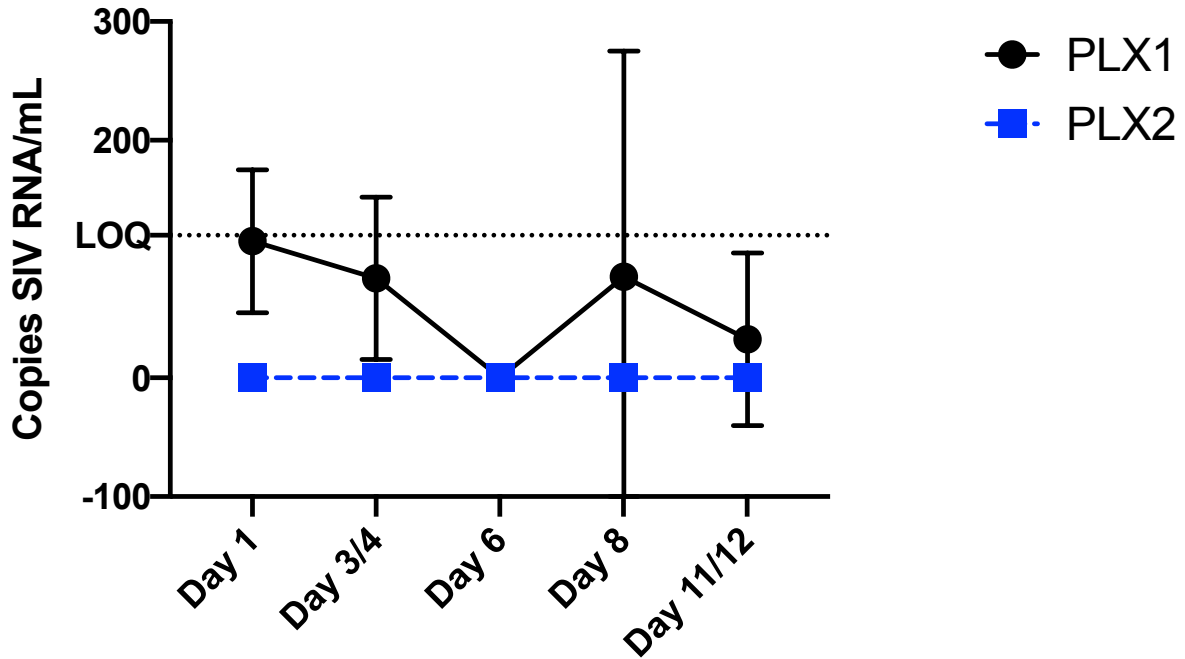
**Figure 4-5. Viral outgrowth of microglia isolated from SIV-infected macaques treated with PLX3397 and released from ART.** Virus RNA was detectable in the supernatants of microglia isolated from the brain of PLX1 (black). However, virus RNA was undetectable in the supernatants of microglia isolated from the brain of PLX2 (blue). Limit of quantitation (LOQ) was 120 copies viral RNA/mL. Limit of detection was 1 copy viral RNA/mL.
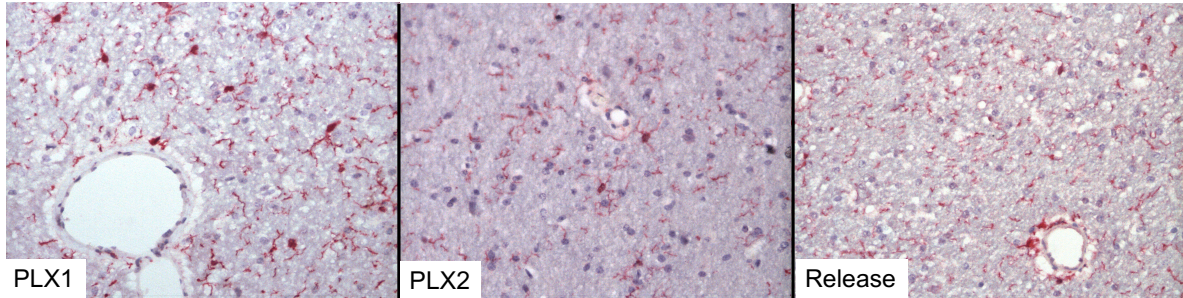
**Figure 4-6. The effect of PLX3397 treatment on microglial viability *in vivo*.** IBA1+ immunostaining (red) in frontal cortex white matter of PLX1 showed a change in microglial morphology, including enlarged nuclei and longer projections compared to procedural controls (Release group as detailed in methods). In PLX2, there was a reduction in IBA1+ staining compared to procedural controls. Additionally, the microglia remaining had similar morphologic changes seen in PLX1.
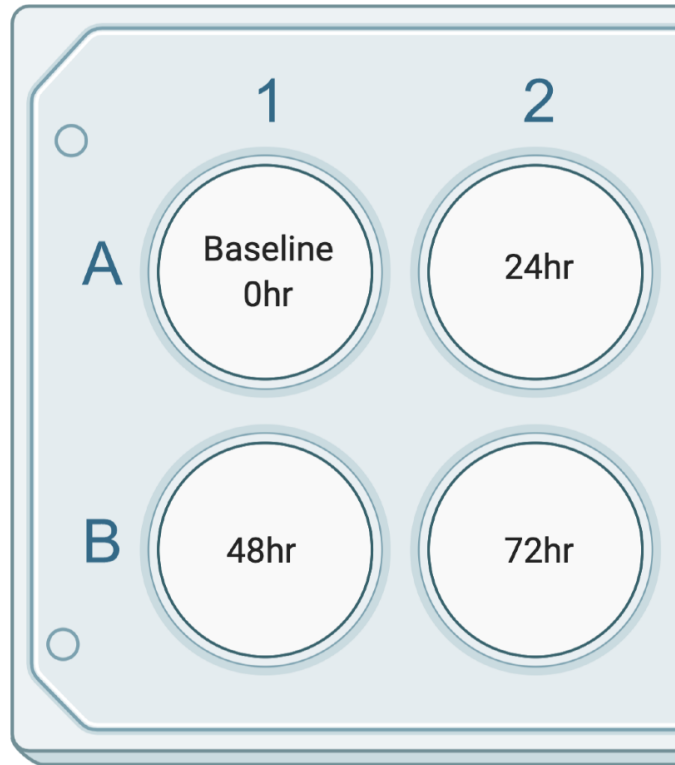
**Supplemental Figure 4-1. Microglia *in vitro* experiment template.** For all microglia *in vitro* experiments described, microglia were plated in four wells of a six-well plate in duplicate. Brightfield images, live/dead immunofluorescence staining and imaging, and cell lysates for interferon-beta qPCR were collected at the timepoints indicated above.

**Chapter V.**

**Summary and Future Directions**

HIV associated neurocognitive disorders (HAND) remain a significant issue in the ART era (Saylor et al. 2016). The work presented here elucidated the role of chronic microglial activation, specifically via colony stimulating factor 1 (CSF1) and its receptor colony stimulating factor 1 receptor (CSF1R), in HAND using an accelerated SIV/pigtailed macaque model of HIV CNS disease (Beck et al. 2015; Beck et al. 2018; Beck et al. 2015). In **Chapter II**, we showed that in this model, *CSF1* mRNA levels were significantly increased with the development of SIV encephalitis in the frontal cortex, and this increase was strongly positively correlated with several genes associated with increased stress and immune activation in the brain. CSF1R protein levels were also significantly increased in the frontal cortex with SIV encephalitis. Interestingly, this increase in CSF1R protein levels continued despite suppressive ART.

**Chapter III** further illustrated microglial responses to chronic SIV infection in the brain. Here I explored expression changes of TREM2, a receptor with several of the same downstream effects of CSF1R signaling and similarly associated with neurodegenerative diseases (Yeh et al. 2017; Akiyama et al. 1996). TREM2 mRNA was significantly increased after 84 days of SIV infection in the brain. TREM2 mRNA was also significantly positively correlated with CSF1 and CSF1R. However, unlike CSF1R, TREM2 protein returned to baseline with suppressive ART. Therefore, although similar, TREM2 and CSF1R have distinct roles in CNS inflammation, specifically in the context of chronic SIV infection.

Interestingly, while CSF1R protein remained elevated with suppressive ART, *CSF1R* mRNA returned to baseline in these animals. This suggests that post-translational modifications or decreased protein degradation maintained CSF1R in this chronically stressed environment. Consequently, we hypothesized that CSF1R is a marker of microglial

priming. Microglial priming is a type of innate immune memory, in which microglia that

have responded to an insult in the past will respond stronger and faster to a second insult.

Because of this, these primed microglia can cause more damage to less stimulus (Neher and

Cunningham 2019). Thus, CSF1R may also be a target for suppressing chronic immune

stimulation that persists in the CNS despite ART.

In **Chapter IV**, we showed evidence that CSF1R is an intriguing target to remove the

latent SIV reservoir in the brain and reset primed microglia. The small molecule CSF1R

inhibitor, PLX3397, effectively killed primary pigtailed macaque microglia *in vitro. In vivo*,

PLX3397 treatment of SIV infected macaques prevented viral rebound in the CSF in one of

two animals. This suggested that CSF1R inhibition can reduce the latent viral reservoir in the

brain. PLX3397 treatment consistently reduced the number of microglia in rodent brain over

90% (Han et al. 2017; Elmore et al. 2015; Jin et al. 2017; Li et al. 2017; Szalay et al. 2016).

While this was the case for nonhuman primate microglia *in vitro*, microglia were not

depleted to this extent *in vivo*. This is likely because maximal drug concentrations were not

achieved in this preliminary study. It is also important to note that rodent microglia and

primate microglia, including human microglia, are quite different (Geirsdottir et al 2019).

There is a core signature of microglia genes across species, including classic markers of

microglia, such as SPI1, P2RY12, and TREM2. However, metabolic and immune pathway

genes diverge from rodents to primates. Importantly, genes associated with

neurodegeneration in humans were poorly correlated with those seen in mouse models of

these diseases. Macaque microglial signatures, however, were closely correlated to those in

human Alzheimer's disease and Parkinson's disease (Geirsdottir et al. 2019). Consequently,

it is also possible that *in vivo*, CSF1R signaling may not be as vital to cell survival in

primates. When plated, microglia adopt an activated immunophenotype (Bohlen et al 2017). Thus, we hypothesize that CSF1R signaling is essential for the survival of activated microglia, but resting microglia may not be as sensitive to CSF1R inhibition.

Interestingly, the microglia that remained had a different morphology compared to other animals released from ART. These microglia had longer, more branched projections, representing a surveilling or resting phenotype compared to the ameboid, activated phenotype seen in the other SIV-infected release animals (Hanisch and Kettenmann 2007; Kreutzberg 1996). This suggests that CSF1R signaling is also important for microglial activation and immune responses in addition to survival. It has also been proposed that in addition to depleting microglia, CSF1R inhibition 'stuns' microglia, preventing microglial replication (Gerber et al 2018). Future studies with BrdU labeling would be necessary to determine changes in microglial replication in PLX3397-treated SIV-infected animals.

Ongoing, we will determine how CSF1R signaling directly impacts microglial phenotype and immune responses including obtaining single-cell RNA sequencing microglia data from PLX3397 treated and untreated animals. We are also interested in identifying the chronic transcriptomic perturbances present in fully suppressed, SIV-infected brain. It has been inferred that chronic inflammation is a major contributor to CNS impairment in fully suppressed HIV infected individuals (Saylor et al. 2016). However, the field's ability to identify clear therapeutic targets and consistent changes is limited by a lack of access to tissues from persons living with HIV. We are performing whole transcriptome sequencing of basal ganglia from SIV/macaque groups outlined in **Table 5-1**.

There are several limitations to doing bulk tissue RNA sequencing in the brain when attempting to characterize glial transcriptomic changes, particularly microglial changes. This

is primarily due to the low percentage of microglial cells in the brain compared to other cells (Lawson et al 1990). To circumvent this limitation, we will be projecting our RNA-sequencing data into single cell transcriptome datasets previously published (Cahoy et al 2008; Li et al 2019; Zamanian et al 2008). Projection analysis allows gene expression data from other related experiments to be visualized, or "projected", into dimensions defined by the dataset of interest (Stein-O'Brien et al. 2019; Sharma et al 2020). We will perform several analyses, including principal component analysis (PCA), clustering, and non-negative matrix factorization (NMF). These analyses will define the dimensions that we will then be able to project into single-cell sequencing datasets as well as other neurodegenerative disease sequencing datasets.

To test the efficacy of projecting our pigtailed macaque sequencing datasets into human data, we projected the PCA from our Nanostring dataset described in **Chapter II** into HIV data. As we saw from the Nanostring panel described in **Chapter II** (Knight et al. 2018; Meulendyke et al. 2014), *SOD2* and *GFAP* mRNA counts were significantly upregulated after 84 days of SIV infection (**Figure 5-1A, B**; $P = 0.002$ and $P = 0.03$ respectively). To determine whether these changes also occurred in individuals infected with HIV, we utilized the National NeuroAIDS Tissue Consortium brain microarray data previously published (Gelman et al. 2012). *SOD2* (**Figure 5-1C**; $P = 0.001$) and *GFAP* (**Figure 5-1D**; $P = 0.0002$) expression was also significantly increased in individuals with HIV encephalitis (HIVE) compared to uninfected individuals.

While this shows similarities in transcriptional changes in SIVE and HIVE, this method is restricted to interrogating a few genes. To be able to determine transcriptional program changes, global analyses must be utilized. To this end, we performed principal

component analysis (PCA) on the normalized Nanostring expression data using the prcomp(.)

function with centering, but not scaling, in R. For this analysis, we utilized data from two

groups: uninfected controls and SIV infected animals with encephalitis. One gene was

removed (*MAP2*) from this analysis because one of the uninfected controls was not

sequenced for this gene.  PC1 accounted for 79.1% of the variance between samples, while

PC2 accounted for 9.15% of the variance (**Figure 5-2A** and data not shown). The SIV group

clusters away from the uninfected controls along PC1. Additionally, SIV animals without

encephalitis (negative) clustered closer to the uninfected animals than the SIV 84d animals

with encephalitis. The weights for individual genes in this PC1 indicate the extent to which

each gene contributes to this major trajectory of expression change in SIV infection. Among

the individual genes driving PC1, *B2M* (MHC I), *SOD2* and *GFAP* were among the top 3

differentially expressed genes (gene weights for PC1 and uncorrected Mann-Whitney p-

values listed in **Supplemental Table 1**).

Using weights from this PCA, data from other experiments can be projected into this

low-dimensional space defined by SIV infection expression change. Gene expression data

from HIV infection (Gelman et al. 2012) was projected into the SIV PC1 using projectR

(https://github.com/genesofeve/projectoR ; Stein-O'Brien et al. 2019; Sharma et al 2020).

Two of the four groups (uninfected and HIVE) in the National NeuroAIDS Tissue

Consortium (NNTC) brain microarray previously published (Gelman et al. 2012) were

included in this analysis. To relate the dynamics of this SIV infection model to HIV

infection, we projected gene expression data from uninfected and HIV-infected with

encephalitis (HIVE) postmortem brain tissue (Gelman et al. 2012) into the transcriptional

space defined by the individual gene weights from PC1 using projectR (Stein-O'Brien et al.

2019; Sharma et al 2020). This projection produced a clear separation between the HIVE

samples and the uninfected control samples (**Figure 5-2B**). The genes primarily driving this

separation are again *B2M*, *SOD2* and *GFAP* (**Supplemental Table 1**). Consequently,

expression changes in *B2M*, *SOD2*, and *GFAP* are characteristic of both SIV encephalitis and

HIV encephalitis. This also highlights a similar transcriptional program change occurring in

both SIVE and HIVE.

      This pilot shows that we can utilize this method to gain insights into transcriptomic

changes in our pigtailed macaque model of HIV CNS disease. We are particularly interested

in cell-specific transcriptomic alterations, in particular microglial changes. This method is

also useful for identifying those changes by projecting into single cell sequencing datasets. In

this way, we will be able to determine specific microglial transcriptomic changes in bulk

tissue RNA sequencing. By better understanding the underlying transcriptomic changes, we

will be able to identify new therapeutic targets that may alleviate symptoms and halt the

progression of HIV CNS disease.

| Group | N | Inoculation | Treatment |
|---|---|---|---|
| **Uninfected control** | 7 | N/A | N/A |
| **SIV-infected with encephalitis (SIVE)** | 7 | SIV/17E-Fr (neurovirulent clone) and SIV/deltaB670 (immunosuppressive swarm) | N/A |
| **SIV-infected suppressed with ART** | 7 | SIV/17E-Fr and SIV/deltaB670 | Subcutaneous injection of 2.5mg/kg Dolutegravir, 20mg/kg PMPA, 40mg/kg FTC |
| **Release** | 12 | SIV/17E-Fr and SIV/deltaB670 | Subcutaneous injection of 2.5mg/kg Dolutegravir, 20mg/kg PMPA, 40mg/kg FTC Released from ART |
| **Release + PLX3397** | 2 | SIV/17E-Fr and SIV/deltaB670 | Subcutaneous injection of 2.5mg/kg Dolutegravir, 20mg/kg PMPA, 40mg/kg FTC + 4 weeks of PLX3397 Released from ART; PLX3397 left onboard |

**Table 5-1. Bulk-tissue RNA-Sequencing group descriptions.**

Figure 5-1

A
**SIV SOD2**

B
**SIV GFAP**

C
**HIV SOD2**

D
**HIV GFAP**

113
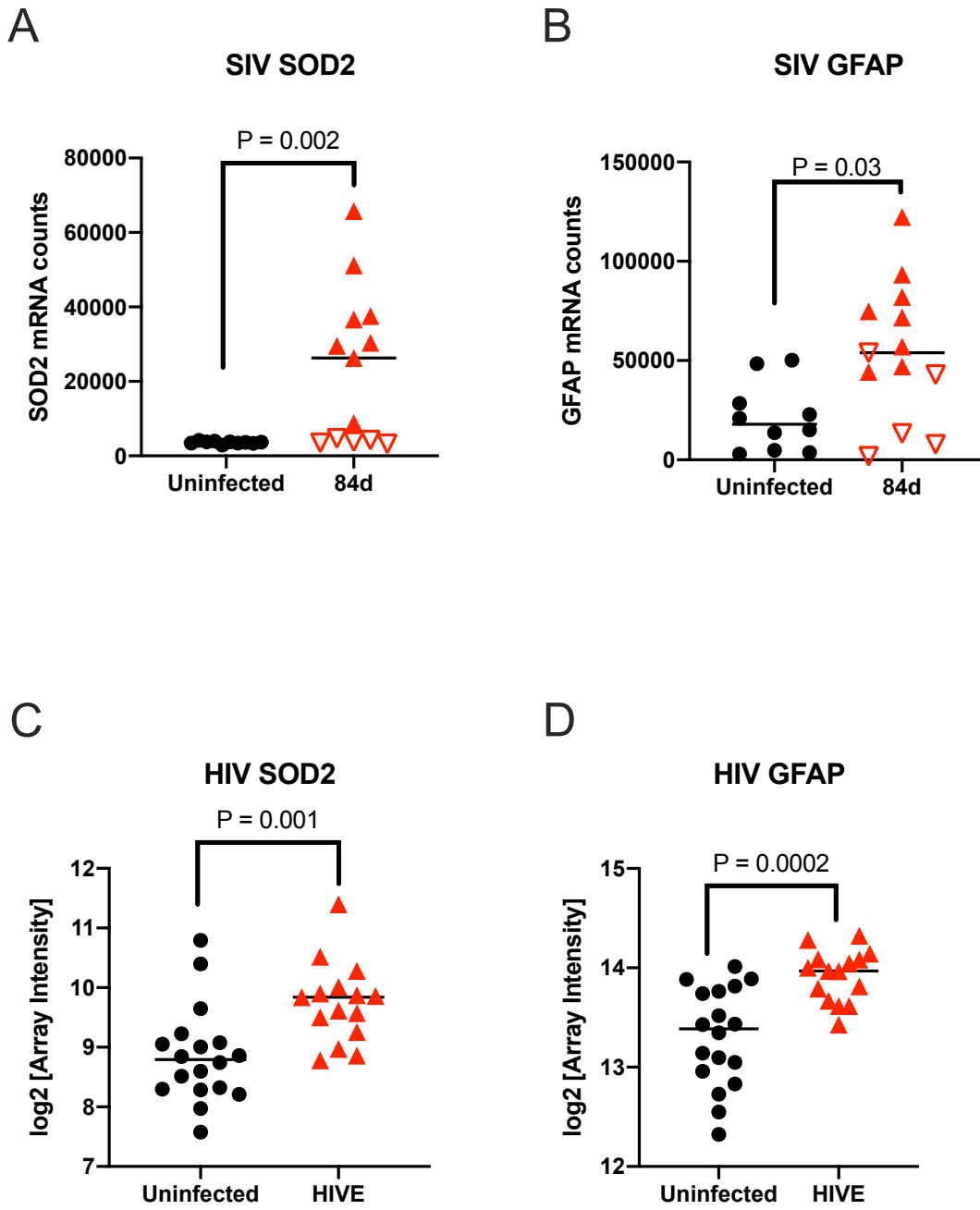
**Figure 5-1. SOD2 and GFAP increase in the brain with SIV and HIV encephalitis.** (A)

SOD2 mRNA counts in the Nanostring panel are significantly increased with SIV infection

at 84 days post infection (dpi) (P = 0.002, Mann-Whitney). Open symbols represent SIV-

infected animals without encephalitis and have the lowest expression of SOD2. (B) GFAP

also increases with SIV at 84dpi (P = 0.03) and is not as elevated in animals without

encephalitis (No encephalitis = ▽; Encephalitis = ▲). Similarly, in HIV encephalitis, SOD2

(C) and GFAP (D) are significantly increased compared to uninfected individuals (P = 0.001,

P = 0.0002 respectively; Mann-Whitney).
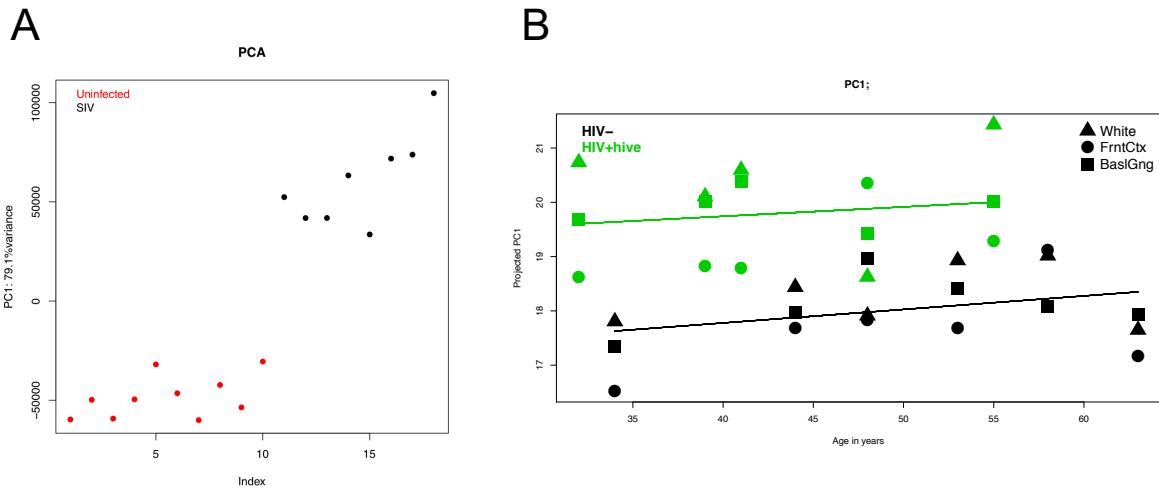
**Figure 5-2. Principal component analysis and subsequent projection from a pigtailed macaque Nanostring panel into a microarray of human brain samples reveals a common transcriptional program in SIV encephalitis and HIV encephalitis.** (A) The first principal component of the PCA from the Nanostring panel separated pigtailed macaques based on SIV encephalitis status. Top genes driving this PC were *B2M*, *GFAP*, and *SOD2*. (B) When this PC was projected into the HIV dataset, it similarly separated samples based on HIV encephalitis status.

115

**Supplemental Table 5-1**

| Gene | SIV.MannWhitney.p | HIV.MannWhitney.p | PC1.weight |
|---|---|---|---|
| B2M | 4.57E-05 | 2.31E-08 | 0.735169457 |
| GFAP | 5.48E-04 | 2.31E-04 | 0.54268943 |
| SOD2 | 4.57E-05 | 1.35E-03 | 0.296681069 |
| UBC | 4.57E-05 | 2.59E-01 | 0.157194288 |
| MX1 | 4.46E-04 | 1.87E-07 | 0.122299989 |
| SIV17E | 4.22E-04 | NA | 0.082118928 |
| CXCL10 | 4.57E-05 | 2.33E-06 | 0.040687098 |
| SLC1A3 | 5.45E-02 | 3.64E-02 | 0.036079262 |
| STAT1 | 4.57E-05 | 9.80E-07 | 0.031145509 |
| GLUL | 4.39E-03 | 5.19E-03 | 0.027469492 |
| ACTB | 2.66E-02 | 7.08E-01 | 0.019467035 |
| CCL2 | 4.46E-04 | 6.29E-04 | 0.016499187 |
| CD163 | 4.57E-05 | 4.58E-03 | 0.014398034 |
| MAOB | 1.37E-03 | 2.02E-02 | 0.013546421 |
| VCAM1 | 4.46E-04 | 8.59E-04 | 0.013346693 |
| GPX1 | 4.57E-05 | 1.06E-02 | 0.012288761 |
| CCL8 | 4.43E-04 | 3.07E-06 | 0.010320694 |
| PRDX1 | 1.37E-03 | 1.90E-01 | 0.010304154 |
| IRF1 | 4.46E-04 | 9.80E-07 | 0.008489555 |
| SOD1 | 8.31E-02 | 8.17E-01 | 0.007267817 |
| SOD3 | 4.57E-05 | 5.32E-01 | 0.006597271 |
| PRDX6 | 1.55E-02 | 5.87E-03 | 0.006594438 |
| STAT3 | 4.57E-05 | 2.33E-06 | 0.006339418 |
| STAT2 | 4.46E-04 | 4.55E-04 | 0.005707637 |
| TGFB2 | 9.14E-05 | 2.10E-04 | 0.005457601 |
| SAMHD1 | 4.57E-05 | 6.29E-04 | 0.005446866 |
| CD68 | 4.57E-05 | 4.03E-03 | 0.004846397 |
| CD14 | 4.57E-05 | 1.18E-02 | 0.004794605 |
| TXN | 3.15E-01 | 4.21E-01 | 0.004664084 |
| IDO1 | 4.40E-04 | 4.21E-01 | 0.004528903 |
| PECAM1 | 4.57E-05 | 5.19E-03 | 0.004461488 |
| ALOX5AP | 4.46E-04 | 9.30E-02 | 0.004397729 |
| CXCL11 | 4.40E-04 | 1.79E-03 | 0.004291584 |
| ICAM1 | 4.46E-04 | 3.81E-01 | 0.004052754 |
| IL18BP | 4.57E-05 | 1.39E-02 | 0.003953579 |
| IRF7 | 4.46E-04 | 5.79E-08 | 0.003941605 |

| | | | |
|---|---|---|---|
| CXCL3 | 4.43E-04 | 7.35E-02 | 0.003933452 |
| CSF1 | 4.57E-05 | 5.18E-06 | 0.003620457 |
| CXCL2 | 4.46E-04 | 3.86E-04 | 0.003573592 |
| CCL3 | 4.40E-04 | 8.60E-02 | 0.003557519 |
| GLRX | 4.57E-05 | 2.15E-01 | 0.00338539 |
| SOCS3 | 4.37E-04 | 1.87E-03 | 0.003308956 |
| CLEC4A | 4.46E-04 | 2.29E-01 | 0.003153184 |
| MAOA | 6.19E-02 | 1.45E-01 | 0.002852908 |
| TLR2 | 4.43E-04 | 6.63E-03 | 0.002671742 |
| TXNRD1 | 1.37E-03 | 3.01E-02 | 0.002645311 |
| IRF3 | 2.16E-03 | 1.61E-04 | 0.002565541 |
| TLR4 | 3.20E-04 | 9.43E-03 | 0.002329879 |
| ZFP36 | 4.46E-04 | 1.00E-03 | 0.00211074 |
| GPX3 | 9.29E-01 | 9.29E-01 | 0.002097262 |
| CXCL9 | 4.40E-04 | 1.26E-01 | 0.002026642 |
| ITGAM | 4.46E-04 | 8.60E-02 | 0.001981872 |
| PCNA | 4.57E-05 | 7.32E-02 | 0.001973239 |
| CCL19 | 4.46E-04 | 2.02E-02 | 0.001939058 |
| SRXN1 | 1.17E-02 | 7.35E-01 | 0.001855749 |
| TGFB1 | 1.17E-02 | 4.03E-03 | 0.001811702 |
| RPS9 | 9.12E-02 | 1.55E-01 | 0.001797939 |
| CCBL2 | 8.55E-03 | 8.17E-01 | 0.00178486 |
| IL18 | 3.43E-02 | 6.63E-03 | 0.001621556 |
| TLR3 | 4.57E-05 | 2.25E-03 | 0.001597187 |
| CAT | 1.17E-02 | 1.06E-02 | 0.001440789 |
| CXCL12 | 4.39E-03 | 7.08E-01 | 0.001240178 |
| STAT5A | 4.46E-04 | 5.87E-03 | 0.001212507 |
| CCL4L1 | 4.43E-04 | NA | 0.001154275 |
| CYBA | 8.68E-04 | 6.63E-03 | 0.001124932 |
| COMT | 2.66E-02 | 3.10E-03 | 0.001083953 |
| TJP2 | 1.82E-01 | 1.82E-02 | 0.001023283 |
| APOBEC3G | 4.31E-04 | 4.01E-01 | 0.000973043 |
| DES | 4.46E-04 | 9.57E-01 | 0.000931278 |
| IL1B | 3.86E-03 | 6.56E-01 | 0.000919173 |
| SOCS1 | 4.43E-04 | 3.25E-01 | 0.000917126 |
| CCR1 | 1.83E-04 | 5.87E-03 | 0.000905665 |
| MMP2 | 9.99E-04 | 7.36E-04 | 0.000899559 |
| TLR1 | 1.37E-03 | 6.74E-02 | 0.000895813 |
| KYNU | 4.40E-04 | 3.43E-01 | 0.000869042 |

| | | | |
|---|---|---|---|
| PDGFA | 2.74E-01 | 1.82E-02 | 0.00086899 |
| TGFB3 | 9.12E-02 | 8.17E-01 | 0.000857405 |
| TYK2 | 5.48E-04 | 1.61E-04 | 0.000820597 |
| EDN1 | 4.39E-03 | 2.24E-02 | 0.000809721 |
| GZMB | 4.46E-04 | 1.87E-03 | 0.000760621 |
| CCR5 | 4.40E-04 | 1.18E-02 | 0.000755522 |
| CD16 | 4.43E-04 | NA | 0.000734899 |
| TBXAS1 | 4.40E-04 | 3.61E-01 | 0.000725665 |
| PTPRC | 4.46E-04 | 1.32E-02 | 0.000725176 |
| FAS | 4.46E-04 | 2.73E-02 | 0.000691356 |
| CD4 | 5.04E-03 | 3.43E-01 | 0.000687411 |
| TLR8 | 4.46E-04 | 9.29E-01 | 0.000670881 |
| CCL24 | 1.55E-02 | 4.86E-01 | 0.000657373 |
| TNFRSF10B | 4.46E-04 | 4.42E-01 | 0.000650675 |
| PDLIM1 | 2.46E-03 | 1.32E-06 | 0.000639734 |
| GSTZ1 | 3.06E-03 | 7.35E-01 | 0.000639177 |
| SELE | 6.04E-04 | 2.06E-03 | 0.000637933 |
| MKI67 | 4.28E-04 | 8.17E-01 | 0.000597115 |
| TP53 | 4.57E-05 | 5.67E-03 | 0.000572586 |
| KMO | 4.40E-04 | 6.56E-01 | 0.000568687 |
| TLR6 | 2.90E-03 | 7.08E-01 | 0.00054887 |
| CCL5 | 6.16E-04 | 1.06E-02 | 0.000529295 |
| PRDX4 | 2.63E-02 | 4.64E-01 | 0.000511853 |
| TNFRSF10A | 1.83E-04 | 5.32E-01 | 0.000494198 |
| GSR | 7.53E-02 | 1.18E-02 | 0.000469111 |
| ALOX5 | 1.59E-03 | 6.00E-01 | 0.000440451 |
| IFNB1 | 4.31E-04 | 9.71E-01 | 0.000427732 |
| TNFA | 4.25E-04 | NA | 0.000416894 |
| HMBS | 2.63E-02 | 3.31E-02 | 0.000409937 |
| IL6 | 4.34E-04 | 4.04E-03 | 0.000376125 |
| OGT | 5.15E-01 | 7.32E-02 | 0.000366476 |
| TLR7 | 1.20E-01 | 4.70E-01 | 0.000348253 |
| IL7 | 4.40E-04 | 1.61E-04 | 0.000342663 |
| NGF | 6.22E-03 | 6.30E-01 | 0.000333833 |
| CCL7 | 4.40E-04 | 6.30E-01 | 0.000321639 |
| CXCR4 | 2.16E-03 | 5.22E-02 | 0.000316939 |
| GSS | 4.50E-01 | 8.45E-01 | 0.000295468 |
| CD69 | 6.04E-04 | 2.47E-02 | 0.000291231 |
| IFNAR1 | 4.50E-01 | 5.36E-04 | 0.000254843 |

| | | | |
|---|---|---|---|
| TNFSF10 | 4.03E-02 | 1.32E-02 | 0.000254065 |
| GPX7 | 6.62E-03 | 5.51E-01 | 0.000225074 |
| QPRT | 1.68E-01 | 1.56E-03 | 0.000200203 |
| MMP9 | 3.22E-03 | 9.86E-01 | 0.000180675 |
| MPV17 | 7.53E-02 | 6.56E-01 | 0.000179366 |
| TLR5 | 2.34E-02 | 3.10E-03 | 0.000168241 |
| SLC2A1 | 8.39E-03 | 2.87E-02 | 0.000168083 |
| EGF | 2.07E-02 | 3.10E-03 | 0.000166419 |
| CNTF | 2.30E-01 | 8.17E-01 | 0.000152269 |
| CCL11 | 8.56E-03 | 6.30E-01 | 0.000128756 |
| CCR2 | 1.09E-03 | 9.43E-03 | 0.000123929 |
| IL4 | 2.92E-02 | 2.59E-01 | 0.000118935 |
| PLA2G6 | 1.55E-01 | 2.29E-01 | 0.000114646 |
| IL13 | 7.59E-03 | 8.45E-01 | 0.000112405 |
| DGCR8 | 7.22E-01 | 1.34E-04 | 9.84E-05 |
| SELP | 4.98E-02 | 3.61E-01 | 9.81E-05 |
| PDGFB | 1.20E-01 | 8.60E-02 | 9.77E-05 |
| NOS2 | 9.09E-02 | 4.21E-01 | 9.29E-05 |
| TDO2 | 4.04E-02 | 1.53E-01 | 8.30E-05 |
| CCL20 | 7.28E-03 | 2.72E-03 | 6.16E-05 |
| FASLG | 3.57E-02 | 6.56E-01 | 5.80E-05 |
| CD8B | 2.88E-02 | 5.09E-01 | 5.67E-05 |
| XCL1 | 1.55E-01 | 8.45E-01 | 5.65E-05 |
| IFNG | 9.59E-03 | 2.74E-01 | 5.37E-05 |
| MBL2 | 8.13E-02 | 1.43E-01 | 5.25E-05 |
| IFNA1 | 5.34E-01 | 9.86E-01 | 4.38E-05 |
| LIN28A | 1.41E-01 | 1.55E-01 | 4.38E-05 |
| GPR35 | 1.40E-01 | 1.78E-01 | 4.28E-05 |
| CCR7 | 1.41E-03 | 2.90E-01 | 4.03E-05 |
| PTGES | 1.67E-01 | 5.69E-02 | 3.68E-05 |
| IL17F | 2.28E-02 | 2.29E-01 | 3.50E-05 |
| SDHA | 8.29E-01 | 3.07E-01 | 3.31E-05 |
| IL27 | 1.52E-01 | 1.78E-01 | 2.76E-05 |
| ALOX15B | 3.49E-01 | 4.37E-02 | 2.68E-05 |
| IL25 | 5.33E-01 | 2.29E-01 | 2.48E-05 |
| IL12A | 6.61E-02 | 2.90E-01 | 2.44E-05 |
| NTF4 | 2.08E-01 | NA | 2.34E-05 |
| IL29 | 3.06E-01 | NA | 2.05E-05 |
| IL9 | 1.80E-01 | 5.32E-01 | 1.88E-05 |

| | | | |
|---|---|---|---|
| ASMT | 5.03E-01 | 5.56E-01 | 1.86E-05 |
| CXCR3 | 2.65E-01 | 1.08E-01 | 1.52E-05 |
| IL2 | 5.61E-01 | 7.08E-01 | 1.12E-05 |
| AGER | 2.12E-01 | 1.00E-01 | 1.07E-05 |
| PTGS2 | 4.09E-02 | 7.95E-02 | 9.72E-06 |
| IL10 | 3.47E-01 | 9.86E-01 | 9.20E-06 |
| SLC6A3 | 2.76E-01 | 1.08E-01 | 8.67E-06 |
| NOX5 | 6.23E-01 | 6.30E-01 | 2.79E-06 |
| ALOX12 | 4.76E-01 | 8.45E-01 | 1.40E-06 |
| IL4I1 | 8.24E-01 | 2.73E-02 | 1.16E-06 |
| CD3D | 4.77E-01 | 1.17E-01 | -3.09E-07 |
| AANAT | 7.89E-01 | 4.01E-01 | -1.56E-06 |
| IL11 | 6.22E-01 | 9.29E-01 | -1.91E-06 |
| IL12RB2 | 8.24E-01 | 6.56E-01 | -2.13E-06 |
| CSF2 | 9.29E-01 | 8.73E-01 | -2.17E-06 |
| SLC6A4 | 9.29E-01 | 9.86E-01 | -2.62E-06 |
| TLR9 | 9.64E-01 | 4.37E-02 | -5.73E-06 |
| TH | 6.56E-01 | 2.02E-01 | -6.01E-06 |
| TPH2 | 5.93E-01 | 6.56E-01 | -6.91E-06 |
| IL8RA | 1.00E+00 | NA | -7.60E-06 |
| PTGIS | 9.64E-01 | 8.73E-01 | -7.67E-06 |
| GDNF | 8.94E-01 | 4.86E-01 | -8.89E-06 |
| MPL | 8.59E-01 | 6.56E-01 | -1.07E-05 |
| STAT5B | 1.00E+00 | 9.30E-02 | -1.07E-05 |
| EPO | 7.88E-01 | 5.32E-01 | -1.20E-05 |
| MMP7 | 2.27E-01 | 5.04E-01 | -1.48E-05 |
| FOXP3 | 4.76E-01 | 4.64E-01 | -1.49E-05 |
| PF4 | 1.29E-01 | 7.35E-01 | -1.55E-05 |
| MPO | 6.56E-01 | 4.01E-01 | -1.74E-05 |
| AOX1 | 2.26E-01 | 9.57E-01 | -1.75E-05 |
| THPO | 9.29E-01 | 9.29E-01 | -1.93E-05 |
| CCL1 | 3.25E-01 | 3.20E-01 | -1.98E-05 |
| PLA2G2A | 8.06E-02 | 6.52E-02 | -2.06E-05 |
| CCR3 | 3.25E-01 | 7.89E-01 | -2.07E-05 |
| CLEC4C | 3.97E-01 | 5.09E-01 | -2.23E-05 |
| IL17A | 7.20E-01 | 8.85E-01 | -2.62E-05 |
| CCR4 | 2.83E-01 | 9.86E-01 | -2.69E-05 |
| VEGFA | 8.59E-01 | 1.00E+00 | -3.64E-05 |
| DDC | 9.02E-02 | 1.78E-01 | -3.66E-05 |

| | | | |
|---|---|---|---|
| ARG1 | 1.18E-01 | 2.74E-01 | -3.90E-05 |
| IL12B | 8.14E-02 | 5.56E-01 | -4.26E-05 |
| TPO | 4.22E-01 | 5.09E-01 | -4.37E-05 |
| IDO2 | 6.02E-02 | 5.56E-01 | -4.42E-05 |
| DAO | 2.85E-01 | 2.02E-01 | -4.64E-05 |
| CYP1A1 | 2.66E-01 | 7.62E-01 | -5.22E-05 |
| ARG2 | 5.73E-01 | 1.17E-01 | -5.67E-05 |
| CHRNA7 | 7.56E-01 | NA | -6.52E-05 |
| VEGFC | 7.56E-01 | 5.32E-01 | -6.54E-05 |
| TNRC6A | 7.62E-01 | 4.78E-02 | -6.82E-05 |
| NTF3 | 6.17E-02 | 3.07E-01 | -7.91E-05 |
| EIF2C2 | 8.97E-01 | NA | -8.03E-05 |
| TBP | 5.94E-01 | 9.01E-01 | -8.65E-05 |
| TGFA | 4.49E-01 | 4.01E-01 | -8.70E-05 |
| PDGFC | 9.65E-01 | 1.82E-02 | -8.86E-05 |
| PDGFD | 1.81E-01 | 7.62E-01 | -9.53E-05 |
| ALOX15 | 8.09E-02 | 4.01E-01 | -0.000127142 |
| HAAO | 4.23E-01 | 1.08E-01 | -0.000152081 |
| TARBP2 | 2.86E-01 | 1.55E-01 | -0.000173737 |
| PRDX3 | 9.65E-01 | 9.29E-01 | -0.000191979 |
| PTGS1 | 1.85E-02 | 3.43E-01 | -0.000202329 |
| VEGFB | 3.15E-01 | 6.74E-02 | -0.000223901 |
| CAMK2D | 9.65E-01 | 7.94E-02 | -0.000228758 |
| CCBL1 | 6.89E-01 | 7.35E-01 | -0.000229115 |
| CCS | 4.08E-02 | 4.58E-03 | -0.000246011 |
| TRIM32 | 6.89E-01 | 5.80E-01 | -0.000251882 |
| TXNRD2 | 2.47E-01 | 1.64E-02 | -0.000283047 |
| TPH1 | 8.31E-02 | 3.43E-01 | -0.000330341 |
| AADAT | 4.44E-03 | 6.05E-01 | -0.000381198 |
| GLS2 | 1.46E-01 | 7.89E-01 | -0.000386027 |
| BDNF | 7.22E-01 | 9.28E-01 | -0.000522046 |
| PTGES2 | 1.42E-01 | 1.00E+00 | -0.000679475 |
| DICER1 | 6.22E-03 | 3.54E-03 | -0.000735301 |
| CHRNA4 | 1.01E-01 | 1.53E-01 | -0.00076971 |
| CNOT8 | 1.37E-03 | 2.15E-01 | -0.001111782 |
| EIF2C1 | 2.05E-02 | NA | -0.001121491 |
| TJP1 | 3.60E-01 | 4.55E-04 | -0.001614356 |
| GOT2 | 8.55E-03 | 1.45E-01 | -0.001634541 |
| GPX4 | 1.01E-01 | 9.57E-01 | -0.001638447 |

| | | |
|---|---|---|
| DROSHA | 2.05E-02 | 6.56E-01 | -0.00169264 |
| CX3CR1 | 4.34E-02 | 2.74E-01 | -0.002187448 |
| GLUD1 | 1.46E-01 | 6.05E-01 | -0.002279373 |
| PRDX2 | 1.83E-04 | 9.01E-01 | -0.002399655 |
| CHRNB2 | 1.60E-03 | 3.07E-01 | -0.002428287 |
| STK25 | 2.03E-01 | 1.78E-01 | -0.002452983 |
| GOT1 | 4.57E-05 | 5.32E-01 | -0.002750809 |
| CAMK2G | 2.05E-02 | 4.21E-01 | -0.003074029 |
| CX3CL1 | 3.60E-01 | 9.86E-01 | -0.003219831 |
| TUBB3 | 5.45E-02 | 4.64E-01 | -0.003931965 |
| HPRT1 | 2.06E-03 | 5.09E-01 | -0.005920692 |
| RPL13A | 4.60E-01 | 7.94E-02 | -0.006246049 |
| CAMK2B | 1.01E-01 | 4.70E-01 | -0.007263731 |
| PRNP | 1.46E-01 | 7.08E-01 | -0.007819734 |
| GLS | 9.14E-05 | 5.80E-01 | -0.009282091 |
| RBFOX3 | 4.34E-02 | 9.86E-01 | -0.00934925 |
| PTGDS | 6.33E-01 | 4.86E-01 | -0.010164182 |
| ENO2 | 3.06E-03 | 5.32E-01 | -0.013313325 |
| SYP | 5.48E-04 | 1.00E+00 | -0.014818987 |
| CAMK2A | 1.01E-01 | 7.08E-01 | -0.016681366 |
| DLG4 | 5.45E-02 | 8.73E-01 | -0.016972488 |
| GAPDH | 8.55E-03 | 3.25E-01 | -0.022098575 |
| APP | 8.68E-04 | 5.32E-01 | -0.027132085 |
| YWHAZ | 1.37E-03 | 7.35E-01 | -0.040272758 |
| TSPAN7 | 6.22E-03 | 4.42E-01 | -0.054687197 |
| MBP | 2.37E-01 | 6.30E-01 | -0.057582173 |
| SNAP25 | 2.66E-02 | 2.15E-01 | -0.063145012 |
| SLC1A2 | 6.22E-03 | 7.89E-01 | -0.094505575 |

**Supplemental Table 5-1. Genes from the pigtailed macaque Nanostring panel PC1 projected into the HIV encephalitis microarray panel that had a weight greater than or less than zero.** Weights closer to +1 or -1 have the strongest effect in the sample separation in the projection. Because the HIVE samples separated higher than the uninfected samples, genes with a positive PC weight have the strongest effect. Similar to the SIV PC1, B2M, GFAP, and SOD2 have the strongest weight in separating HIVE from uninfected samples. NAs indicate genes that were not included in the HIV microarray panel. The red to blue gradient represents the strongest positive (red) and strongest negative (blue) PC1 weights.

**REFERENCES**

**Chapter I**

Abreu CM, Veenhuis RT, Avalos CR, Graham S, Queen SE, Shirk EN, Bullock BT, Li M, Metcalf Pate KA, Beck SE, Mangus LM, Mankowski JL, Clements JE, Gama L. (2019) Infectious virus persists in CD4+ T cells and macrophages in antiretroviral therapy-suppressed simian immunodeficiency virus-infected macaques. J Virol. Doi: 10.1128/JVI.00065-19

Akiyama H, Nishimura T, Kondo H, Ikeda K, Hayashi Y, McGeer PL (1994) Expression of the receptor for macrophage colony stimulating factor by brain microglia and its upregulation in brains of patients with Alzheimer's disease and amyotrophic lateral sclerosis. Brain Res. Doi: 10.1016/0006-8993(94)91779-5

Antiretroviral Therapy Cohort, Collaboration (2017) Survival of HIV-positive patients starting antiretroviral therapy between 1996 and 2013: a collaborative analysis of cohort studies. Lancet HIV. Doi: 10.1016/S2352-3018(17)30066-8

Barre-Sinoussi F, Chermann JC, Rey F, Nugeyre MT, Chamaret S, Gruest J, Dauguet C, Axler-Blin C, Vezinet-Brun F, Rouzioux C, Rozenbaum W, Montagnier L (1983) Isolation of a T-lymphotropic retrovirus from a patient at risk for acquired immune deficiency syndrome (AIDS). Science. Doi: 10.1126/science.6189183

Bashiri K, Rezaei N, Nasi M, Cossarizza A (2018) The role of latency reversal agents in the cure of HIV: A review of current data. Immunol Lett. Doi: 10.1016/j.imlet.2018.02.004

Beck SE, Kelly KM, Queen SE, Adams RJ, Zink MC, Tarwater PM, Mankowski JL (2015) Macaque species susceptibility to simian immunodeficiency virus: increased

incidence of SIV central nervous system disease in pigtailed macaques versus rhesus

    macaques. J Neurovirol. Doi: 10.1007/s13365-015-0313-7

Beck SE, Queen SE, Metcalf Pate KA, Mangus LM, Abreu CM, Gama L, Witwer KW,

    Adams RJ, Zink MC, Clements JE, Mankowski JL (2018) An SIV/Macaque model

    targeted to study HIV-associated neurocognitive disorders. J Neurovirol. Doi:

    10.1007/s13365-017-0582-4

Bonsignori M, Montefiori DC, Wu X, Chen X, Hwang KK, Tsao CY, Kozink DM, Parks RJ,

    Tomaras GD, Crump JA, Kapiga SH, Sam NE, Kwong PD, Kepler TB, Lio HX,

    Mascola JR, Haynes BF (2012) Two distinct broadly neutralizing antibody

    specificities of different clonal lineages in a single HIV-1 infected donor:

    implications for vaccine design. J Virol. Doi: 10.1128/JVI.07163-11

Cartier N, Lewis CA, Zhang R, Rossi FM (2014) The role of microglia in human disease:

    therapeutic tool or target? Acta Neuropathol. Doi: 10.1007/s00401-014-1330-y

Chen NC, Partridge AT, Sell C, Torres C, Martin-Garcia J (2017) Fate of microglia during

    HIV-1 infection: From activation to senescence? Glia. Doi: 10.1002/glia.23081

Clutton GT and Jones RB (2018) Diverse impacts of HIV latency-reversing agents on CD8+

    T-cell function: Implications for HIV cure. Front Immunol. Doi:

    10.3389/fimmu.2018.01452

Colonna M and Butovsky O (2017) Microglia function in the central nervous system during

    health and neurodegeneration. Annu Rev Immunol. Doi: 10.1146/annurev-immunol-

    051116-052358

Day TA and Kublin JG (2013) Lessons learned from HIV vaccine clinical efficacy trials.

    Curr HIV Res. Doi: 10.2174/1570162x113116660051

Dohgu S and Banks WA (2013) Brain pericytes increase the lipopolysaccharide-enriched

transcytosis of HIV-1 free virus across the in vitro blood-brain barrier: evidence for

cytokine-mediated pericyte-endothelial cell crosstalk. Fluids Barriers CNS. Doi:

10.1186/2045-8118-10-23

Duh EJ, Maury WJ, Folks TM, Fauci AS, Rabson AB (1989) Tumor necrosis factor alpha

activates human immunodeficiency virus type 1 through induction of nuclear factor

binding to the NF-kappa B sites in the long terminal repeat. Proc Natl Acad Sci USA.

Doi: 10.1073.86.15.5974

Elmore MR, Najafi AR, Koike MA, Dagher NN, Spangenberg EE, Rice RA, Kitazawa M,

Matusow B, Nguyen H, West BL, Green KN (2014) Colony-stimulating factor 1

receptor signaling is necessary for microglia viability, unmasking a microglia

progenitor cell in the adult brain. Neuron. Doi: 10.1016/j.neuron.2014.02.040

Erblich B, Zhu L, Etgen AM, Dobrenis K, Pollard JW (2011) Absence of colony stimulation

factor-1 receptor results in loss of microglia, disrupted brain development and

olfactory deficits. PLoS One. Doi: 10.1371/journal.pone.0026317

Ferdin J, Goricar K, Dolzan V, Plemenitas A, Martin JN, Peterlin BM, Deeks SG, Lenassi M

(2018) Viral protein Nef is detected in plasma of half of HIV-infected adults with

undetectable plasma HIV RNA. PLoS One. Doi: 10.1371/journal.pone.0191613

Freed EO (2001) HIV-1 replication. Somat Cell Mol Genet. Doi: 10.1023/a:1021070512287

Gallo RC, Salahuddin SZ, Popovic M, Shearer GM, Kaplan M, Haynes BF, Palker TJ,

Redfield R, Oleske J, Safai B et al. (1984) Frequent detection and isolation of

cytopathic retroviruses (HTLV-III) from patients with AIDS and at risk for AIDS.

Science. Doi: 10.1126/science.6200936

Gama L, Abreu CM, Shirk EN, Price SL, Li M, Paird GM, Pate KA, Wietgrefe SW, O'Connor SL, Pianowski L, Haase AT, Van Lint C, Siliciano RF, Clements JE, LRA-SIV Study Group (2017) Reactivation of simian immunodeficiency virus reservoirs in the brain of virally suppressed macaques. AIDS. Doi: 10.1097/QAD.0000000000001267

Gomez-Nicola D, Fransen NL, Suzzi S, Perry VH (2013) Regulation of microglial proliferation during chronic neurodegeneration. J Neurosci. Doi: 10.1523/JNEUROSCI.4440-12.2013

Groopman JE and Gottlieb MS (1983) Acquired immune deficiency syndrome. AIDS: the widening gyre. Nature. Doi: 10.1038/303575a0

Hahn BH, Shaw GM, De Cock KM, Sharp PM (2000) AIDS as a zoonosis: scientific and public health implications. Science. Doi: 10.1126/science.287.5453.607

High KP, Brennan-Ing M, Clifford DB, Cohen MH, Currier J, Deeks SG, Deren S, Effros RB, Gebo K, Goronzy JJ, Justice AC, Landay A, Levin J, Miotti PG, Munk RJ, Nass H, Rinaldo CR, Shlipak MG, Tracy R, Valcour V, Vance DE, Walston JD, Volberding P, OAR Working Group on HIV Aging (2012) HIV and aging: state of knowledge and areas of critical need for research: A report to the NIH office of AIDS research by the HIV and aging working group. J Acquir Immune Defic Syndr. Doi: 10.1097/QAI.0b013e31825a3668

Ke R, Conway JM, Margolis DM, Perelson AS (2018) Determinants of the efficacy of HIV latency-reversing agents and implications for drug and treatment design. JCI Insight. Doi: 10.1172/jci.insight.123052

Korber B, Muldoon M, Theiler J, Gao F, Gupta R, Lapedes A, Hahn BH, Wolinsky S,

    Bhattacharya T (2000) Timing the ancestor of the HIV-1 pandemic strains. Science.

    Doi: 10.1126/science.288.5472.1789

Levy JA (2007) HIV and the pathogenesis of AIDS, 3rd edition

Menassa DA, Gomez-Nicola D (2018) Microglial dynamics during human brain

    development. Front Immunol. Doi: 10.3389/fimmu.2018.01014

Montoya JL, Campbell LM, Paolillo EW, Ellis RJ, Letendre SL, Jeste DV, Moore DJ (2019)

    Inflammation relates to poorer complex motor performance among adults living with

    HIV on suppressive antiretroviral therapy. J Acquir Immune Defic Syndr. Doi:

    10.1097/QAI.0000000000001881

Mylvaganam GH, Silvestri G, Amara RR (2015) HIV therapeutic vaccines: moving towards

    a functional cure. Curr Opin Immunol. Doi: 10.1016/j.coi.2015.05.001

Papasavvas E, Kostman JR, Mounzer K, Grant RM, Gross R, Gallo C, Azzoni L, Foulkes A,

    Thiel B, Pistilli M, Mackiewicz A, Shull J, Montaner LJ (2004) Randomized,

    controlled trial of therapy interruption in chronic HIV-1 infection. PLoS Med. Doi:

Pau AK, George JM (2014) Antiretroviral therapy: current drugs. Infect Dis Clin North Am.

    Doi: 10.1016/j.idc.2014.06.001

Perry VH, Holmes C (2014) Microglial priming in neurodegenerative disease. Doi:

    10.1038/nneurol.2014.38

Saylor D, Dickens AM, Sacktor N, Haughey N, Slusher B, Pletnikov M, Mankowski JL,

    Brown A, Volsky DJ, McArthur JC (2016) HIV-associated neurocognitive disorder –

    pathogenesis and prospects for treatment. Nat Rev Neurol. Doi:

    10.1038/nrneurol.2016.53

Sengupta S, Siliciano RF (2018) Targeting the latent reservoir for HIV-1. Immunity. Doi: 10.1016/j.immuni.2018.04.030

Siliciano JD, Kajdas J, Finzi D, Quinn TC, Chadwick K, Margolick JB, Kovacs C, Gange SJ, Siliciano RF (2003) Long-term follow-up studies confirm the stability of the latent reservoir for HIV-1 in resting CD4+ T cells. Nat Med. Doi: 10.1038/nm880

Silvestri G, Paiardini M, Pandrea I, Lederman MM, Sodora DL (2007) Understanding the benign nature of SIV infection in natural hosts. J Clin Invest. Doi: 10.1172/JCI33034

Sominsky L, De Luca S, Spencer SJ (2018) Microglia: Key players in neurodevelopment and neuronal plasticity. Int J Biochem Cell Biol. Doi: 10.1016/j.biocel.2017.11.012

Thion MS, Ginhoux F, Garel S (2018) Microglia and early brain development: An intimate journey. Science. Doi: 10.1126/science.aat0474

Van Heuverswyn F, Peeters M (2007) The origins of HIV and implications for the global epidemic. Curr Infect Dis Rep. Doi: 10.1007/s11908-007-0052-x

Wallet C, De Rovere M, Van Ssche J, Daouad F, De Wit S, Gautier V, Mallon PWG, Marcello A, Van Lint C, Rohr O Schwartz C (2019) Microglial cells: The main HIV-1 reservoir in the brain. Front Cell infect Microbiol. Doi: 10.3389/fcimb.2019.00362

Williams DW, Calderon TM, Lopez L, Carvallo-Torres L, Gaskill PJ, Eugenin EA, Morgello S, Berman JW (2013) Mechanisms of HIV entry into the CNS: increased sensitivity of HIV infected CD14+CD16+ monocytes to CCL2 and key roles for CCR2, JAM-A, and ALCAM in diapedesis. PLoS One. Doi: 10.1371/journal.pone.0069270

Williams DW, Veenstra M, Gaskill PJ, Morgello S, Galderon TM, Berman JW (2014) Monocytes mediate HIV neuropathogenesis: mechanisms that contribute to HIV

associated neurocognitive disorders. Curr HIV Res. Doi:

10.2174/1570162x12666140526114526

Wong ME, Jaworowski A, Hearps AC (2019) The HIV reservoir in monocytes and

macrophages. Front Immunol. Doi: 10.3389/fimmu.2019.01435


**Chapter II**

Akiyama H, Nishimura T, Kondo H, Ikeda K, Hayashi Y, McGeer PL (1994) Expression of

the receptor for macrophage colony stimulating factor by brain microglia and its

upregulation in brains of patients with Alzheimer's disease and amyotrophic lateral

sclerosis. Brain Res. Doi: 10.1016/0006-8993(94)91779-5

Beck SE, Kelly KM, Queen SE, Adams RJ, Zink MC, Tarwater PM, Mankowski JL (2015)

Macaque species susceptibility to simian immunodeficiency virus: increased

incidence of SIV central nervous system disease in pigtailed macaques versus rhesus

macaques. J Neurovirol. Doi: 10.1007/s13365-015-0313-7

Beck SE, Queen SE, Metcalf Pate KA, Mangus LM, Abreu CM, Gama L, Witwer KW,

Adams RJ, Zink MC, Clements JE, Mankowski JL (2018) An SIV/macaque model

targeted to study HIV-associated neurocognitive disorders. J Neurovirol. Doi:

10.1007/s13365-017-0582-4

Beck SE, Queen SE, Witwer KW, Metcalf Pate KA, Mangus LM, Gama L, Adams RJ,

Clements JE, Christine Zink M, Mankowski JL (2015) Paving the path to HIV

neurotherapy: Predicting SIV CNS disease. Eur J Pharmacol. Doi:

10.1016/j.ejphar.2015.03.018

Cardenas VA, Meyerhoff DJ, Studholme C, Kornak J, Rothlind J, Lampiris H, Neuhaus J, Grant RM, Chao LL, Truran D, Weiner MW (2009) Evidence for ongoing brain injury in human immunodeficiency virus-positive patients treated with antiretroviral therapy. J Neurovirol. Doi: 10.1080/13550280902973960

Dagher NN, Najafi AR, Kayala KM, Elmore MR, White TE, Medeiros R, West BL, Green KN (2015) Colony-stimulating factor 1 receptor inhibition prevents microglial plaque association and improves cognition in 3xTg-AD mice. J Neuroinflammation. Doi: 10.1186/s12974-015-0366-9

De I, Nikodemova M, Steffen MD, Sokn E, Maklakova VI, Watters JJ, Collier LS (2014) CSF1 overexpression has pleiotropic effects on microglia in vivo. Glia. Doi: 10.1002/glia.22717

Dheen ST, Kaur C, Ling EA (2007) Microglial activation and its implications in the brain diseases. Curr Med Chem. Doi: 10.2174/092986707780597961

Elmore MR, Najafi AR, Koike MA, Dagher NN, Spangenberg EE, Rice RA, Kitazawa M, Matusow B, Nguyen H, West BL, Green KN (2014) Colony-stimulating factor 1 receptor signaling is necessary for microglia viability, unmasking a microglia progenitor cell in the adult brain. Neuron. Doi: 10.1016/j.neuron.2014.02.040

Erblich B, Zhu L, Etgen AM, Dobrenis K, Pollard JW (2011) Absence of colony stimulation factor-1 receptor results in loss of microglia, disrupted brain development and olfactory deficits. PLoS One. Doi: 10.1371/journal.pone.0026317

Gerngross L, Fisher T (2015) Evidence for cFMS signaling in HIV production by brain macrophages and microglia. J Neurovirol. Doi: 10.1007/s13365-014-0270-6

Gerngross L, Lehmicke G, Belkadi A, Fischer T (2015) Role for cFMS in maintaining

    alternative macrophage polarization in SIV infection: implications for HIV

    neuropathogenesis. J Neuroinflammation. Doi: 10.1186/s12974-015-0272-1

Gomez-Nicola D, Fransen NL, Suzzi S, Perry VH (2013) Regulation of microglial

    proliferation during chronic neurodegeneration. J Neurosci.

    Doi:10.1523/JNEUROSCI.4440-12.2013

Gruber MF, Weih KA, Boone EJ, Smith PD, Clouse KA (1995) Endogenous macrophage

    CSF production is associated with viral replication in HIV-1-infected human

    monocyte-derived macrophages. J Immunol.

Jin WN, Shi SX, Li Z, Li M, Wood K, Gonzales RJ, Liu Q (2017) Depletion of microglia

    exacerbates postischemic inflammation and brain injury. J Cereb Blood Flow Metab.

    Doi: 10.1177/0271678X17694185

Kalter DC, Nakamura M, Turpin JA, Baca LM, Hoover DL, Dieffenbach C, Ralph P,

    Gendelman HE, Meltzer MS (1991) Enhanced HIV replication in macrophage

    colony-stimulating factor-treated monocytes. J Immunol.

Klegeris A, McGeer PL (2003) Toxicity of human monocytic THP-1 cells and microglia

    toward SH-SY5Y neuroblastoma cells is reduced by inhibitors of 5-lipoxygenase and

    its activating protein FLAP. J Leukoc Biol. Doi: 10.1189/jlb.1002482

Lall D, Baloh RH (2017) Microglia and C9orf72 in neuroinflammation and ALS and

    frontotemporal dementia. J Clin Invest. Doi: 10.1172/JCI90607

Martinez FO, Gordon S (2014) The M1 and M2 paradigm of macrophage activation: time for

    reassessment. F1000Prime Rep. Doi: 10.12703/P6-13

Martinez-Muriana A, Mancuso R, Francos-Quijorna I, Olmos-Alonso A, Osta R, Perry VH, Navarro X, Gomez-Nicola D, Lopez-Vales R (2016) CSF1R blockade slows the progression of amyotrophic lateral sclerosis by reducing microgliosis and invasion of macrophages into peripheral nerves. Sci Rep. Doi: 10.1038/srep25663

Meulendyke KA, Ubaida-Mohien C, Drewes JL, Liao Z, Gama L, Witwer KW, Graham DR, Zink MC (2014) Elevated brain monoamine oxidase activity in SIV- and HIV-associated neurological disease. J Infect Dis. Doi: 10.1093/infdis/jiu194

Mitrasinovic OM, Murphy GM (2003) Microglial overexpression of the M-CSF receptor augments phagocytosis of opsonized Abeta. Neurobiol Aging. Doi: 10.1016/s0197-4580(02)00237-3

Muffat J, Li Y, Yuan B, Mitalipova M, Omer A, Corcoran S, Bakiasi G, Tsai LH, Aubourg P, Ransohoff RM, Jaenisch R (2016) Efficient derivation of microglia-like cells from human pluripotent stem cells. Nat Med. Doi: 10.1038/nm.4189

Ohashi T, Aoki M, Tomita H, Akazawa T, Sato K, Kuze B, Mizuta K, Hara A, Nagaoka H, Inoue N, Ito Y (2017) M2-like macrophage polarization in high lactic acid-producing head and neck cancer. Cancer Sci. Doi: 10.1111/cas.13244

Ransohoff RM (2016) A polarizing question: do M1 and M2 microglia exist? Nat Neurosci. Doi: 10.1038/nn.4338

Ransohoff RM, El Khoury J (2015) Microglia in Health and Disease. Cold Spring Harb Perspect Biol. Doi: 10.1101/cshperspect.a020560

Sasaki A (2017) Microglia and brain macrophages: An update. Neuropathology. Doi: 10.1111/neup.12354

Saylor D, Dickens AM, Sacktor N, Haughey N, Slusher B, Pletnikov M, Mankowski JL, Brown A, Volsky DJ, McArthur JC (2016) HIV-associated neurocognitive disorder – pathogenesis and prospects for treatment. Nat Rev Neurol. Doi: 10.1038/nrneurol.2016.53

Sherr CJ (1990) Colony-stimulating factor-1 receptor. Blood.

Spudich SS (2016) Immune activation in the central nervous system throughout the course of HIV infection. Curr Opin HIV AIDS. Doi: 10.1097/COH.0000000000000243

Stanley ER Chitu V (2014) CSF-1 receptor signaling in myeloid cells. Cold Spring Harb Perspect Biol. Doi: 10.1101/cshperspect.a021857

Williams DW, Veenstra M, Gaskill PJ, Morgello S, Galderon TM, Berman JW (2014) Monocytes mediate HIV neuropathogenesis: mechanisms that contribute to HIV associated neurocognitive disorders. Curr HIV Res. Doi: 10.2174/1570162x12666140526114526

Zelante T, Ricciardi-Castagnoli P (2012) The yin-yang nature of CSF1R-binding cytokines. Nat Immunol. Doi: 10.1038/ni.2375

**Chapter III**

Akiyama H, Nishimura T, Kondo H, Ikeda K, Hayashi Y, McGeer PL (1994) Expression of the receptor for macrophage colony stimulating factor by brain microglia and its upregulation in brains of patients with Alzheimer's disease and amyotrophic lateral sclerosis. Brain Res 639:171-174

Beck SE, Kelly KM, Queen SE, Adams RJ, Zink MC, Tarwater PM, Mankowski JL (2015) Macaque species susceptibility to simian immunodeficiency virus: increased

incidence of SIV central nervous system disease in pigtailed macaques versus rhesus macaques. J Neurovirol. Doi: 10.1007/s13365-015-0313-7

Beck SE, Queen SE, Metcalf Pate KA, Mangus LM, Abreu CM, Gama L, Witwer KW, Adams RJ, Zink MC, Clements JE, Mankowski JL (2018) An SIV/Macaque model targeted to study HIV-associated neurocognitive disorders. J Neurovirol. Doi: 10.1007/s13365-017-0582-4

Beck SE, Queen SE, Witwer KW, Metcalf Pate KA, Mangus LM, Gama L, Adams RJ, Clements JE, Christine Zink M, Mankowski JL (2015) Paving the path to HIV neurotherapy: predicting SIV CNS disease. Eur J Pharmacol. Doi: 10.1016/j.ejphar.2015.03.018

Brenchley JM, Douek DC (2012) Microbial translocation across the GI tract. Annu Rev Immunol. Doi: 10.1146/annurev-immunol-020711-075001

Chitu V, Gokhan S, Nandi S, Mehler MF, Stanley ER (2016) Emerging roles for CSF-1 receptor and its ligands in the nervous system. Trends Neurosci. Doi: 10.1016/j.tins.2016.03.005

Dardiotis E, Siokas V, Pantazi E, Dardioti M, Rikos D, Xiromerisiou G, Markou A, Papadimitriou D, Speletas M, Hadjigeorgiou GM (2017) A novel mutation in TREM2 gene causing Nasu-Hakola disease and review of the literature. Neurobiol Aging. Doi: 10.1016/j.neurobiolaging.2017.01.015

Elmore MR, Najafi AR, Koike MA, Dagher NN, Spangenberg EE, Rice RA, Kitazawa M, Matusow B, Nguyen H, West BL, Green KN (2014) Colony-stimulating factor 1 receptor signaling is necessary for microglia viability, unmasking a microglia progenitor cell in the adult brain. Neuron. Doi: 10.1016/j.neuron.2014.02.040

Fields JA, Spencer B, Swinton M, Qvale EM, Marquine MJ, Alexeeva A, Gough S, Soontornniyomkij B, Valera E, Masliah E, Achim CL, Desplats P (2018) Alteration in brain TREM2 and amyloid-beta levels are associated with neurocognitive impairment in HIV-infected persons on antiretroviral therapy. J Neurochem. Doi: 10.1111/jnc.14582

Gisslén M, Heslegrave A, Veleva E, Yilmaz A, Andersson LM, Hagberg L, Spudich S, Fuchs D, Price RW, Zetterberg H (2018) CSF concentrations of soluble TREM2 as a marker of microglial activation in HIV-1 infection. Neurol Neuroimmunol Neuroinflamm. Doi: 10.1212/NXI.0000000000000512

Guan Z, Kuhn JA, Wang X, Colquitt B, Solorzano C, Vaman S, Guan AK, Evans-Reinsch Z, Braz J, Devor M, Abboud-Werner SL, Lanier LL, Lomvardas S, Basbaum AI (2016) Injured sensory neuron-derived CSF1 induces microglial proliferation and DAP12-dependent pain. Nat Neurosci. Doi: 10.1038/nn.4189

Guerreiro R, Wojtas A, Bras J, Carrasquillo M, Rogaeva E, Majounie E, Cruchaga C, Sassi C, Kauwe JS, Younkin S, Hazrati L, Collinge J, Pocock J, Lashley T, Williams J, Lambert JC, Amouyel P, Goate A, Rademakers R, Morgan K, Powell J, St George-Hyslop P, Singleton A, Hardy J (2013) TREM2 variants in Alzheimer's disease. N Engl J Med. Doi: 10.1056/NEJMoa1211851

Holtman IR, Raj DD, Miller JA, Schaafsma W, Yin Z, Brouwer N, Wes PD, Möller T, Orre M, Kamphuis W, Hol EM, Boddeke EWGM, Eggen BJL (2015) Induction of a common microglia gene expression signature by aging and neurodegenerative conditions: a co-expression meta-analysis. Acta Neuropathol Commun. Doi: 10.1186/s40478-015-0203-5

Irons DL, Meinhardt T, Allers C, Juroda MJ, Kim WK (2019) Overexpression and activation

    of colony-stimulating factor 1 receptor in the SIV/macaque model of HIV infection

    and neuroHIV. Brain Pathol. Doi: 10.1111/bpa.12731

Jay TR, Miller CM, Cheng PJ, Graham LC, Bemiller S, Broihier ML, Xu G, Margevicius D,

    Karlo JC, Sousa GL, Cotleur AC, Butovsky O, Bekris L, Staugaitis SM, Leverenz JB,

    Pimplikar SW, Landreth GE, Howell GR, Ransohoff RM, Lamb BT (2015) TREM2

    deficiency eliminates TREM2+ inflammatory macrophages and ameliorates

    pathology in Alzheimer's disease mouse models. J Exp Med. Doi:

    10.1084/jem.20142322

Jonsson T, Stefansson H, Steinberg S, Jonsdottir I, Jonsson PV, Snaedal J, Bjornsson S,

    Huttenlocher J, Levey AI, Lah JJ, Rujescu D, Hampel H, Giegling I, Andreassen OA,

    Engedal K, Ulstein I, Djurovic S, Ibrahim-Verbaas C, Hofman A, Ikram MA, van

    Duijn CM, Thorsteinsdottir U, Kong A, Stefansson K (2013) Variant of TREM2

    associated with the risk of Alzheimer's disease. N Engl J Med. Doi:

    10.1056/NEJMoa1211103

Knight AC, Brill SA, Queen SE, Tarwater PM, Mankowski JL (2018) Increased microglial

    CSF1R expression in the SIV/macaque model of HIV CNS disease. J Neuropathol

    Exp Neurol. Doi: 10.1093/jnen/nlx115

Kobayashi M, Konishi H, Sayo A, Takai T, Kiyama H (2016) TREM2/DAP12 signal elicits

    proinflammatory response in microglia and exacerbates neuropathic pain. J Neurosci.

    Doi: 10.1523/JNEUROSCI.1238-16.2016

Kober DL, Brett TJ (2017) TREM2-ligand interactions in health and disease. J Mol Biol.

    Doi: 10.1016/j.jmb.2017.04.004

Konishi H, Kiyama H (2018) Microglial TREM2/DAP12 signaling: a double-edged sword in

    neural diseases. Front Cell Neurosci. Doi: 10.3389/fncel.2018.00206

Krasemann S, Madore C, Cialic R, Baufeld C, Calcagno N, El Fatimy R, Beckers L,

    O'Loughlin E, Xu Y, Fanek Z, Greco DJ, Smith ST, Tweet G, Humulock Z, Zrzavy

    T, Conde-Sanroman P, Gacias M, Weng Z, Chen H, Tjon E, Mazaheri F, Hartmann

    K, Madi A, Ulrich JD, Glatzel M, Worthmann A, Heeren J, Budnik B, Lemere C,

    Ikezu T, Heppner FL, Litvak V, Holtzman DM, Lassmann H, Weiner HL, Ochando J,

    Haass C, Butovsky O (2017) The TREM2-APOE pathway drives the transcriptional

    phenotype of dysfunctional microglia in neurodegenerative diseases. Immunity. Doi:

    10.1016/j.immuni.2017.08.008

Laast VA, Shim B, Johanek LM, Dorsey JL, Hauer PE< Tarwater PM, Adams RJ, Pardo CA,

    McArthur JC, Ringkamp M, Mankowski JL (2011) Macrophage-mediated dorsal root

    ganglion damage precedes altered nerve conduction in SIV-infected macaques. Am J

    Pathol. Doi: 10.1016/j.ajpath.2011.07.047

Li JT, Zhang Y (2018) TREM2 regulates innate immunity in Alzheimer's disease. J

    Neuroinflammation. Doi: 10.1186/s12974-018-1148-y

Martinez-Muriana A, Mancuso R, Francos-Quijorna I, Olmos-Alonso A, Osta R, Perry VH,

    Navarro X, Gomez-Nicola D, Lopez-Vales R (2016) CSF1R blockade slows the

    progression of amyotrophic lateral sclerosis by reducing microgliosis and invasion of

    macrophages into peripheral nerves. Sci Rep. Doi: 10.1038/srep25663

Otero K, Turnbull IR, Poliani PL, Vermi W, Cerutti E, Aoshi T, Tassi I, Takai T, Stanley SL,

    Miller M, Shaw AS, Colonna M (2009) Macrophage colony-stimulating factor

induces the proliferation and survival of macrophages via a pathway involving DAP12 and β-catenin. Nat Immunol. Doi: 10.1038/ni.1744

Satoh J, Asahina N, Kitano S, Kino Y (2014) A comprehensive profile of ChIP-Seq-based PU.1/Spi1 target genes in microglia. Gene Regul Syst Bio. Doi: 10.4137/GRSB.S19711

Saylor D, Dickens AM, Sacktor N, Haughey N, Slusher B, Pletnikov M, Mankowski JL, Brown A, Volsky DJ, McArthur JC (2016) HIV-associated neurocognitive disorder – pathogenesis and prospects for treatment. Nat Rev Neurol. Doi: 10.1038/nrneurol.2016.53

Schmid CD, Sautkulis LN, Danielson PE, Cooper J, Hasel KW, Hilbush BS, Sutcliffe JG, Carson MJ (2002) Heterogeneous expression of the triggering receptor expressed on myeloid cells-2 on adult murine microglia. J Neurochem. 83:1309-20

Stanley ER, Chitu V (2014) CSF-1 receptor signaling in myeloid cells. Cold Spring Harb Perspect Biol. Doi: 10.1101/cshperspect.a021857

Thelen M, Razquin C, Hernandez I, Gorostidi A, Sanchez-Valle R, Ortega-Cubero S, Wolfsgruber S, Drichel D, Fliessbach K, Duenkel T, Damian M, Heilmann S, Slotosch A, Lennarz M, Seijo-Martinez M, Rene R, Kornhuber J, Peters O, Luckhaus C, Jahn H, Hull M, Ruther E, Wiltfang J, Lorenzo E, Gascon J, Lleo A, Llado A, Campedalacreu J, Moreno F, Ahmadzadehfar H, Dementia Genetics Spanish, Consortium, Fortea J, Indakoetxea B, Heneka MT, Wetter A, Pastor MA, Riverol M, Becker T, Frolich L, Tarraga L, Boada M, Wagner M, Jessen F, Maier W, Clarimon J, Lopez de Munain A, Ruiz A, Pastor P, Ramirez A (2014) Investigation of the role

of rare TREM2 variants in frontotemporal dementia subtypes. Neurobiol Aging. Doi: 10.1016/j.neurobiolaging.2014.06.018

Uden M, Morley GM, Dibb NJ (1999) Evidence that downregulation of the M-CSF receptor is not dependent upon receptor kinase activity. Oncogene. Doi: 10.1038/sj.onc.1202743

Wang Y, Ulland TK, Ulrich JD, Song W, Tzaferis JA, Hole JT, Yuan P, Mahan TE, Shi Y, Gilfillan S, Cella M, Grutzendler S, DeMattos RB, Cirrito JR, Holtzman DM, Colonna M (2016) TREM2-mediated early microglial response limits diffusion and toxicity of amyloid plaques. J Exp Med. Doi: 10.1084/jem.20151948

Yarandi SS, Peterson DA, Treisman GJ, Moran TH, Pasricha PJ (2016) Modulatory effects of gut microbiota on the central nervous system: how gut could play a role in neuropsychiatric health and disease. J Neurogastroenterol Motil. Doi: 10.5056/jnm15146

Yeh FL, Hansen DV, Sheng M (2017) TREM2, microglia, and neurodegenerative diseases. Trends Mol Med. Doi: 10.1016/j.molmed.2017.03.008

**Chapter IV**

Abreu CM, Veenhuis RT, Avalos CR, Graham S, Parilla DR, Ferreira EA, Queen SE, Shirk EN, Bullock BT, Li M, Metcalf Pate KA, Beck SE, Mangus LM, Mankowski JL, Mac Gabhann F, O'Connor SL, Gama L, Clements JE (2019) Myeloid and CD4 T cells comprise the latent reservoir in antiretroviral therapy-suppressed SIVmac251-infected macaques. mBio. Doi: 10.1128/mBio.01659-19

Abreu CM, Veenhuis RT, Avalos CR, Graham S, Queen SE, Shirk EN, Bullock BT, Li M, Metcalf Pate KA, Beck SE, Mangus LM, Mankowski JL, Clements JE, Gama L

(2019) Infectious virus persists in CD4+ T cells and macrophages in antiretroviral therapy-suppressed simian immunodeficiency virus-infected macaques. J Virol. Doi: 10.1128/JVI.00065-19

Akiyama H, Nishimura T, Kondo H Ikeda K, Hayashi Y, McGeer PL (1994) Expression of the receptor for macrophage colony stimulating factor by brain microglia and its upregulation in brains of patients with Alzheimer's disease and amyotrophic lateral sclerosis. Brain Res. Doi: 10.1016/0006-8993(94)91779-5

Ao JY, Zhu XD, Chai ZT, Cai H, Zhang YY, Zhang KZ, Kong LQ, Zhang N, Ye BG, Ma DN, Sun HC (2017) Colony-stimulating factor 1 receptor blockade inhibits tumor growth by altering the polarization of tumor-asociated macrophages in hepatocellular carcinoma. Mol Cancer Ther. Doi: 10.1158/1535-7163.MCT-16-0866

Avalos CR, Abreu CM, Queen SE< Li M, Price S, Shirk EN, Engle EL, Forsyth E, Bullock BT, MacGabhann F, Wietgrefe SW, Haase AT, Zink MC, Mankowski JL, Clements JE, Gama L (2017) Brain macrophages in simian immunodeficiency virus-infected antiretroviral-suppressed macaques: a functional latent reservoir. mBio. Doi: 10.1128/mBio.01186-17

Barber SA, Herbst DS, Bullock BT, Gama L, Clements JE (2004) Innate immune responses and control of acute simian immunodeficiency virus replication in the central nervous system. J Neurovirol. Doi: 10.1080/753312747

Beck SE, Kelly KM, Queen SE, Adams RJ, Zink MC, Tarwater PM, Mankowski JL (2015) Macaque species susceptibility to simian immunodeficiency virus: increased incidence of SIV central nervous system disease in pigtailed macaques versus rhesus macaques. J Neurovirol. Doi: 10.1007/s13365-015-0313-7

Beckmann N, Giorgetti E, Neuhaus A, Zurbruegg S, Accart N, Smith P, Perdoux J, Perrot L, Nash M, Desrayaud S, Wipfli P, Frieauff W, Shimshek DR (2018) Brain region-specific enhancement of remyelination and prevention of demyelination by the CSF1R kinase inhibitor BLZ945. Acta Neuropathol Commun. Doi: 10.1186/s40478-018-0510-8

Bohlen CJ, Bennett FC, Tucker AF, Collins HY, Mulinyawe SB, Barres BA (2017) Diverse requirements for microglial survival, specification, and function revealed by defined-medium cultures. Neuron. Doi: 10.1016/j.neuron.2017.04.043

Cannarile MA, Weisser M, Jacob W, Jegg, AM, Ries CH, Ruttinger D (2017) Colony-sitmulating factor 1 receptor (CSF1R) inhibitors in cancer therapy. J Immunother Cancer. Doi: 10.1186/s40425-017-0257-y

Cartier N, Lewis CA, Zhang R, Rossi RM (2014) The role of microglia in human disease: therapeutic tool or target? Acta Neuropathol. Doi: 10.1007/s00401-014-1330-y

Chitu V, Gokhan S, Nandi S, Mehler MF, Stanley ER (2016) Emerging roles for CSF-1 receptor and its ligands in the nervous system. Trends Neurosci. Doi: 10.1016/j.tins.2016.03.005

Coleman LG, Zou J, Crews FT (2020) Microglial depletion and repopulation in brain slice culture normalizes sensitized proinflammatory signaling. J Neuroinflammation. Doi: 10.1186/s12974-019-1678-y

Cunyat F, Rainho JN, West B, Swainson L, McCune JM, Stevenson M (2016) Colony-stimulating factor 1 receptor antagonists sensitize human immunodeficiency virus type 1-infected macrophages to TRAIL-mediated killing. J Virol. Doi: 10.1128/JVI.00231-16

Dagher NN, Najafi AR, Kayala KM, Elmore MR, White TE, Medeiros R, West BL, Green
KN (2015) Colony-stimulating factor 1 receptor inhibition prevents microglial plaque
association and improves cognition in 3xTg-AD mice. J Neuroinflammation. Doi:
10.1186/s12974-015-0366-9

Dammeijer F, Lievense LA, Kaijen-Lambers ME, van Nimwegen M, Bezemer K, Hegmans
JP, van Hall T, Hendriks RW, Aerts JG (2017) Depletion of tumor-associated
macrophages with a CSF-1R kinase inhibitor enhances antitumor immunity and
survival induced by DC immunotherapy. Cancer Immunol Res. Doi: 10.1158/2326-
6066.CIR-16-0309

Elmore MR, Lee RJ, West BL, Green KN (2015) Characterizing newly repopulated
microglia in the adult mouse: impacts on animal behavior, cell morphology, and
neuroinflammation. PLoS One. Doi: 10.1371/journal.pone.0122912

Elmore MR, Najafi AR, Koike MA, Dagher NN, Spangenberg EE, Rice RA, Kitazawa M,
Matusow B, Nguyen H, West BL, Green KN (2014) Colony-stimulating factor 1
receptor signaling is necessary for microglia viability, unmasking a microglia
progenitor cell in the adult brain. Neuron. Doi: 10.1016/j.neuron.2014.02.040

Geirsdottir L, David E, Keren-Shaul H, Weiner A, Bohlen SC, Neuber J, Balic A, Giladi A,
Sheban F, Dutertre CA, Pfeifle C, Peri F, Raffo-Romero A, Vizioli J, Matiasek K,
Scheiwe C, Meckel S, Matz-Rensing K, van der Meer F, Thormodsson FR,
Stadelmann C, Zikha N, Kimchi T, Ginhoux F, Ulitsky I, Erny D, Amit I, Prinz M
(2019) Cross-species single-cell analysis reveals divergence of the primate microglia
program. Cell. Doi: 10.1016/j.cell.2019.11.010

Gomez-Nicola D, Fransen NL, Suzzi S, Perry VH (2013) Regulation of microglial

    proliferation during chronic neurodegeneration. J Neurosci.

    Doi:10.1523/JNEUROSCI.4440-12.2013

Han J, Harris RA, Zhang XM (2017) An updated assessment of microglia depletion: current

    concepts and future directions. Mol Brain. Doi: 10.1186/s13041-017-0307-x

Jin WN, Shi SX, Li Z, Li M, Wood K, Gonzales RJ, Liu Q (2017) Depletion of microglia

    exacerbates postischemic inflammation and brain injury. J Cereb Blood Flow Metab.

    Doi: 10.1177/0271678X17694185

Knight AC, Brill SA, Queen SE, Tarwater PM, Mankowski JL (2018) Increased microglial

    CSF1R expression in the SIV/macaque model of HIV CNS disease. J Neuropathol

    Exp Neurol. Doi: 10.1093/jnen/nlx115

Lamb YN (2019) Pexidartinib: First Approval. Drugs. Doi: 10.1007/s40265-019-01210-0

Li M, Li Z, Ren H, Jin WN, Wood K, Liu Q, Sheth KN, Shi FD (2017) Colony stimulating

    factor 1 receptor inhibition eliminates microglia and attenuates brain injury after

    intracerebral hemorrhage. J Cereb Blood Flow Metab. Doi:

    10.1177/0271678X16666551

Mancuso R, Fryatt G, Cleal M, Obst J, Pipi E, Monzon-Sandoval J, Ribe E, Winchester L,

    Webber C, Vevado A, Jacobs T, Austin N, Theunis C, Grauwen K, Daniela Ruiz E,

    Mudher A, Vicente-Rodriguez M, Parker CA, Simmons C, Cash D, Richardson J,

    Nima Consortium, Jones DNC, Lovestone S, Gomez-Nicola D, Perry VH (2019)

    CSF1R inhibitor JNJ-40346527 attenuates microglial proliferation and

    neurodegeneration in P301S mice. Brain. Doi: 10.1093/brain/awz241

Martinez-Muriana A, Mancuso R, Francos-Quijorna I, Olmos-Alonso A, Osta R, Perry VH,

    Navarro X, Gomez-Nicola D, Lopez-Vales R (2016) CSF1R blockade slows the

    progression of amyotrophic lateral sclerosis by reducing microgliosis and invasion of

    macrophages into peripheral nerves. Sci Rep. Doi: 10.1038/srep25663

Mitrasinovic OM and Murphy GM (2003) Microglial overexpression of the M-CSF receptor

    augments phagocytosis of opsonized Abeta. Neurobiol Aging. 10.1016/s0197-

    4580(00237-3

Nissen JC, Thompson KK, West BL, Tsirka SE (2018) Csf1R inhibition attenuates

    experimental autoimmune encephalomyelitis and promotes recovery. Exp Neurol.

    Doi: 10.1016/j.expneurol.2018.05.021

Olmos-Alonso A, Schetters ST, Sri S, Askew K, Mancuso R, Vargas-Caballero M, Holscher

    C, Perry VH, Gomez-Nicola D (2016) Pharmacological targeting of CSF1R inhibits

    microglial proliferation and prevents the progression of Alzheimer's-like pathology.

    Brain. Doi: 10.1093/brain/awv379

Sassi C, Nalls MA, Ridge PG, Gibbs JR, Lupton MK, Troakes C, Lunnon K, Al-Sarraj S,

    Brown KS, Medway C, Lord J, Turton J, Bras J, Aruk Consortium, Blumenau S,

    Thielke M, Josties C, Freyer D, Dietrich A, Hammer M, Baier M, Dirnagl U, Morgan

    K, Powell JF, Kauwe JS, Cruchaga C, Goate AM, Singleton AB, Guerreiro R,

    Hodges A, Hardy J (2018) Mendelian adult-onset leukodystrophy genes in

    Alzheimer's disease: critical influence of CSF1R and NOTCH3. Neurobiol Aging.

    Doi: 10.1016/j.neurobiolaging.2018.01.015

Saylor D, Dickens AM, Sacktor N, Haughey N, Slusher B, Pletnikov M, Mankowski JL,

    Brown A, Volsky DJ, McArthur JC (2016) HIV-associated neurocognitive disorder –

pathogenesis and prospects for treatment. Nat Rev Neurol. Doi:
10.1038/nrneurol.2016.53

Schneider CA, Rasband WS, Eliceiri KW (2012) NIH Image to ImageJ: 25 years of image
analysis. Nat Mathods. Doi: 10.1038/nmeth.2089

Sonsa J, Philipp S, Albay R, Reyes-Ruiz JM, Baglietto-Vargas D, LaFerla FM, Glabe CG
(2018) Early long-term administration of the CSF1R inhibitor PLX3397 ablates
microglia and reduces accumulation of intraneuronal amyloid, neuritic plaque
deposition and pre-fibrillar oligomers in 5xFAD mouse model of Alzheimer's
disease. Mol Neurodegener. Doi: 10.1186/s13024-018-0244-x

Spangenberg EE, Lee RJ< Najafi AR, Rice RA, Elmore MR, Blurton-Jones M, West BL<
Green KN (2016) Eliminating microglia in Alzheimer's mice prevents neuronal loss
without modulating amyloid-beta pathology. Brain. Doi: 10.1093/brain/aww016

Stanley ER and Chitu V (2014) CSF-1 receptor signaling in myeloid cells. Cold Spring Harb
Perspect Biol. Doi: 10.1101/cshperspect.a021857

Szalay G, Martinecz B, Lenart N, Kornyei Z, Orsolits B, Judak L, Csaszar E, Fekete R, West
BL< Katona G, Rozsa B, Denes A (2016) Microglia protect against brain injury and
their selective elimination dysregulates neuronal network activity after stroke. Nat
Commun. Doi: 10.1038/ncomms11499

Tahmasebi F, Pasbakhsh P, Mortezaee K, Madadi S, Barati S, Kashani IR (2019) Effect of
the CSF1R inhibitor PLX3397 on remyelination of corpus callosum in a cuprizone-
induced demyelination mouse model. J Cell Biochem. Doi: 10.1002/jcb.28344

Tap WD, Wainberg ZA, Anthony SP, Ibrahim PN, Zhang C, Healey JH, Chmielowski B,
Staddon AP, Cohn AL, Shapiro GI, Keedy VL, Singh AS, Puzanov I, Kwak EL,

Wagner AJ, Von Hoff DD, Weiss GJ, Ramanathan RK, Zhang J, Habets G, Zhang Y, Burton EA, Visor G, Sanftner L, Severson P, Nguyen H, Kim MJ, Marimuthu A, Shellooe R, Gee C, West BL, Hirth P, Nolop K, van de Rijn M, Hsu HH, Peterfy C, Lin PS, Tong-Starksen S, Bollag G (2015) Structure-guided blockade of CSF1R kinase in tenosynovial giant-cell tumor. N Engl J Med. Doi: 10.1056/NEJMoa1411366

Wallet C, De Rovere M, Van Ssche J, Daouad F, De Wit S, Gautier V, Mallon PWG, Marcello A, Van Lint C, Rohr O Schwartz C (2019) Microglial cells: The main HIV-1 reservoir in the brain. Front Cell infect Microbiol. Doi: 10.3389/fcimb.2019.00362

Williams DW, Veenstra M, Gaskill PJ, Morgello S, Calderon TM, Berman JW (2014) Monocytes mediate HIV neuropathogenesis: mechanisms that contribute to HIV associated neurocognitive disorders. Doi: 10.2174/1570162x12666140526114526

Witwer KW, Gama L, Li M, Bartizal CM, Queen SE, Varrone JJ, Brice AK, Graham DR, Tarwater PM, Mankowski JL, Zink MC, Clements JE (2009) Coordinated regulation of SIV replication and immune responses in the CNS. PLoS One. Doi: 10.1371/journal.pone.0008129

**Chapter V**

Akiyama H, Nishimura T, Kondo H, Ikeda K, Hayashi Y, McGeer PL (1994) Expression of the receptor for macrophage colony stimulating factor by brain microglia and its upregulation in brains of patients with Alzheimer's disease and amyotrophic lateral sclerosis. Brain Res. Doi: 10.1016/0006-8993(94)91779-5

Beck SE, Kelly KM, Queen SE, Adams RJ, Zink MC, Tarwater PM, Mankowski JL (2015)
Macaque species susceptibility to simian immunodeficiency virus: increased
incidence of SIV central nervous system disease in pigtailed macaques versus rhesus
macaques. J Neurovirol. Doi: 10.1007/s13365-015-0313-7

Beck SE, Queen SE, Metcalf Pate KA, Mangus LM, Abreu CM, Gama L, Witwer KW,
Adams RJ, Zink MC, Clements JE, Mankowski JL (2018) An SIV/Macaque model
targeted to study HIV-associated neurocognitive disorders. J Neurovirol. Doi:
10.1007/s13365-017-0582-4

Beck SE, Queen SE, Witwer KW, Metcalf Pate KA, Mangus LM, Gama L, Adams RJ,
Clements JE, Christine Zink M, Mankowski JL (2015) Paving the path to HIV
neurotherapy: predicting SIV CNS disease. Eur J Pharmacol. Doi:
10.1016/j.ejphar.2015.03.018

Bohlen CJ, Bennett FC, Tucker AF, Collins HY, Mulinyawe SB, Barres BA (2017) Diverse
requirements for microglial survival, specification, and function revealed by defined-
medium cultures. Neuron. Doi: 10.1016/j.neuron.2017.04.043

Cahoy JD, Emery B, Kaushal A, Foo LC, Zamanian JL, Chistopherson KS, Xing Y,
Lubischer JL, Krieg PA, Krupenko SA, Thompson WJ, Barres BA (2008) A
transcriptome database for astrocytes neurons, and oligodendrocytes: a new resource
for understanding brain development and function. J Neurosci. Doi:
10.1523/JNEUROSCI.4178-07.2008

Elmore MR, Lee RJ, West BL, Green KN (2015) Characterizing newly repopulated
microglia in the adult mouse: impacts on animal behavior, cell morphology, and
neuroinflammation. PLoS One. Doi: 10.1371/journal.pone.0122912

Gerber YN, Saint-Martin GP, Bringuier CM, Bartolami S, Goze-Bac C, Noristani HN, Perrin
FE (2018) CSF1R inhibition reduces microglia proliferation, promotes tissue
preservation and improves motor recovery after spinal cord injury. Front Cell
Neurosci. Doi: 10.3389/fncel.2018.00368

Geirsdottir L, David E, Keren-Shaul H, Weiner A, Bohlen SC, Neuber J, Balic A, Giladi A,
Sheban F, Dutertre CA, Pfeifle C, Peri F, Raffo-Romero A, Vizioli J, Matiasek K,
Scheiwe C, Meckel S, Matz-Rensing K, van der Meer F, Thormodsson FR,
Stadelmann C, Zikha N, Kimchi T, Ginhoux F, Ulitsky I, Erny D, Amit I, Prinz M
(2019) Cross-species single-cell analysis reveals divergence of the primate microglia
program. Cell. Doi: 10.1016/j.cell.2019.11.010

Gelman BB, Chen T, Lisinicchia JG, Soukup VM, Carmical JR, Starkey JM, Masliah E,
Commins DL, Brandt D, Grant I, Singer EJ, Levine AJ, Miller J, Winkler JM, Fox
HS, Luxon BA, Morgello S, National NeuroAIDS Tissue Consortium (2012) The
National NeuroAIDS Tissue Consortium brain gene array: two types of HIV-
associated neurocognitive impairment. PLoS One. Doi:
10.1371/journal.pone.0046178

Han J, Harris RA, Zhang XM (2017) An updated assessment of microglia depletion: current
concepts and future directions. Mol Brain. Doi: 10.1186/s13041-017-0307-x

Hanisch UK, Kettenmann H (2007) Microglia: active sensor and versatile effector cells in the
normal and pathologic brain. Nat Neurosci. Doi: 10.1038/nn1997

Jin WN, Shi SX, Li Z, Li M, Wood K, Gonzales RJ, Liu Q (2017) Depletion of microglia
exacerbates postischemic inflammation and brain injury. J Cereb Blood Flow Metab.
Doi: 10.1177/0271678X17694185

Knight AC, Brill SA, Queen SE, Tarwater PM, Mankowski JL (2018) Increased microglial

    CSF1R expression in the SIV/macaque model of HIV CNS disease. J Neuropathol

    Exp Neurol. Doi: 10.1093/jnen/nlx115

Kreutzberg GW (1996) Microglia: a sensor for pathological events in the CNS. Trends

    Neurosci. Doi: 10.1016/0166-2236(96)10049-7

Lawson LJ, Perry VH, Dri P, Gordon S (1990) Heterogeneity in the distribution and

    morphology of microglia in the normal adult mouse brain. Neuroscience. Doi:

    10.1016/0306-4522(90)90229-w

Li M, Li Z, Ren H, Jin WN, Wood K, Liu Q, Sheth KN, Shi FD (2017) Colony stimulating

    factor 1 receptor inhibition eliminates microglia and attenuates brain injury after

    intracerebral hemorrhage. J Cereb Blood Flow Metab. Doi:

    10.1177/0271678X16666551

Li Q, Cheng Z, Zhou L, Darmanis S, Neff NF, Okamoto J, Gulati G, Bennett ML, Sun LO,

    Clarke LE, Marschallinger J, Yu G, Quake SR, Wyss-Coray T, Barres BA (2019)

    Developmental heterogeneity of microglia and brain myeloid cells revealed by deep

    single-cell RNA sequencing. Neuron. Doi: 10.1016/j.neuron.2018.12.006

Neher JJ, Cunningham C (2019) Priming microglia for innate immune memory in the brain.

    Trends Immunol. Doi: 10.1016/j.it.2019.02.001

Meulendyke KA, Ubaida-Mohien C, Drewes JL, Liao Z, Gama L, Witwer KW, Graham DR,

    Zink MC (2014) Elevated brain monoamine oxidase activity in SIV- and HIV-

    associated neurological disease. J Infect Dis. Doi: 10.1093/infdis/jiu194

Saylor D, Dickens AM, Sacktor N, Haughey N, Slusher B, Pletnikov M, Mankowski JL,

    Brown A, Volsky DJ, McArthur JC (2016) HIV-associated neurocognitive disorder –

pathogenesis and prospects for treatment. Nat Rev Neurol. Doi:
10.1038/nrneurol.2016.53

Sharma G, Colantuoni C, Goff LA, Fertig EJ, Stein-O'Brien G (2020) projectR: An
R/Bioconductor package for transfer learning via PCA, NMF, correlation, and
clustering. Bioinformatics. Doi: 10.1093/bioinformatics/btaa183

Stein-O'Brien GL, Clark BS< Sherman T, Zibetti C, Hu Q, Sealfon R, Liu S, Qian J,
Colantuoni C, Blackshaw S, Goff LA, Fertig EJ (2019) Decomposing cell identity for
transfer learning across cellular measurements, platforms, tissues, and species. Cell
Syst. Doi: 10.1016/j.cels.2019.04.004

Szalay G, Martinecz B, Lenart N, Kornyei Z, Orsolits B, Judak L, Csaszar E, Fekete R, West
BL, Katona G, Rozsa B, Denes A (2016) Microglia protect against brain injury and
their selective elimination dysregulates neuronal network activity after stroke. Nat
Commun. Doi: 10.1038/ncomms11499

Yeh FL, Hansen DV, Sheng M (2017) TREM2, microglia, and neurodegenerative diseases.
Trends Mol Med. Doi: 10.1016/j.molmed.2017.03.008

Zamanian JL, Xu L, Foo LC, Nouri N, Zhou L, Giffard RG, Barres BA (2012) Genomic
analysis of reactive astrogliosis. J Neurosci. Doi: 10.1523/JNEUROSCI.6221-
11.2012

Zhang Y, Chen K, Sloan SA, Bennett ML, Scholze AR, O'Keeffe S, Phatnani HP, Guarnieri
P, Caneda C, Ruderisch N, Deng S, Liddelow SA, Zhang C, Daneman R, Maniatis T,
Barres BA, Wu JQ (2014) An RNA-sequencing transcriptome and splicing database
of glia, neurons, and vascular cells of the cerebral cortex. J Neurosci. Doi:
10.1523/JNEUROSCI.1860-14.2014

# CURRICULUM VITAE

**Audrey C. Knight**
Department of Molecular and Comparative Pathobiology
Johns Hopkins University School of Medicine,
733 North Broadway, MRB 820, Baltimore, MD 21205
Work #: (443) 287-7088    Cell #: (314) 920-2936    Email: aknigh12@jhmi.edu

## Education

**Johns Hopkins University School of Medicine, Baltimore, MD**
 Pathobiology PhD Candidate; PI: Joseph Mankowski, DVM, PhD
 Anticipated Completion: May 2020

**Illinois College, Jacksonville, IL**
 BS in Biology, May 2014
 Minors: Chemistry, French
 Honors: Phi Beta Kappa
 GPA: 3.97

## Research Experience

**Johns Hopkins School of Medicine, Baltimore, MD**
*Graduate Student Thesis Project*
- The Immunoregulatory Role of Microglial CSF1R in the SIV Model of HIV CNS Disease
  - Tracked alterations in CSF1R and TREM2 mRNA and protein expression in the CNS throughout disease progression including latency.
  - Characterized viral dynamics and microglial cell biology *in vitro* (primary cell culture) and *in vivo* (NHP).
  - Developed and executed an RNA-Seq transcriptome-based project to characterize dysregulation of microglial and astrocyte immune activation and its impact on neurodegeneration in this model.
  - Designed and completed a pilot pre-clinical drug trial with PLX3397 (CSF1R inhibitor) in SIV-infected pigtailed macaques.

*Graduate Student Rotation Projects*
- Development of an Anti-Viral IgE screen from patient serum
  - Developed an IgE capture technique to be used with viral Phage Immunoprecipitation (PhIP) sequencing; used this capture technique to develop an ELISA to measure IgE levels in human serum.
  - Analyzed anti-viral IgE from patients with peanut allergy and asthma
- Development of an Anti-Prostate Cancer Virus-Like-Particle Vaccine
  - Cultured VLPs and conjugated prostate cancer antigens; injected conjugated VLPs in mice and tested for T cell response via FACS

## Grants, Publications, Presentations, and Awards

*Grants*
**NIH R25 Pilot Grant**: 2018; Translational Research in NeuroHIV and Mental Health
Title: Dysregulation of central nervous system glial immune responses in a cART-suppressed SIV/macaque model of chronic HIV CNS disease
Role: Principal Investigator
Amount: $20,000; 1 year

*Publications*
**Knight AC**, Brill SA, Solis CV, Richardson MR, McCarron ME, Queen SE, Bailey CC, Mankowski JL. "Differential Regulation of TREM2 and CSF1R in CNS Macrophages in an SIV/Macaque Model of HIV CNS Disease." *J Neurovirol*. Submitted 4 December 2019.

**Knight AC**, Brill SA, Queen SE, Tarwater PM, Mankowski JL. "Increased Microglial CSF1R Expression in the SIV/Macaque Model of HIV CNS Disease." *J Neuropathol Exp Neurol*. 2018. PMID: 29319808

Mangus LM, Weinberg RL, **Knight AC**, Queen SE, Adams RJ, Mankowski JL. "SIV-Induced Immune Activation and Metabolic Alterations in the Dorsal Root Ganglia During Acute Infection." *J Neuropathol Exp Neurol.* 2018. PMID: 30500918

Yokoya K, Zettler LW, Kendon JP, Bidartondo MI, Stice AL, Skarha S, Corey LL, **Knight AC**, Sarasan V. "Preliminary findings on identification of mycorrhizal fungi from diverse orchids in the Central Highlands of Madagascar." *Mycorrhiza*. 2015. PMID: 25771863

*Presentations*
**Conference on Retroviruses and Opportunistic Infections;** 2020
Poster presentation: "CSF1R Inhibition Targets CNS Macrophages in an SIV/Macaque Model of HIV CNS Disease."

**NeuroHIV Lecture Series;** 2019
Invited talk: "Markers of Microglial Priming in an SIV/Macaque Model of HIV CNS Disease."

**Society for NeuroImmune Pharmacology Annual Meeting**; 2019
Poster Presentation: "Differential Regulation of TREM2 and CSF1R in CNS Macrophages in the SIV/Macaque Model."

**International Symposium on Neurovirology**; 2019, 2018
2019 Poster Presentation: "TREM2 and CSF1R as markers of chronic CNS inflammation in an SIV pigtailed macaque model of HIV CNS disease"
2018 Oral and Poster Presentation: "TREM2 Expression Increases with SIV Encephalitis in a Macaque Model of HIV CNS Disease"

**Wistar Neurovirology and Neuroimmunology Symposium at the University of Pennsylvania**; 2017

Poster presentation: "Increased Microglial CSF1R Expression in the SIV/Macaque Model of HAND"

**The Johns Hopkins School of Medicine Pathology Young Investigators Day**; 2018
Poster presentation: "TREM2 expression increases with SIV encephalitis in a macaque model of HIV CNS disease."

**Pathobiology Graduate Program Retreat**
2019 Invited Oral Presentation: "The Role of CSF1R in an SIV/Macaque Model of HIV CNS Disease"
2018 Poster: "The Discordant Regulation of TREM2 and CSF1R in an SIV/Macaque Model of HIV CNS Disease"
2017 Poster: "Increased Microglial CSF1R Expression in the SIV/Macaque Model of HAND"
2016 Poster: "Heme Oxygenase-1 Expression in SIV+ Pigtailed Macaques"
*Awards*
**New Investigator Scholarship;** Conference on Retroviruses and Opportunistic Infections, 2020
**Early Career Investigators in Training Travel Scholarship**; International Symposium on Neurovirology, 2018
**Best 2nd Year Graduate Student Poster Presentation**; Pathobiology Graduate Program Retreat, 2016

*Awards*
**New Investigator Scholarship;** Conference on Retroviruses and Opportunistic Infections, 2020
**Early Career Investigators in Training Travel Scholarship**; International Symposium on Neurovirology, 2018
**Best 2nd Year Graduate Student Poster Presentation**; Pathobiology Graduate Program Retreat, 2016


**Teaching, Mentorship, and Leadership Experience**

**Baltimore Montessori Public Charter School Science Education**; 2019-2020
- Worked with Dr. Carlo Colantuoni to develop lesson plans for multiple sections of science education for 4th and 5th grade students; topics covered the big bang, evolution, comparative anatomy, cell biology, and genetics.
- Executed these lessons in the classroom starting in December and will continue through the spring.

**Mentorship of Undergraduate Summer Student**; 2019
- Developed a research project for the student characterizing and quantifying PU.1 protein expression in the SIV/macaque model.
- Worked one-on-one with the student training her in different laboratory techniques, how to find and read the relevant literature, and how to analyze data. I also provided career advice and guidance.

**Johns Hopkins Teaching Academy Teaching Institute**; 2018

- Participated in a three-day intensive course focused on preparing PhD-level scientists for teaching at the undergraduate level. Activities included basic pedagogy, teaching strategies, flipped-classroom design, and syllabus generation.

**Teaching in Pathobiology: Pathobiology for Graduate Students, Basic Mechanisms**
**Teaching Assistant**; 2016
- Presented a mini-lecture on basic infectious disease immunohistochemistry.
- Assisted the class proctor with grading, facilitating in-class discussions, and answering student questions.

**Co-organizer of the Johns Hopkins Pathobiology Sabin Pathology Club**; 2017 - 2019
- Organized meeting topics and presenters in several-month rotating shifts.
- Presented lectures on various pathology topics including autoimmune cardiomyopathy and neurotropic viruses

**Admissions Committee Member**; 2017 and 2018 admissions cycle

*Undergraduate Teaching Experience; Illinois College*
- Student director of the Campus Writing Center; 2012-2014
  - Apprentice Coordinator; 2011-2012: Designed and executed a training program for Writing Center Consultants
  - Writing Center Consultant; 2011-2014: Assist peers through the writing process
- Teaching Assistant: Genetics; Introduction to Physics II
  - Taught one class per week for each course; class focus was on working through problem sets and reviewing the course material from the previous week